CHALMERS
UNIVERSITY OF TECHNOLOGY

Dynamics and amorphous state stability of pharmaceuticals in hot melt extruded solid dispersions

Master's thesis in Applied Physics

Gustav Ferrand-Drake del Castillo

Department of Applied Physics
CHALMERS UNIVERSITY OF TECHNOLOGY
Gothenburg, Sweden 2015-06-10

Acknowledgements

I wish to acknowledge support from AstraZeneca and the department of Pharmaceutical Development in Mölndal, Sweden. I am very thankful for the kind support of my supervisors Susanna Alami Abrahamsén, and Hanna Matic who provided scientific competence combined with their industrial experience. Apart from the help of my supervisors, Anders Borde, Anna Viridén and Johan Breiholtz also made significant contributions in helping me with my work at AstraZeneca. I wish to acknowledge the support from Chalmers University of Technology. My supervisor prof. Anette Larsson at the division of Pharmaceutical Technology at the department of Chemistry and Chemical Engineering has been an excellent support and provided me with valuable insights. I wish to thank the department of Applied Physics and the division of Condensed Matter Physics. I wish to give a special thanks to the staff at the division of Condensed Matter Physics whom I have a lot of time with throughout the course of this thesis, the help from my colleagues and their cheerful attitude has helped and inspired me. Finally I would like to thank my examiner and supervisor prof. Aleksandar Matic who has been a source of inspiration and motivation.

1 Abstract

Drug discovery methods seek to generate new drugs with higher potency and specificity[1]. These methods result in drug molecules that display increased molecular weight and greater lipophilic character and as a consequence lower solubility. Already, it is estimated that 40% of marketed drugs display insufficient solubility in order to be used in oral administration[2]. Due to the ease-of-use, and high patient compliance in relation to other methods of drug administration, oral administration is the most common method of drug administration, and will continue to be a preferred method of drug administration[3-5]. Formulation of Active Pharmaceutical Ingredients (API) in the glass state is a method of raising solubility which could enable oral administration of insufficiently soluble compounds[6]. Glasses are however metastable with respect to the crystal state making physical stability over time and reliable release behavior a concern[7-9]. As a consequence so-called amorphous solid dispersions where the API is stabilized in the amorphous state has emerged as a promising formulation strategy[7,10].

In this thesis improvement of API solubility and glass stability through preparation of amorphous solid dispersions using hot melt extrusion was evaluated. Three pharmaceutical glasses of ibuprofen, felodipine, cilostazol and hot melt extruded amorphous solid dispersions of all three APIs were characterized using Differential Scanning Calorimetry, Dielectric spectroscopy, and Raman spectroscopy. Felodipine solubility in an amorphous solid dispersion was raised by 6 times the crystalline solubility, while maintaining increased glass stability relative to the neat state. The dynamics and relaxations within the solid dispersion was studied, characterized and compared with neat felodipine. The combined approach of physical characterization of pharmaceutical glasses and release performance testing may facilitate identification of common denominators between method of preparation, crystallization suppression, and release functionality. A primary contribution of this work is to show that it is possible to study the dynamics of an API confined within a polymer carrier matrix.

2 Table of Contents

3 Introduction

The demand of drugs exhibiting both high potency and selectivity has lead to new drug candidates becoming increasingly complex in their molecular structure[2]. Recently it was estimated that 40 % of all marketed drugs display low solubility in water[2]. Predictions on currently developed pharmaceutical compounds indicate that above 50% of new drug candidates are highly lipophilic, and as a consequence they display insufficient bioavailability[11]. Bioavailability is a term used to describe how effectively the drug substance enters the body, and reaches its intended target with therapeutic activity as a result[2].

Oral administration is the most frequently used drug formulation method[4]. It offers several advantages in relation to other methods. Oral administration is simple, convenient and the safest method of drug administration. It offers high patient compliance in relation to other methods such as intravenous injections[4]. Although high sanitary conditions during manufacturing are absolutely necessary, the over-all need of sterility is lower compared to other formulation methods[4]. Therefore, despite challenges in oral drug delivery of modern Active Pharmaceutical Ingredients (API), displaying low bioavailability, intensive efforts are being put into developing oral formulations with sufficient performance[2]. Bioavailability in terms of oral administered tablets depend primarily on two factors, firstly the ability of the drug molecule to dissolve and enter the gastric fluid molecularly dispersed, secondly, it must be absorbed within the gastrointestinal system in order to enter the bloodstream and reach its intended target.

Simply increasing the dose of the API as a formulation method may be an effective way of achieving higher uptake, however it raises may compromise safety and result in release profiles that are difficult to predict[12]. This raises the question of achieving a controlled release formulation. Apart from raising solubility of insufficiently soluble APIs, a controlled release is a crucial aspect when developing pharmaceutical formulations. A formulation capable of raising the solubility of a compound should not only result in a concentration within the body where therapeutic effect is observed. It is also of highest priority to prevent toxic concentrations of API within the body. The release profile of a solubility enhancing release formulation should therefore reliably stabilize within the window of therapeutic efficiency concentration, and the toxic concentration. This is illustrated in Figure 3.1 where blood concentration profiles as a function of time are shown that model instant and controlled release cases.

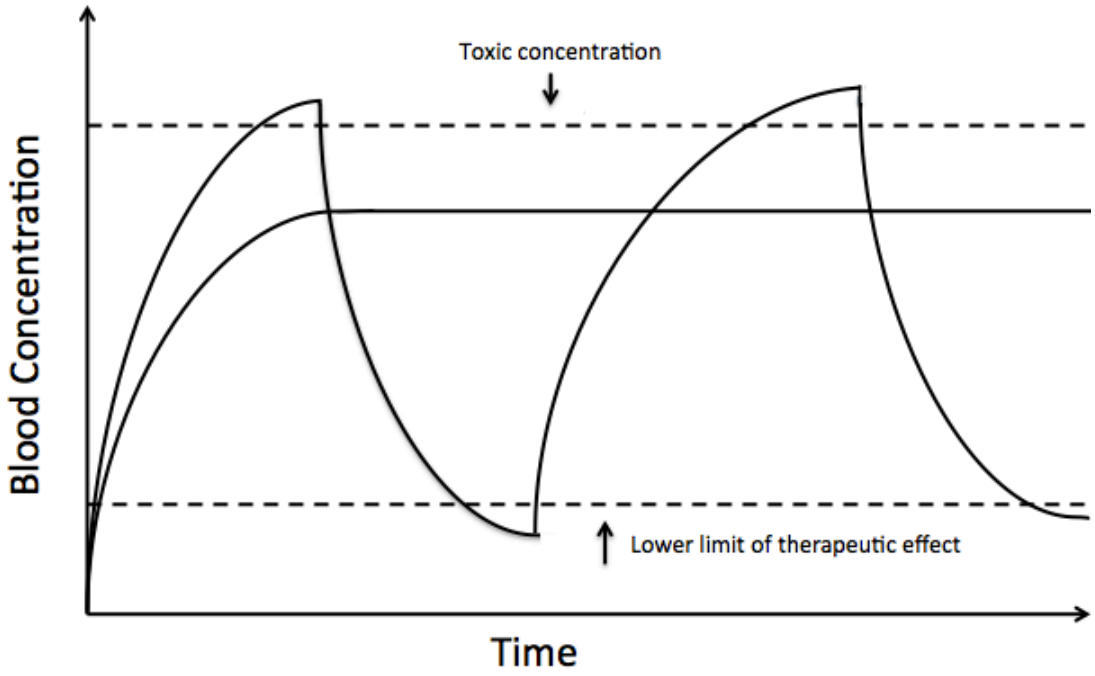

Figure 3.1.Blood plasma concentration shown as a function of time for two formulations. The traditional un-optimized oral formulation may require frequent administration, during administration toxic and insufficient concentrations may be reached. The second formulation profile shown is the controlled release profile; result in a stable blood concentration requiring less frequent administration. Adapted from Aulton with modifications[4].

The profile shown in Figure 3.1 identifies another important aspect of controlled release. Apart from reaching appropriate concentration within a patient, a pharmaceutical formulation should also give rise to an extended release profile. This means that the frequency of supplying new doses is kept as low as possible. An issue with many oral immediate release formulations is the frequency at which new doses need to be administered in order to maintain therapeutic effect[4]. In a report by WHO patient adherence in developed nations was estimated to be as low as 50%[5,13]. Patient adherence means the extent to which the prescribed treatment is followed. It is also expected that the number may be even lower in developing nations. It is crucial that a patient is able to fulfill its prescribed treatment in the way it is intended. The consequence of failure in patient adherence is estimated to cost US$100 billion in the United States each year due to hospitalizations required as a result[5]. Complex medication schemes have been identified to increase the risk of failure in successfully treating the patient. By achieving extended release formulations requiring less frequent administration efficiency would increase along with patient compliance.

To achieve both increased solubility and extended release amorphous solid dispersions have been identified as a potential formulation strategy[10,12,14]. An amorphous solid dispersion is a pharmaceutical formulation, which consists of an Active Pharmaceutical Ingredient in the amorphous state within a carrier matrix. Amorphous state, or the glass state as it is also called, is a solid with non-crystalline structure[4,8,15]. A glass is in a higher energy state compared to its crystalline

counterpart. The higher energy state gives glasses the potential to dissolve more rapidly[4]. Dissolving glasses may also temporarily reach concentrations that exceed the crystalline solubility[6,16]. As with other tablet formulations, the inclusion of swellable hydrophilic polymers enables an extended release[14]. The combination of using an amorphous API within hydrophilic polymer acting as a carrier matrix provides the potential to deliver poorly soluble APIs more rapidly and at higher concentrations than what is possible in crystalline tablet formulation methods.

This enables a potential increase in solubility. Due to its solid properties the amorphous state of the pharmaceutical has the potential of raising solubility compared to the crystalline counterpart[6,16]. Apart from solubility enhancement an amorphous solid dispersion has the potential of extended release properties. Extended release properties are achieved by the use of a polymer additive able to sustain high concentration of the pharmaceutical within the gastric fluid. Enhanced solubility may enable lower drug doses of tablets compared to existing crystalline state formulations, limiting the risk of reaching concentrations where unwanted side-effects and toxic levels[6].

Apart from amorphous solid dispersion several formulation strategies are being developed with aim to increase solubility and permeability of APIs[2]. Examples of such strategies include, polymorphism, co-crystal formation, co-solvents, cyclodextrins, particle size reduction strategies, and lipid based formulations[2]. In each of these examples it is customary to include some type of additive in order to achieve the solubility or permeability enhancement. An example of such a case is for instance nano-suspensions in which additives are used to stabilize nano-sized particles[17]. Additives are crucial in many formulation techniques and amorphous solid dispersions are no exception since they contain polymer carriers. However amorphous solid dispersions have the potential of not only relying on the additive in order to achieve enhanced solubility, instead the intrinsic physical state of the API is responsible for solubility enhancement.

The success of amorphous solid dispersions as pharmaceutical formulation suffers from the fact that glasses are metastable in relation to the crystal form. It is generally recognized that the susceptibility to crystallization is a major issue[2,6]. Added to the uncertainty of glass instability, there is also lack of a fundamental understanding of the formation of glasses[8].

To deal with amorphous API instability considerable efforts have been directed towards tuning the polymer additive properties[2,7,12]. The polymer additives developed for amorphous solid dispersion stabilize the amorphous state of the API by acting as a physical barrier towards external environment, by increasing the viscosity of the multi-component system, slowing down motion and dynamics of the API, and by intermolecular interactions with the API and the polymer[18]. In addition to tuning polymer properties, the method of manufacture has proven to be important in realizing amorphous solid dispersions with sufficient stability.

Despite intensive research on amorphous solid dispersions for oral release applications, relatively few cases of amorphous solid dispersion formulations have become marketed products[19]. The number of products available utilizing hot melt extruded amorphous solid dispersions has increased[7]. In 2013, there was 13 hot melt extruded amorphous solid dispersion formulations on the market. Still it was recently commented that the number of amorphous solid dispersions formulations marketed products is strikingly low[18]. Although the use of hot melt extrusion as pharmaceutical manufacturing technique is now employed in marketed products, the potential of further use and development is predicted to be large[7]. Especially downstream processing solutions of hot melt extruded amorphous solid dispersions to achieve desired properties is considered to be a promising area of development[18].

In this work the possibility of increasing API solubility through amorphous solid dispersion preparation of selected model drugs is investigated. The aim of this thesis is to determine the physical properties of amorphous pharmaceuticals in their neat state, and how these are affected when incorporated in solid dispersions using different preparation methods. To evaluate physical properties of the pharmaceutical glasses and dispersions several characterization techniques have been used; differential scanning calorimetry, dielectric spectroscopy, Raman spectroscopy, and thermal gravimetry analysis. The preparation methods of amorphous solid dispersions considered are hot melt extrusion and solvent film-casting.

To render an API amorphous one essentially need to either; i) melt the API, ii) dissolve it in a suitable organic solvent, or iii) mechanically grind the crystalline material to provide sufficient shear to disrupt the long range order of the crystal. There exist many methods of achieving amorphous state, all of which are characterized by certain advantages and disadvantages from a laboratory and industrial perspective. Melting may result in thermal degradation, solvent dissolution put heavy requirement on evaporation without residual solvent in the product, mechanical grinding may also result in degradation but may primarily present a challenge in terms of producing a homogenously amorphous material.

The manufacturing technique of making solid dispersions primarily considered in this report is hot melt extrusion (HME). Hot melt extrusion is a combination of thermal treatment resulting in melting of the API and mechanical shear which leads to a blending of the material with the polymer[12]. A combination of thermal treatments results in less damage of the final product. By careful choice of the polymer additive, temperature and process speed, thermal degradation can be avoided.

Another method considered in this work is film-casting using organic solvents. The preparation method is used primarily as a reference to hot melt extruded amorphous solid dispersions. Film casted solid dispersions are prepared by mixing dissolved API in a solution with a polymer, resulting in a homogenous liquid, followed by solvent evaporation. The level of mixing is close to ideal providing a

reference to how homogenously prepared the hot melt extruded solid dispersions are. Homogenous mixing of the API with the polymer at the molecular level is considered to be of crucial importance in terms of amorphous state stability[20-22]. The primary disadvantage of solvent-casted solid dispersions is the need of organic solvents, which may be environmentally harmful as well as toxic to the patient, if residual solvents are present within the tablet.

The emphasis of the thesis is to elucidate the dynamics of amorphous pharmaceuticals confined within the polymer matrix of a solid dispersion. Dielectric Spectroscopy (DS) is particularly useful in studying dynamics of glasses and liquids[23]. Pharmaceutical glasses have been extensively studied in their neat state using dielectric spectroscopy[6,24,25]. A reason for the large interest in characterizing dynamics of pharmaceutical glasses is the suggested role of molecular mobility in determining glass stability[6,24]. Both the liquid behavior of pharmaceuticals as a function of temperature, and the crystallization kinetics as a function of time at fixed temperature has been investigated thoroughly[24]. Limited efforts have also been dedicated to characterize dynamics of pharmaceuticals within solid dispersions. Recently it was concluded that the interpretation of DS experiments performed on amorphous solid dispersions is a complex issue[26]. In general multi-component systems are difficult to study using DS[23]. However there exist examples of DS studies performed on plasticized polymer systems[27]. In such studies differences of the liquid behavior of small molecules within polymers could be effectively characterized. These non-pharmaceutical systems bear several similarities to amorphous solid dispersions. There is reason to believe that similar studies can be performed in amorphous solid dispersions. If so, important information regarding the dynamics of pharmaceuticals within amorphous solid dispersions may be extracted. Specifically, the ability of most pharmaceuticals and polymer matrices to hydrogen-bond can be studied. Hopefully this can help to explain the role of hydrogen bonding in amorphous solid dispersion stability.

4 Aim & Objectives

4.1 Aim

The aim of this thesis is to determine how amorphous solid dispersions of model drugs and extended release matrix formers can enhance pharmaceutical tablet performance in terms of storage and dissolution behavior.

4.2 Objectives

The objectives of this thesis will either relate to determining and understanding i) the physical stability of amorphous solid dispersions, or ii) determining and understanding the dissolution and release behavior of amorphous solid dispersions.

- Characterization of three selected pharmaceutical compounds and two polymer carriers that could be of interest in amorphous solid dispersions.
- Evaluation of how properties of these materials affect amorphous solid dispersion formation and performance.
- Determine the crystallization properties of model drugs from undercooled melts and to characterize and compare the crystallization kinetics between the three substances.
- Study the relaxation processes in neat API undercooled melts and compare the structural relaxation between the APIs.
- Study how the relaxation behavior of APIs changes when confined within amorphous solid dispersions. Investigate possible interactions between the API and polymer.
- Determine the solubility of amorphous solid dispersions and the possibility of achieving supersaturated concentrations of API in solution.
- Examine the release mechanisms by which supersaturation is achieved. Determine the relative contribution played by the polymer release.
- Investigate the robustness of amorphous solid dispersions. How stable is the amorphous state within the tablet during solution exposure?
- Evaluate the role of manufacturing method HME in achieving increased stability and solubility performance.
- To what degree is it possible to control the state of the API within hot melt extruded solid dispersions? Could one prepare amorphous and crystalline felodipine solid dispersions depending on extrusion temperature and if so, would this affect the release profile significantly?

5 Theory

The theoretical background of this work will include a presentation of glasses. A general description of the glass transition, thermodynamic properties, and the potential solubility enhancement of glasses will be described. This is followed by descriptions of amorphous solid dispersions and methods to stabilize pharmaceutical glasses. Extended release matrix formers and their properties will be presented. The manufacturing technique hot melt extrusion used for pharmaceutical application is also presented. Finally release mechanisms of amorphous solid dispersions are reviewed.

5.1 The amorphous state

Amorphous materials are solids with disordered structure that lack long-range order[28]. Contrary to crystals they do not possess a long-range translational order. A subset of amorphous materials is glasses. What distinguishes glasses from other amorphous materials is the method of preparation[15]. Glasses form when a melt is quenched at a sufficiently rapid rate where crystallization is avoided and the melt undergoes the so-called glass transition[15]. Materials with disorder occur frequently in nature, humans have cultural traditions of producing glasses that trace back thousands of years back in time. In modern time amorphous materials due to their unique properties has become a key ingredient in many technologies such as fiber optics, telescope mirrors, food industry, and increasingly so in pharmaceutical industry[8,15]. Even though materials with purposely made disordered structure are being increasingly incorporated in our everyday life, there are still several aspects of amorphous materials and the glass transition that remain unknown. To date a theory that can satisfactory describe experimentally observed glass dynamics has not yet been presented[15,29,30].

5.1.1 The glass transition

Our current knowledge of amorphous materials has taught us that the ability to form glasses is universal[15]. A glass forming liquid can occur in atomic and molecular systems regardless of what interactions and bonding mechanisms are present within the material, be it covalent, ionic, metallic, hydrogen, or van der Waals bonding liquids. Volume, entropy and enthalpy are continuous throughout the glass transition, see Figure 5.1.

When a liquid melt is cooled past its melting temperature it may crystallize. Crystallization occurs when randomly moving molecules or atoms lock into a structure corresponding to an energy minima of the energy landscape and leads to a discontinuity of volume as a function of temperature[29]. This is characteristic of a first order phase transition, see Figure 5.1.

If the melt of a substance is cooled at a sufficiently high rate below the melting temperature crystallization is avoided. The liquid enters a supercooled liquid state that is metastable with respect to the stable crystalline state; this can be seen in Figure 5.1. As the temperature is lowered the supercooled liquid exhibits a rapid increase in viscosity corresponding to several orders of magnitude. By further cooling of the supercooled liquid the glass transition is eventually reached. The glass transition manifests itself for instance by a change in the slope of the volume as a function of temperature, see Figure 5.1. The glass transition is can also be observed as a step-like change in heat capacity. The temperature where the change in slope is observed is denoted T_g. The glass transition resembles a second order phase transition due to the observed volume and heat capacity dependency on temperature during the transition. The sensitivity to applied heating rate introduces a kinetic factor to the transition, due to this it cannot be considered a true phase transition[15,28].

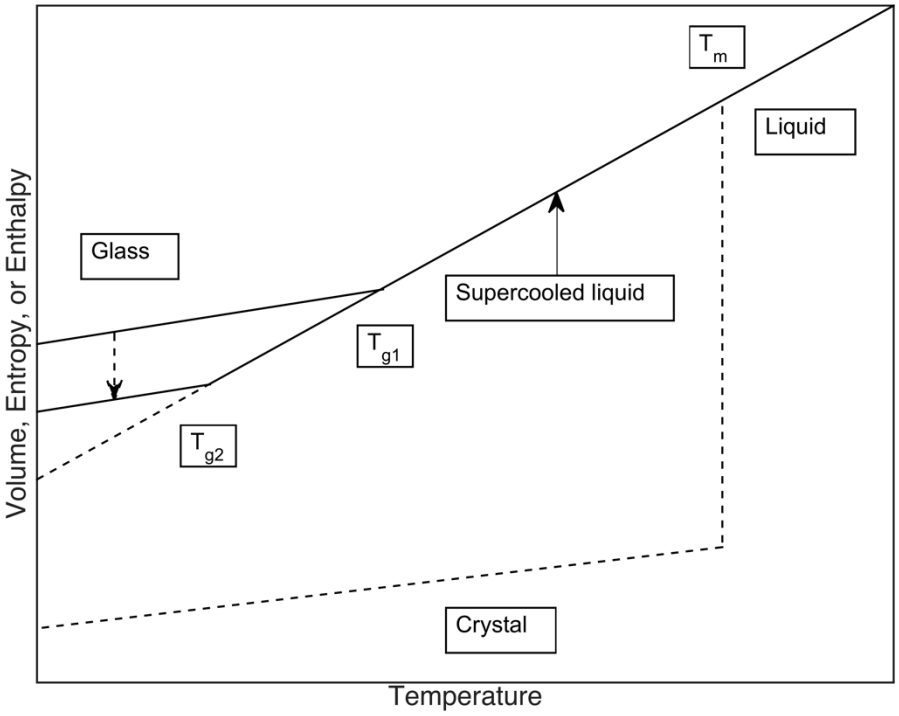

Figure 5.1. Schematic behavior of volume, entropy, and enthalpy as a function of temperature. Crystallization corresponds to a step-like change in volume as a function of temperature. If the cooling rate is high, the glass is formed at a relatively high temperature, T_{g1}. If the cooling rate is lower the glass is formed at a lower temperature, T_{g2}. This illustrates the kinetic nature of the glass formation.

When a liquid is cooled through its glass transition the system falls out of equilibrium[8,15]. The relaxation time of the system, which is an intrinsic property of the material, crosses the experimental timescale. The glass transition is a temperature range where the average relaxation time changes from 0.1s to 100s.

In all liquids there exist a relaxation time due to structural rearrangement within the liquid, also called the α-relaxation, which by all practical means cease to occur in the glassy state. In addition glasses and liquids can also exhibit several other motions giving rise to additional characteristic relaxation times. Such dynamics are generally tied to the chemistry of the molecules within the solution rather than to the liquid. Examples of such motions are local reorientations of molecules, motion of polymer side groups independent of its backbone motion, internal reorientations of molecules and their bonds. These relaxations are called secondary relaxations.

5.1.2 Canonical features of viscous liquids

Viscous liquids display non-Arrhenius behavior of structural relaxation time and viscosity over a wide temperature range. Two extremes are identified. The first is the near Arrhenius temperature dependence of relaxation time, $\tau \propto \ln(1/T)$. Examples of the few liquids that follow a near Arrhenius temperature are SiO_2 and GeO_2, such liquids are called "Strong". The second extreme behavior displayed by viscous liquids is the substantial deviation from Arrhenius temperature dependence. Examples of such liquids are molecular compounds with aromatic chemistry, van der Waals bonding liquids, and hydrogen bonding liquids. Such liquids are called Fragile. A comparison between strong and fragile liquids is given in Figure 5.2 where the relaxation time as a function of inverse temperature, scaled with respect to T_g is shown. As emphasized above, the same behavior is observed when examining the viscous liquid in terms of viscosity as a function of temperature.

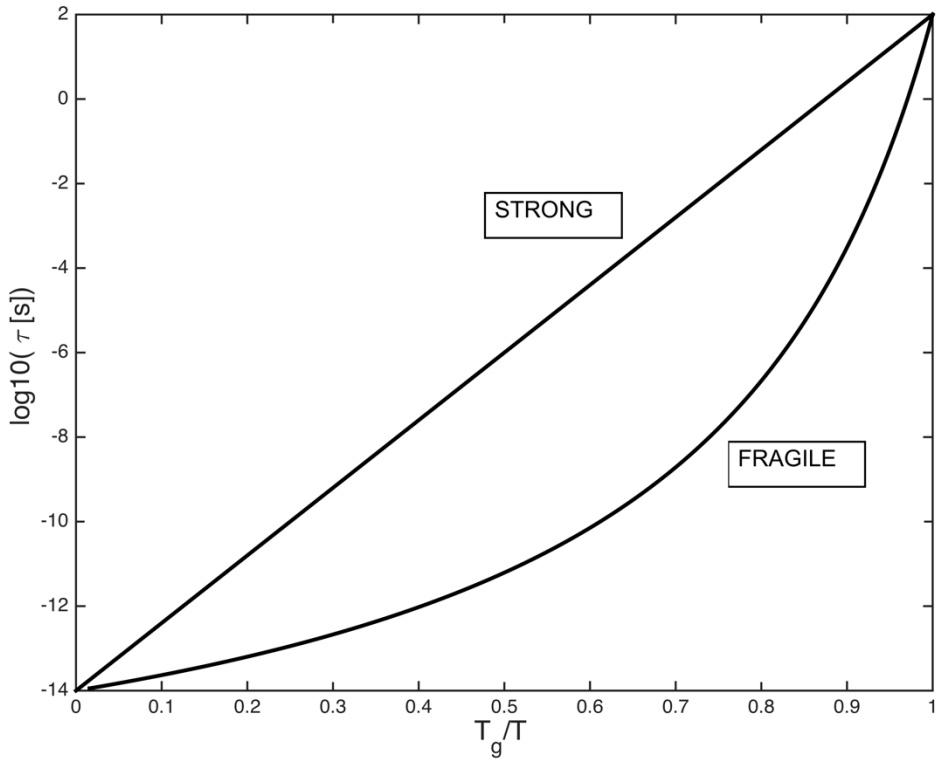

Figure 5.2. Relaxation time of viscous liquids shown as a function of T_g over temperature. The two extreme behaviors of viscous liquids are shown, fragile liquids that deviate from Arrhenius temperature dependence, and strong liquids displaying Arrhenius (exponential) temperature dependence. The figure is adapted from[8].

The behavior of viscous liquid relaxation time and viscosity as a function of temperature can be described by the VFT (Vogel-Tamman-Fulcher) equation **(1)**.

$$\tau = \tau_0 \exp\left(\frac{DT_0}{T - T_0}\right) \qquad (1)$$

The parameter D in equation **(1)** distinguishes between strong and fragile liquids, a large D value corresponds to a strong liquid, and a small D value results in fragile liquid behavior. The glass transition is defined to occur at $\tau_\alpha = 10^2 s$. The prefactor of equation **(1)** is set to be $\tau_0=10^{-13}$s. Another measure of fragility of a liquid is the derivative of the structural relaxation time of the liquid, with respect to temperature at the point of the glass transition, equation (2).

$$m = \left. \frac{d\left(\log_{10} \tau_\alpha (T)\right)}{d\left(\frac{T_g}{T}\right)} \right]_{T=T_g} \quad (2)$$

A characteristic of the α-relaxation of viscous liquids is a non-exponential decay as a function of time. A model that approximately fits most experimental data is the Kohlrausch-Williams-Watts function **(3)**. The stretching parameter β_{KWW} can be adjusted to fit the behavior of many different liquids of different chemistry and structure.

$$\phi(t) = \exp\left(-\left[\frac{t}{\tau}\right]^{\beta_{KWW}}\right) \quad (3)$$

Data collected from a large amount of viscous liquid indicate that a fragile liquids displaying deviations of relaxation time from Arrhenius temperature dependence is also likely to exhibit exponential deviations of relaxation time as a function of time.

5.2 Experimental characterization of glasses

Primarily two methods of studying the glass transition and behavior of glasses have been employed in this thesis. Differential Scanning Calorimetry and Dielectric Spectroscopy. Differential scanning calorimetry is relatively simple method of determining T_g, and crystallization and melting temperatures. Dielectric spectroscopy can be used to study relaxation processes due to the large frequency range where measurements can be performed.

5.2.1 Differential Scanning Calorimetry

Differential Scanning Calorimetry (DSC) is a widely used method in which the heat flux between a sample of interest and a reference sample is monitored[31]. In doing so the response of a material as a function of thermal exposure can be detected revealing processes such as glass transitions, crystallization, melting and its heat capacity. The experimental method is not material demanding requiring a sample amount in milligrams. A DSC measurement produce what is called a thermogram, where heat flow is recorded as a function of temperature, see Figure 5.3.

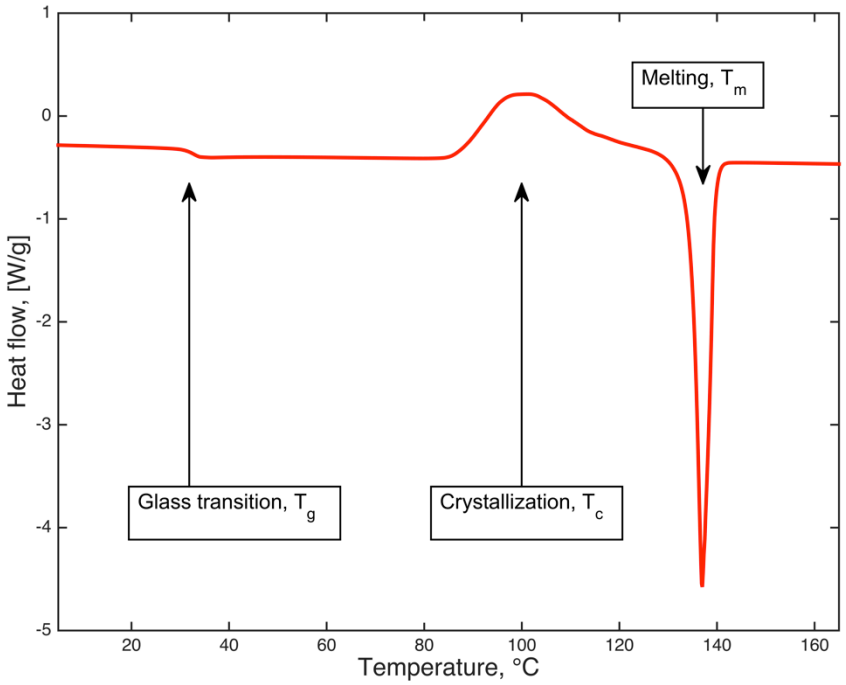

Figure 5.3. DSC thermogram where the heat flow is shown as a function of temperature. Exothermic events point upwards, endothermic events downwards. The characteristic signatures of the glass transition, crystallization, and melting are indicated.

Apart from observing the presence of thermal transitions one can also measure the difference in heat capacity, and if the equipment is properly calibrated, on an absolute scale for instance by integration of the peak, the heat released or uptake throughout a phase transition can be determined.

Some materials exhibits glass transitions with very small heat capacity change between glass and viscous liquid state. The transition may then be very difficult to detect by the use of a standard DSC experiments. The use of a modulated temperature signal, so-called MDSC measurement may be a useful method in such a case. The modulated heat flow is a sinusoidal heat flow signal applied in addition to an average heat flow. Through Fourier analysis the heat flow response of the material can be separated into reversible and non-reversing heat flow. The sum of

the two heat flow signals is the total heat flow measured during a standard DSC experiment. In the reversing heat flow signal the glass transition can be detected. The additional information required to perform a MDSC experiment is the amplitude and period of the sinusoidal heat flow.

5.2.2 Dielectric spectroscopy

The dielectric function of materials describes how a material responds to electromagnetic fields. Dielectric spectroscopy (DS) is a useful tool to study the dynamics within liquids and glasses[23]. In a DS experiment a molecular ensemble is exposed to an electric field. Molecules that exhibit a dipole moment respond by reorientational motion as a function of the electric field. The molecular dipoles depend on the molecular structure, such as the content of polar functional groups. The collective reorientational motion of molecular dipoles enables study of the structural relaxation (α-relaxation) and intramolecular reorientational relaxations (β-relaxations). Using DS the frequency and temperature dependence of viscous liquid relaxation can be covered over large intervals, 10^{-2}-10^{7}Hz and 100-600K.

In the theoretical treatment of dielectric relaxation measurements the material considered will be assumed to be an isotropic medium[29]. When an electric field is applied to the investigated material there exist a linear relation between the polarization field, $\boldsymbol{P}$, and the electric field, $\boldsymbol{E}$, according to equation **(4)** [23,29]. The linear relation is valid as long as the electric field is not too large.

$$\boldsymbol{P} = (\varepsilon - 1)\varepsilon_0 \boldsymbol{E} \tag{4}$$

Polarization of the material occur due to; (i) displacement of the electronic clouds of atoms (electronic polarization), (ii) displacement of atoms (atomic polarization), (iii) or dipolar polarization within the material aligning in direction of the electric field[23,29]. Polarization of a material due to (i) and (ii) occurs at very high frequency scale (10^{12}Hz). Dipolar reorientational motion occurs instead within the frequency range 10^{-2}-10^{7}Hz. Introduction of an electric displacement, $\boldsymbol{D}$, results in equation **(5)**.

$$\boldsymbol{D} = \varepsilon_0 \boldsymbol{E} + \boldsymbol{P} = \varepsilon\varepsilon_0 \boldsymbol{E} \tag{5}$$

Applying a harmonic electric field $E(t) = E_0 \exp(i\omega t)$, the displacement field is given by $D(t) = D_0 \exp(i(\omega t - \delta(\omega)))$. The dielectric properties of the material dictate the amplitude, D_0, and the phase shift, $\delta(\omega)$, of the displacement field. The dielectric function is calculated given the given the harmonic electric field and displacement field using equation **(6)**.

$$\varepsilon^*(\omega) = \varepsilon'(\omega) - i\,\varepsilon''(\omega) = \frac{D(\omega)}{\varepsilon_0\, E(\omega)} = \frac{D_0}{\varepsilon_0 E_0} \exp(-i\,\delta(\omega)) \tag{6}$$

The real and imaginary parts of the permittivity function are mutually related through the Kramers-Kronig relations according to equation **(7)** and **(8)**. A consequence of the Kramers-Kronig relations is that the derivative of the real part of the dielectric function is proportional to the imaginary dielectric function.

$$\varepsilon'(\omega) = 1 + \frac{2}{\pi} P \left[\int_0^\infty \frac{v\varepsilon''(v)}{v^2 - \omega^2} dv \right] \tag{7}$$

$$\varepsilon''(\omega) = \frac{2\omega}{\pi} P \left[\int_0^\infty \frac{\varepsilon'(v) - 1}{v^2 - \omega^2} dv \right] \tag{8}$$

The imaginary part of the dielectric function is often referred to as the dielectric loss, or dielectric dissipation. This is based upon the observation that the power loss during one cycle is proportional to the imaginary part of the dielectric function. A material investigated by DS may have a non-zero contribution of conductivity. The conductivity in an experiment contributes to the dielectric loss as

$$\varepsilon_{exp} = \varepsilon(\omega) - i \frac{\sigma_0}{\omega \varepsilon_0}. \tag{9}$$

When analyzing the reorientational motion of dipoles it is important to be aware of the potential presence of conductivity. Also, it is important through sample preparation to avoid impurities (mobile charge carriers) and to adjust the thickness of the sample to minimize the contribution of conductivity.

5.2.2.1 Experimental details of Dielectric Spectroscopy

A schematic electrical circuit of the experimental set-up of a dielectric measurement is shown in Figure 5.4.

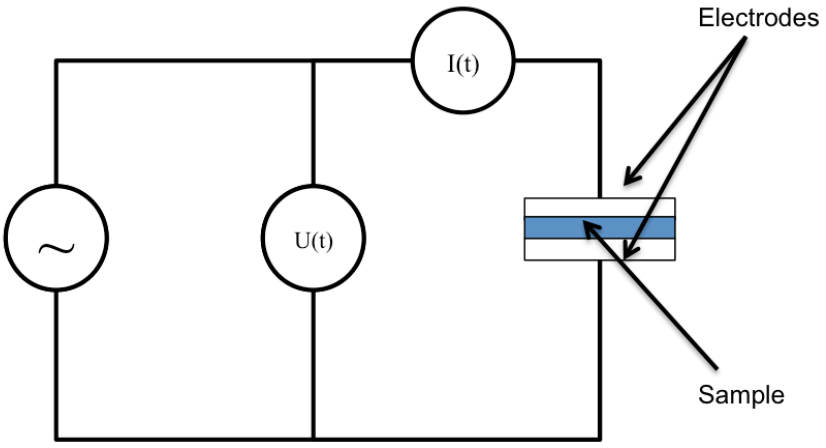

Figure 5.4. Schematic view of the circuit of a dielectric spectrometer.

During a dielectric measurement a voltage, $U(t) = U_0 \exp(i\omega t)$, is applied over the sample[29]. In response a current, $I(t) = I_0 \exp(i(\omega t - \phi(\omega)))$, will flow across the sample where the amplitude, I_0 , and phase, $\phi(\omega)$, are recorded. The impedance is then calculated according to equation (10).

$$Z^*(\omega) = Z'(\omega) - i\,Z''(\omega) = \frac{U^*(\omega)}{I^*(\omega)} \qquad (10)$$

Through the impedance the dielectric function is computed through

$$\varepsilon^*(\omega) = \varepsilon'(\omega) - i\,\varepsilon''(\omega) = \frac{-i}{\omega C_0 Z(\omega)}, \qquad (11)$$

where C_0 is the vacuum capacitance[23,29]. To achieve optimal resolution during a measurement the capacity of the material should have a value around 100pF for the instrument used in this work[29]. To adjust this value the thickness of the sample can be varied. Sample thicknesses ranging between 50-200μm were found to be suitable for the materials considered in this thesis.

5.2.2.2 Interpretation and analysis of the dielectric spectra

Figure 5.5 a) shows a conceptual imaginary part of the dielectric spectrum of a molecular liquid that is kept at a temperature $T>T_g$. The peaks shown in Figure 5.5 each correspond to reorientational motion of molecular dipoles as a function of the applied electric field. A peak signifies that the molecular dipoles in question dissipate energy by fluctuating reorientational motion at the peak position characteristic frequency values.

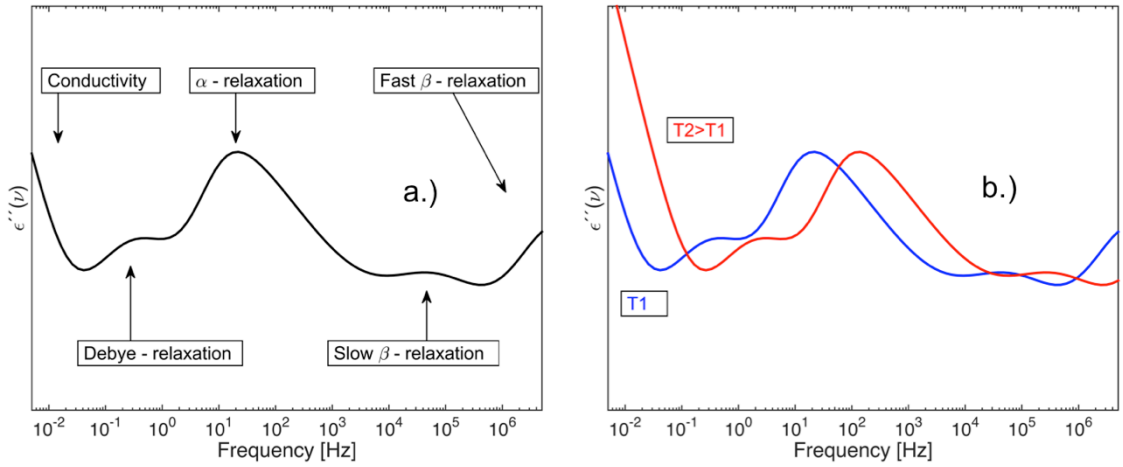

Figure 5.5. Conceptual dielectric spectrum (imaginary part). In a) various relaxation processes and features are indicated, which can appear in measurements of the dielectric function of molecular liquids. Figure b) illustrate how the characteristic frequencies of relaxation processes shift towards higher frequencies as the temperature increases. Adapted with modifications from[23].

Among the typical features of a molecular liquid within this frequency range the α-relaxation can be identified. The value of the α-relaxation peak frequency, f_α, (or any

other relaxation process) converted to the α-relaxation time, τ_α (or any other relaxation time) according to Equation (12).

$$\tau_\alpha = \frac{1}{2\,\pi\,f_\alpha} \qquad (12)$$

If the relaxation time for the α-relaxation in Figure 5.5 is calculated using equation **(13**) this would result in a α-relaxation time below 100s, thus the sample is in the liquid state. The glass transition relaxation time is defined to occur at $\tau_\alpha = 100$s enabling one to determine the T_g of a material using Dielectric spectroscopy[23,30]. This will be frequently utilized when examining the materials considered in this thesis.

At low frequencies the contribution from the conductivity of the material can be observed in Figure 5.5. Conductivity is identified in the dielectric spectrum as a contribution having a constant slope of -1 in a double logarithmic plot; see the conduction part of equation **(9)**. Conductivity arises from charge transport within the measured material across the electric field. The presence of conductivity in the dielectric spectrum is highly dependent on the amount of mobile charge carriers, and the temperature.

The α-relaxation displays an asymmetric peak shape. Typically the high frequency side has a lower slope value than the low frequency side, having a slope of 1. This asymmetric broadening is commonly attributed to the presence of dynamical heterogeneities in the molecular liquid[23]. In addition to the α-relaxation there are secondary β-relaxations. The β-relaxations correspond to intra-molecular dipole dynamics. The intra-molecular dynamics are in general faster, higher in frequency, than the motion of the entire molecule. It is easy to picture how the structural rearrangement (α-relaxations) of a large polymer chain, is slower than the dynamics of its side-groups (β-relaxations). The shape of the β-relaxation relaxation loss peak is usually symmetric.

It has been recognized that not only global molecular mobility of the entire molecular ensemble referred to as α-relaxations is relevant for glass stability[30,32]. Traditionally secondary relaxations have been related primarily to reorientations within the molecule[30]. However the existence secondary relaxation within glasses that should display no or minor intramolecular degrees of freedom has been observed in numerous cases[30]. Due to its general appearance in glasses this secondary relaxation is considered to be of fundamental importance to the glass transition[30]. A distinguished type of relaxation also referred to as the Johari-Goldstein relaxation (JG-relaxation). The JG-relaxation is typically observed below T_g and has been detected using DRS for several molecular glasses[24,25,30,32-34].

Another type of relaxation process is the Debye-relaxation[24,25]. The Debye-relaxation is related to molecular liquids that contain hydrogen-bonding groups.

Figure 5.5 clearly shows that in contrast to the β-relaxations, the Debye-relaxation peak is slower than the α-relaxation. The Debye-relaxation is poorly understood but one proposed explanation is the ability of these molecules to form intermolecular hydrogen-bonded structures or networks[35]. In this way the molecules form non-covalent polymeric chains held together by hydrogen bonds. Of the three APIs considered in this thesis, all have the ability of forming hydrogen bonds, but only ibuprofen has a reported Debye-relaxation in literature[24,25]. It has been suggested that the Debye –relaxation found in ibuprofen is due to dimer or trimer formation molecules arrange in two-by-two formation, or three by three formation[25,36].

The fitting of model functions to the dielectric spectrum is required to extract information regarding relaxation process. This enables one to extract the shape of the relaxation process, the dielectric signal strength (amplitude) and in particular the relaxation time. A function used to fit a general relaxation processes is the Havriliak-Negami function [29].

$$\varepsilon^*(\omega) = \varepsilon_\infty + \frac{\Delta\varepsilon}{(1 + (i\,\omega\,\tau_{HN})^{\beta_{HN}})^{\alpha_{HN}}} \qquad (13)$$

The parameter $\Delta\varepsilon = (\varepsilon_s - \varepsilon_\infty)$ signifies the dielectric strength of the process, τ_{HN} is the average relaxation time, and the two parameters α_{HN} and β_{HN} are defining the shape of the peak. The HN function is shown for some different values of α_{HN} and β_{HN} in Figure 5.6. The shape parameters α_{HN} and β_{HN} corresponds to symmetric and asymmetric broadening of the relaxation function respectively.

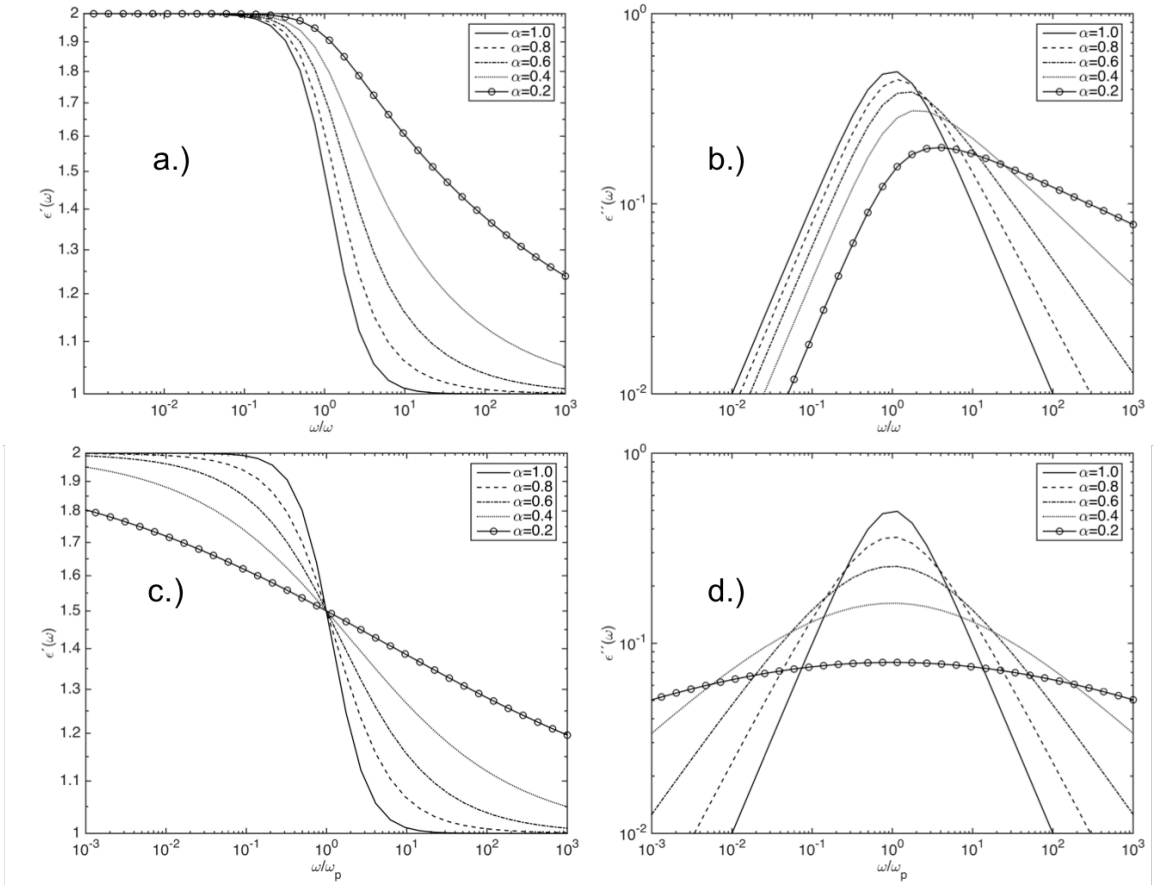

Figure 5.6. Real (left) and imaginary (right) parts of the Cole-Davidson relaxation function a) and b), and the Cole-Cole relaxation function, c) and d) for different values of the shape parameter. In the case of the CD function there is an asymmetric broadening, and in the case of the CC function, there is symmetric broadening. Adapted with modifications from[23].

There are two important cases of the HN relaxation function depending on which shape parameter that is adjusted[23]. The first case shown in Figure 5.6 a) and b) is called the Cole-Davidson, where: $\alpha_{HN} \leq 1, \beta_{HN} = 1$. The CD function is used to fit the α-relaxation, which typically exhibits asymmetric broadening, see Figure 5.6. The second case is the Cole-Cole function which is shown in Figure 5.6 c) and d). Here only symmetric broadening of the relaxation process shape is allowed: $\alpha_{HN} = 1$, $\beta_{HN} \leq 1$. The Cole-Cole function is used to fit β-relaxations processes. A third case is the Debye-relaxation fulfilling: $\alpha_{HN} = 1, \beta_{HN} = 1$. Figure 5.6 illustrates both the imaginary dielectric function, and the real dielectric function. This is done to emphasize that from a DS experiment both the real and imaginary dielectric function is obtained. When fitting reliable results can be obtained if both real and imaginary dielectric parts of the dielectric spectrum are considered.

Now that the model functions are described, the data fit procedure is addressed. In Figure 5.5 the dielectric spectrum obtained from some DS measurement consist of a series of experimental data points. The model function is compared to the experimental data at each frequency according to equation **(14)**. The difference

between the model and the experimental data is then minimized using least square minimization according to

$$\sum_j w_j \left[\varepsilon_j^* - \left(\sum_k \varepsilon_{HN,k}^* - ia\frac{\sigma_0}{\varepsilon_0 {\omega_j}^s}\right)\right]^2 \rightarrow min\,. \qquad (14)$$

The minimization routine contains *k,* HN functions, one for each relaxation process fitted, and a contribution for conductivity where *a* is a factor with dimensionality (Hz^{-1}), σ_0 is the d.c conductivity of the sample, and the parameter ε_0 is the vacuum dielectric permittivity[23]. The factor *s* is set to 1 if polarization of the electrodes is absent. An assumption that is made in equation **(14)** is that the relaxation processes included in the model are additive, and not convoluted. This is generally a good approximation if the relaxation process peaks are sufficiently separated in frequency[23].

An alternative way of fitting the structural relaxation is to take the one sided Fourier transform of the KWW function, equation **(3)**, according to equation **(15)**.

$$\varepsilon^*(\omega) = \varepsilon_\infty + (\varepsilon_0 - \varepsilon_\infty)\int_0^\infty \exp(-i\omega t)\left[-\frac{d\phi(t)}{dt}\right]dt \qquad (15)$$

Fitting the relaxation time, τ_α, and the β_{KWW} parameter a fit of the structural relaxation time can be obtained[23]. The KWW model being asymmetrical does not fit the relaxation behavior of secondary processes. It is worth stressing that both the KWW relaxation model, and the HN relaxation model are empirical, and neither methods is able to fit the structural relaxation behavior of all glass formers. In the absence of a well-defined connection between the shape of the peak maximum of relaxation to that of the molecular structure of the viscous liquid the best one can do is using empirical models [23,29]. An important realization when using relaxation models is that a better fit does not always imply a better physical picture of the viscous liquid behavior[30].

Dielectric spectroscopy performed on multi-component systems can provide information of how structural dynamics of a liquid is affected by inclusion in a matrix[27]. The interpretation of dielectric experiment data is complicated due to the possibility of heterogeneity within the sample that can give rise to charge build-up and polarization as a result[23]. Polarization effects of this type generally occur at frequencies lower than that of dipolar polarization, also the dielectric strength of interfacial polarization exceeds that of dipolar polarization. Another complication is the physical interpretation of structural relaxation taking place within the sample. To be able to fully attribute relaxation processes to one of the substances within a multi-component mixture effective medium analysis needs to be applied.

Effective medium theory distinguishes between two cases[27]. The first is the symmetrical case one is when the two components both significantly contribute to

the dipole reorientational motion within the probed temperature and frequency range. The second case corresponds to one component that display liquid behavior while the other as acts as a matrix. In such a case the liquid dynamics much faster than the polymer matrix which in relation to the liquid dynamics is static. The matrix exert a confining effect upon the liquid by occupying space that is not available to the liquid[37].

Liquid behavior of propylene carbonate, PC, confined within a poly(methyl methacrylate), PMMA is an example of a system in which a liquid is confined within a PMMA matrix[27,37]. When PC is confined within PMMA polymer matrix a change of liquid PC behavior was observed[27]. Neat PMMA polymer display a much higher T_g compared to PC, $T_{g,PMMA}$≈107 °C and $T_{g,PC}$≈-110 °C. This means that at temperatures in the vicinity of PC T_g, the PMMA polymer matrix is static in relation to the dynamics of PC. Neat PC displayed a high α-relaxation dielectric strength compared to the corresponding dielectric spectrum of neat PMMA. Thus, the PC α-relaxation could be studied within the relevant temperature window as a function of concentration within the PMMA matrix. The α-relaxation of PC within the PMMA matrix network was observed to be slower than within neat PC liquid. The shape of the α-relaxation peak loss in imaginary dielectric function was observed to change for PC within the PMMA matrix. Specifically a broadening of the low frequency slope of the α-relaxation was observed. The Havriliak-Negami function, **(13)**, only describes asymmetric broadening on the high frequency side of the α-relaxation. To account for asymmetric broadening on either side of the α-relaxation a different model function was used to fit the experimental data in such a case, Equation **(16)**.

$$\varepsilon''(\omega) = \frac{\varepsilon_p''}{\frac{1-|a-b|}{a+b}\left[b\left(\omega/\omega_p\right)^{-a} + a(\omega/\omega_p)^b\right] + |a-b|} \qquad (16)$$

The α-relaxation peak position is determined by ω_p[27]. The parameters affecting the α-relaxation peak shape are a and b, which fulfill $0 < a, b \leq 1$. The shape parameter a and b of equation **(16)** describe power law behavior of the relaxation loss peak on either side of the peak frequency position, ω_p, with amplitude, ε_p''. The PC in PMMA matrix experiments could be transferred to the problem of studying pharmaceutical dynamics within polymer matrix systems. Here one may also study dynamics of pharmaceutical molecules when confined within amorphous solid dispersions. This can in turn provide valuable insights to how physical stability alters under polymer matrix confinement.

5.3 Crystallization kinetics

The super cooled liquid is metastable with respect to the crystalline state when it is kept below its melting temperature, T_m[8]. The rate of cooling the material through the metastable window needs to exceed the rate of forming crystalline material. The mechanism by which the metastable liquid orders into a crystalline structure is

called nucleation[38]. Nucleation is an event where a significant number of molecules in the liquid state self-assemble into a stable crystalline phase[8]. Nucleation is typically a co-operative motion of a number of molecules exceeding what is required for structural relaxation[8]. The rate of nucleation depends on the material studied and at what temperature within the metastable window the sample is held.

In most materials with few exceptions nucleation induce a transient process in which the entire liquid system eventually crystalizes. The timescale of crystallization, corresponding to the time required to convert half of the sample to crystalline material, is again highly dependent on material and the experimental temperature considered. Characterizing the kinetics of crystallization of a material can provide crucial information for glass manufacturing processes. In many applications no or minimal crystal nucleation can be tolerated.

5.3.1 Thermodynamics and kinetics of crystallization

Crystallization of a liquid substance is the result of two events occurring, nucleation of molecules within the sample forming crystalline particles, and growth of these particles within the material incorporating an increasing number of molecules[8,39]. Depending on the material and the thermal treatment used to study crystallization it may occur primarily in two separate steps, or more or less simultaneously making it difficult to separate a nucleation phase and a growth phase of the process[39].

In order to form a crystal phase within a liquid, energy is required to form a liquid-crystal interface[40]. The free energy gain of forming a crystal may not be enough to overcome the energy required to form a liquid-crystal interface. As an example, consider the formation of a spherical crystal nucleus within a liquid. The competition between energy cost of forming an interface and the gain in forming a crystal nucleus is in such a case given by

$$\Delta G(r) = \frac{4}{3}\pi r^3 \Delta G_b + 4\pi r^2 \gamma_{sl}, \tag{17}$$

here $\Delta G(r)$ is the free energy of forming a nucleus, ΔG_b is the energy difference between the liquid and crystal, and γ_{sl} is the interface energy between the liquid and solid[38,40]. The radius r, is the size of the crystal nucleus. There is a critical size of the nucleus at which the free energy of forming an interface is offset by the gain of forming a crystal given by

$$\Delta G(r^*) = \frac{16\pi {\gamma_{sl}}^3}{3{\Delta G_b}^2}. \tag{18}$$

A thermal fluctuation with sufficient energy to offset the energy of forming the interface leads to the growth of a stable crystal nucleus. Once the barrier of

nucleating a stable crystal is overcome, further growth of the crystal nucleus is energetically favorable[38,40].

The theory of nucleation of pure substances is usually referred to as Classical Nucleation Theory (CNT). CNT predicts a rate of nucleation, I, according to

$$I = A \exp\left[-\frac{16\pi\gamma_{sl}{}^3}{3\Delta G_b{}^2}\frac{1}{k_B T}\right], \tag{19}$$

where $\Delta G(r^*)$ corresponds to the thermodynamic barrier of nucleation and A is a pre-exponential factor[41]. CNT predicts a straight line between log (I) and $1/(T\ \Delta G_b^2)$.[41] The CNT has been tested by experimentally measuring the nucleation rates in glasses and liquids. In several cases the CNT fail to describe experimental results. It should be stressed that the description given here strictly applies to pure substances where no impurities are present and where the effect of surface exposure can be ignored[38]. In general liquids that contain impurities or is exposed to surfaces will display altered nucleation kinetics. Nucleation caused by an external factor such as impurities or exposure to surfaces is called heterogeneous nucleation, whereas nucleation of a pure substance is termed homogenous nucleation. Measurement of homogenous nucleation is difficult partly because of the experimental difficulty in avoiding impurities and surface effects of crystallizing liquids[42].

As equation **(17)** suggest, even though nucleation of a crystalline particle is thermodynamically favored it is not guaranteed that nucleation immediately occurs. The thermodynamic driving force for crystallization increases with lower temperature. However, as the temperature of the liquid approaches T_g a considerable increase in viscosity of several orders of magnitude occur. Thus, a kinetic element related to mass transport, is introduced where thermodynamically favorable nucleation of crystalline particles is prevented on an experimental timescale.

Crystallization kinetics at isothermal conditions is described by equation **(20)**[24,39].

$$X(t) = 1 - \exp\left[-\left(\frac{t-t_0}{\tau_{cryst}}\right)^n\right] \tag{20}$$

Where $X(t)$ is the crystalline content, τ_{cryst} is the characteristic timescale of crystallization, $t_0$is the induction time of crystallization, and n is an integer which provides information regarding the dimensions of growing crystalline nucleus[39]. A schematic view of the degree of crystallinity as a function of time is given in Figure 5.7. The crystalline content first increases rapidly and then the rate of forming new crystalline material decays until full crystallinity is reached.

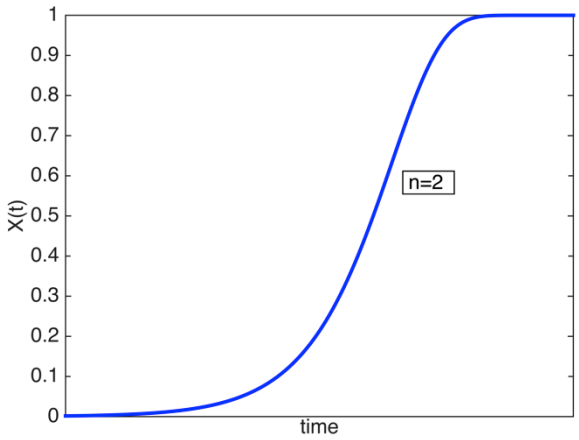

Figure 5.7. Degree of crystallinity shown as a function of time. The exponential factor in equation (19)is set to n=2.

A number of assumptions are made when using equation **(20)**. One assumes that the density of the liquid and the crystal is the same, that nucleus once formed does not move within the remaining melt, and that the direction of growth is linear with respect to the radial distance from the crystal nucleus center. Two methods used to determine the values of τ_{cryst} and n are considered in this thesis, the Avrami and Avramov methods presented in Section 5.3.2.

5.3.2 Experimental probe of crystallization kinetics

The crystal content as a function of time within a sample is measured during a crystallization kinetics experiment. Several techniques are able to do this, such as Dielectric Spectroscopy, X-ray diffraction, Second Harmonic Optical Imaging, and several other diffraction techniques[24,43,44]. In this work Dielectric Spectroscopy is the method for determining crystallization kinetics. An advantage of using DS is that the liquid content (α-relaxation) can be continuously monitored as a function of time[23]. Information on the crystalline content can be gathered on a timescale much smaller than the timescale of crystallization, $t_{exp} \ll \tau_{cryst}$ [43]. A disadvantage of using DS is exposure of the liquid to surfaces can mediate nucleation. DS experiment cannot distinguish between heterogeneous nucleation and homogenous nucleation.

As discussed in Section 5.2.2.2 concerning dielectric spectroscopy measurement interpretation. The α-relaxation has a certain dielectric strength, $\Delta\varepsilon$ [43]. The magnitude of dielectric strength within the sample is proportional to the number of fluctuating molecular dipoles present according to

$$\Delta\varepsilon \propto n\,\mu^2. \tag{21}$$

Each liquid molecule has a dipole moment, μ, with the ability to fluctuate with the electric field applied by the DS system that contribute to the signal strength. The

decrease of signal strength, $\Delta\varepsilon$, is related to crystallization occurring within the sample, as the motion of the molecules becomes arrested when included into the crystal lattice, see Figure 5.8.

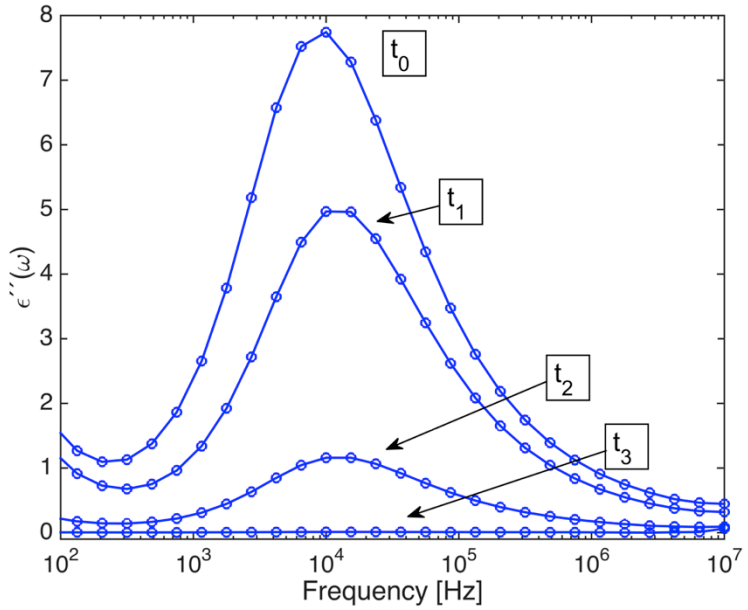

Figure 5.8. Imaginary dielectric spectrum of a crystallizing cilostazol at T=67 °C measured at four different times in the frequency range of the α-relaxation. Crystallization is observed as a decrease in dielectric signal strength of the α-relaxation over time where t_0 is the initial liquid state of the sample and t_3 is the final crystalline state.

Monitoring the structural relaxation as a function of time at a constant temperature such as in Figure 5.8 yields information of the transition from liquid at t_0, to crystal state at t_3. From the data obtained a suitable frequency in the frequency spectrum is picked. The dielectric signal recorded at this frequency as a function of time can be converted to a measure of the degree of crystallinity, $X(t)$, as a function of time according to

$$X(t) \propto \varepsilon'_N(t) = \frac{\varepsilon'(t_0) - \varepsilon'(t)}{\varepsilon'(t_0) - \varepsilon'(\infty)}. \qquad (22)$$

In equation **(22)** $\varepsilon'(t_0)$ is the dielectric function at the selected frequency at the induction time marking the onset of crystallization, $\varepsilon'(\infty)$ correspond to the limit in time when full crystallization of the sample has occurred. The normalized dielectric function follows an exponential decay according to equation **(19)**. Fitting of experimentally determined normalized dielectric function, $\varepsilon'_N(t)$, to the crystallization kinetics parameters offers a comparison between different temperatures and between materials.

The Avrami method consist of taking the double logarithm of the normalized permittivity, $\gamma(\varepsilon_N) = \ln(-\ln(1-\varepsilon_N))$, as a function of $\ln(t)$ and analyzing the

resulting approximately straight line[24,43]. The graphical interpretation is shown in Figure 5.9.

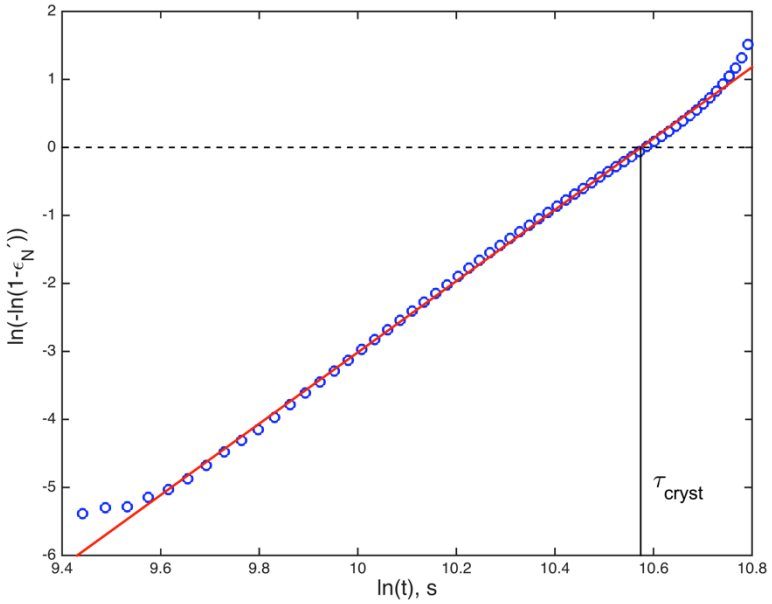

Figure 5.9. Determination of crystallization parameters with the Avrami method. The experimental data is obtained from a DS experiment of felodipine at T=92°C.

The intersection of the linear fit of data points with the x-axis provides an estimation of the timescale of crystallization, τ_{cryst}. The slope of the line corresponds to the estimated n value. A limitation of the Avrami method is that the timescale of crystallization obtained includes the induction time. This can be seen by inserting the normalized permittivity value that sets $\gamma(\varepsilon_N) = 0$.

$$\gamma(\varepsilon_N = 1 - e^{-1}) = \ln(-\ln(1 - \varepsilon_N)) = 0 \qquad (23)$$

By inserting $\varepsilon_N = 1 - e^{-1}$ into equation **(20)** one obtains $\tau_{cryst} = t - t_0$ [43]. The value of the induction time is not obtained directly through the Avrami approach.

It has been observed in several crystallization kinetics studies that the straight line interpretation is difficult due to substantial deviations from linearity, especially for molecular liquids[24,43]. The effect is seen in Figure 5.9 where a deviation from linearity, is observed in both the short and long time limits. The deviations are thought to originate in measurement errors being amplified by the double logarithmic operation on the normalized permittivity leading to an overexpression of these data points in the graph[24].

To circumvent the shortcomings of the Avrami method in determining the crystallization kinetics parameters a different approach was developed by Avramov[24,43]. In this approach the normalized permittivity and its derivative is analyzed as functions of the logarithmic time, see Figure 5.10.

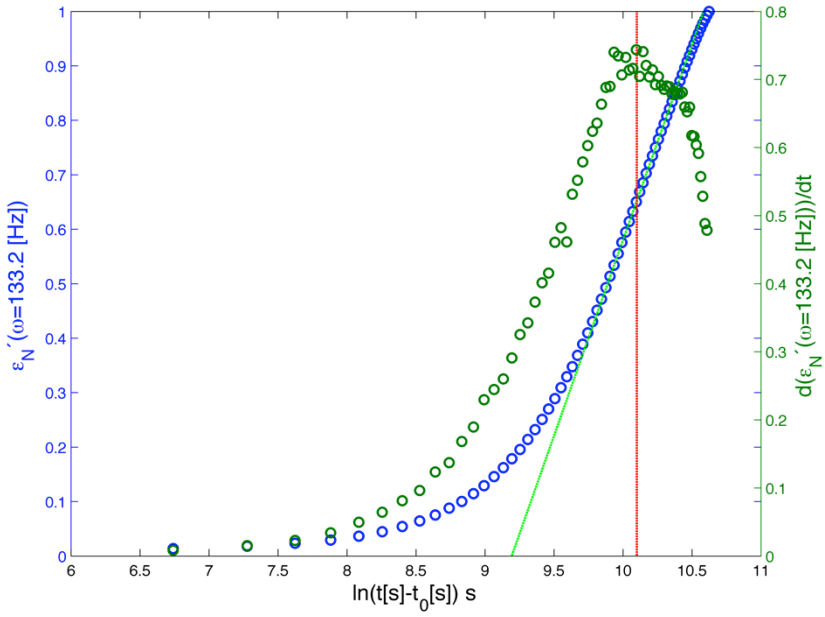

Figure 5.10. Avramov analysis plot of crystallization kinetics. The Normalized permittivity is analyzed as a function of logarithmic time, so is the derivative of the normalized permittivity signal. The highest slope value is identified.

The parameters of equation **(20)** are estimated from Figure 5.10. The peak in the derivative is used to estimate the timescale of crystallization. Also the tangent of the normalized permittivity, drawn at the corresponding point, is used to estimate the *n* parameter according to.

$$n = \frac{e}{\ln(t_1) - \ln(t_2)}. \qquad (24)$$

The Avramov method avoids the systematic errors of the Avrami method. The induction time can be estimated directly using the Avramov method. The induction time may also be estimated by identifying when the drop in dielectric signal strength commences. By neglecting the data points prior to the induction time both the Avrami and Avramov method may be applied[24]. The halftime of crystallization $t_{1/2}$ provide another way of determining the rate of crystallization, $k = {\tau_{cryst}}^{-1}$, according to

$$k = \left(\frac{\ln(2)^{1/n}}{t_{1/2}}\right)^n. \qquad (25)$$

The rate of crystallization *k* can be determined by extracting $t_{1/2}$ from experimentally determined $\varepsilon_N(t_{1/2}) = 0.5$, and by using Avramov or Avrami determined *n*.

5.4 Increased solubility of amorphous pharmaceuticals

Glasses display higher rates of dissolution compared to their crystalline counterparts[4,6,16]. This behavior is explained by comparing the free energy of dissolution of glasses and crystals. In order for any process to occur spontaneously there must be a negative free energy difference. The difference in free energy is given by

$$\Delta G(T) = \Delta H(T) - T\Delta S(T), \tag{26}$$

where $\Delta G(T)$ is the free energy change, and $\Delta H(T)$, and $\Delta S(T)$ is the enthalpy and entropy of change respectively. From Section 5.1.1 and from Figure 5.1 we know that there is a significant difference in enthalpy, and entropy between the glass and crystal state. These differences lead to higher free energy, a higher energy state, of glasses compared to crystals[6]. This in turn leads to a larger free energy change related to dissolution of the glass. This gives glasses the potential to dissolve more rapidly than crystals.

The dissolving glass can potentially give rise to concentrations in solution exceeding the saturated crystalline solubility, C_s. This effect is called supersaturation[2]. A challenge presented when trying to measure supersaturation is the tendency of the dissolved substance to crystallize. In addition to the state of the solid dissolving into a liquid there are several other factors that affect the concentration profile produced in solution. This topic will be treated in Section 5.5.5. Methods of measuring the concentration of dissolving pharmaceuticals in this thesis are treated in the following section.

5.4.1 UV spectrophotometric methods to measure solubility

Quantification of an API in solution is critical when evaluating enhanced dissolution performance of amorphous formulations. Several techniques and experimental set-ups have been developed for this purpose. In this thesis UV-spectrophotometry is mainly used to quantify API presence in solution. UV Spectrophotometry is a commonly used method of quantifying concentration of various compounds exhibiting light excitation when exposed to UV light wavelengths. Two experimental strategies of performing such measurements exists, one in which the experiment is performed in situ, and a second which requires sampling and analysis with a separate equipment[45].

The in-situ fiber optics method offers complete elimination of the sampling stage, since optical UV probes are inserted directly into the dissolution medium calibrated against a reference sample curve of known concentration prior to the measurement [45]. A much more frequent sampling of the dissolution process can be made. A disadvantage of this method is the lack of control of what the UV-probe measures. Excipient and additive material may interfere with the scattering related to the compound. Also, the absorbance of UV light is not tied to if the compound is

dissolved in solution or present as nanoparticles, or micron-sized particles within the solution. Even though correction of excipient and additive contributions may be compensated for, it is extremely difficult to de-convolute contributions arising from particle contributions of the compound in question. The detection of very low concentrations using in situ UV probes may be challenging due to low absorption and difficulty to distinguish the signal from the measured baseline[45]. Drugs with very low solubility may therefore not be present within solution to the extent that in situ UV-probes can detect it.

The second method is an external measurement method where samples are withdrawn from the dissolution vessel at predefined times[45,46]. The sample is either filtered or centrifuged, the filtered liquid or supernatant may then be diluted if there is a risk of particle precipitation of the dissolved compound. Using a suitable chromatography method the compound is separated and quantified using UV spectroscopy or if needed mass spectroscopy. An advantage of this technique is the high resolution obtainable and possibility of detecting very low concentrations. Another advantage is the filtering or centrifuge stage where potentially interfering compounds such as excipients, additives and particulate matter may be separated. Especially the presence of crystalline particles of an API present with a size exceeding the maximum relevant size may be removed. Disadvantages of this technique is the many experimental steps where sample material may be lost, experimental errors such as excessive adhesion to the filter, inexact dilution prior to measurement, and need of dispensable material required to transfer sample material.

5.5 Amorphous solid dispersions

To benefit from a potential solubility increase of an API glass an additive with ability to stabilize the amorphous state is required[20]. In this thesis the addition of a polymer to kinetically stabilize the amorphous state is considered. Systems of this type are called solid dispersions.

One of the first articles published within the field of solid dispersions by Chio and Riegelman in 1971 define solid dispersions as a “dispersion of one or more API in an inert carrier in the solid state, prepared by either melting, solvent or combined melting-solvent method”[7]. Depending on the state of the drug and the carrier a solid dispersion may also be characterized as eutectic mixture, solid solution or glass solution. As research has progressed several systems have been described as solid dispersions, ranging from the two-component mixture of an API with a polymer, to more complex material mixtures such as solidified drug-lipid mixtures, or ternary mixtures where surfactants or cyclodextrins are added to the drug-polymer mixtures. In general the aim of using additives is to enhance stability or dissolution behavior further. In this report a solid dispersion will be referred to as a two-component system of a drug and a polymer unless stated otherwise.

Six types of solid dispersions can be distinguished. The state of the pharmaceutical within the solid dispersion is either: i) present within the polymer dispersion primarily as crystal particles, ii) primarily as amorphous particles, iii) or molecularly dispersed within the polymer carrier. In addition the polymer within the dispersion may either be amorphous, or crystalline. In this thesis fully amorphous polymers are used, thus three cases of solid dispersions can be expected. These are illustrated in Figure 5.11.

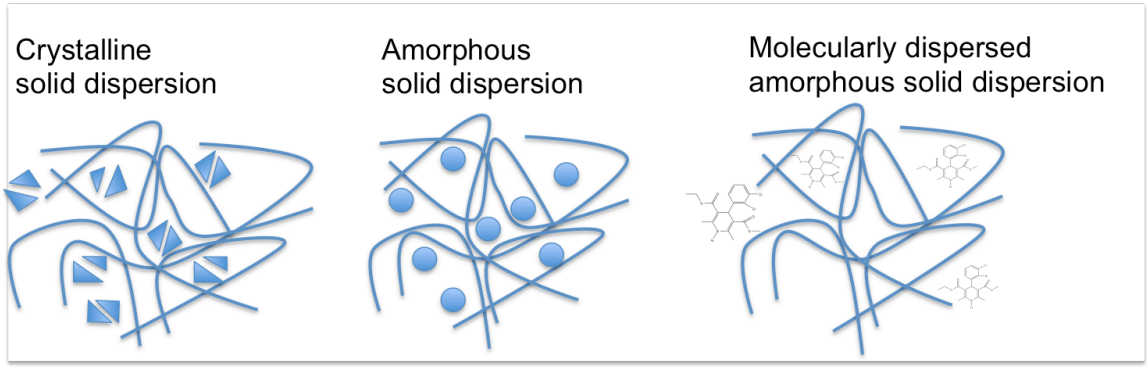

Figure 5.11. Illustrations of three types of solid dispersions considered in this thesis. The API is incorporated into the polymer matrix in crystalline or amorphous particles. A third possibility is molecularly dispersed API in close proximity of the polymer chains.

Stabilization of the amorphous pharmaceutical in an amorphous solid dispersion occurs through creating a physical barrier to the surroundings, through an increase in viscosity reducing diffusive motion of the API within the polymer matrix, and through intermolecular interactions between the API and the polymer[18]. The increased viscosity restricts the movement of the pharmaceutical molecules within the polymer network, compared to the neat pharmaceutical system, lowering diffusive motion that may give rise to nucleated crystals[2]. Chemical interactions such as hydrogen-bond formation between the API and polymer put a further restriction on the molecular rearrangement and have the potential to disrupt interactions between API molecules.

5.5.1 Multi-component mixing

The inclusion of an API within the polymer matrix depends on the free energy of mixing between the two materials. Mixing of two liquids can result in a one-phase mixture, or a two-phase mixture as a result of immediate or delayed phase separation. When preparing amorphous solid dispersions an understanding of the miscibility between the API and polymer is crucial. The theory presented in this section provides a framework for understanding and making simple models of phase behavior of multi-component mixtures. To achieve miscibility, meaning a stable mixed state of two substances, the free energy of mixing of the system needs to be negative[47]. The free energy of mixing, ΔG_{mix}, of a multi-component system, is given by [2,39,47]

$$\Delta G_{mix} = \Delta H_{mix} - T\,\Delta S_{mix}. \tag{27}$$

The simplest case of mixing a multi-component system is an ideal solution. In an ideal solution the molecular interaction between two components, ϵ_{AB} is as large as the interactions between the molecules of the same kind, $\epsilon_{AB} = \epsilon_{AA} = \epsilon_{BB}$ [38]. The enthalpy of mixing in an ideal solution is zero. The energy of mixing in such a system is purely related to entropy gain of mixing. Using statistical mechanics and by making a mean field assumption one obtains

$$\Delta S_{mix} = -k_B(n_1 + n_2)(x_1 \ln(x_1) + x_2 \ln(x_2)). \tag{28}$$

The ideal solution model is obviously not suitable to describe a system such as a pharmaceutical substance within a polymer matrix. To describe a more realistic solution, enthalpic contributions are needed. Such a model, the regular solution model would allow two compounds to be miscible at some high temperature, and but exhibit a phase separation at some lower temperature. The regular solution model is given by

$$\Delta G_{mix} = k_B T(n_1 + n_2)(x_1 \ln(x_1) + x_2 \ln(x_2) + \chi x_1 x_2). \tag{29}$$

The main difference is the addition of an enthalpy term where an important contribution is the so-called interaction parameter, χ. A phase diagram is shown in Figure 5.12. In the phase diagram the free energy of mixing is computed using equation **(29)** for varying compositions at several temperatures, where the temperature dependence was attributed to the interaction parameter, χ. The free energy of mixing is shown for several fictive temperature of the system. For a high temperature the phase diagram exhibit only one minimum, see T_2 of Figure 5.12 a.). The two-component system displays miscibility in all concentrations. As the temperature is lowered multiple minima appear, see T_1 of Figure 5.12 b.). The two-component system at T_1 will be unstable for some concentrations.

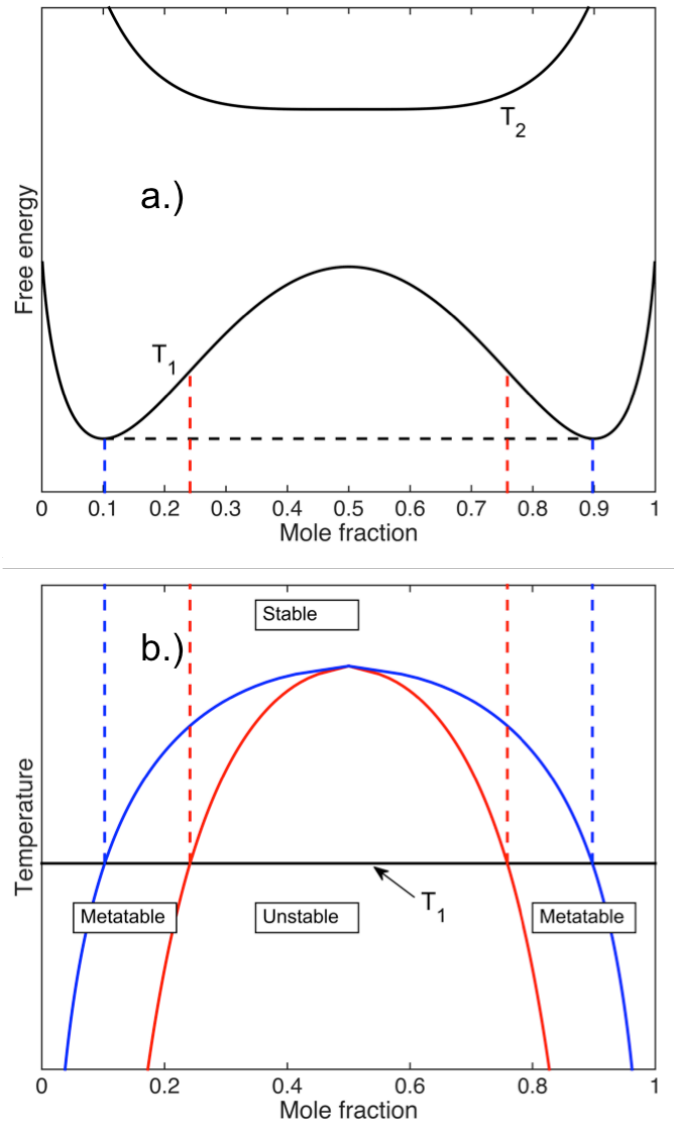

Figure 5.12. Top figure: Free energy diagram as a function of mole fraction at temperature T1. Bottom figure: Temperature dependence of the binodal and spinodal locus curves as a function of mole fraction. Adapted with modifications from[39].

The compositions at T_1 that are not stable are those that are within the tangent drawn between the two minima. The blue solid curve of Figure 5.12 is called the phase envelope. In polymer science the blue curve is also referred to as the cloud point curve[39,47]. It is obtained by collecting the tangent drawn for each temperature where multiple minimums exist. Within the phase envelope an important distinction between unstable compositions is made, metastable compositions and unstable compositions. The inflection point of the free energy curve in of Figure 5.12 a.) is used to separate metastable and unstable compositions. The inflection point shown as a function of temperature in Figure 5.12 b.) is called the spinodal curve. The spinodal curve separates unstable compositions in terms of what mechanism of phase separation occurs.

The regular solution model provide a simplified description of a two-component system[47]. Despite its simplicity it is able to describe on a conceptual level stability of the two-component mixture and mechanisms of phase separation that takes place within a liquid-liquid solution[47].

Phase separation occurs through one of following mechanisms, nucleation or spinodal decomposition[38]. The mechanism of phase separation depend on if the second derivative of the free energy is negative or positive. In a case where it is positive the composition is metastable and phase separation occur through nucleation. Nucleation has already been described in terms of crystallization. Similar to nucleation of crystals within a liquid there is an energy penalty of forming an interface between the new phase and the old phase. If however the system is exposed to a sufficient energy input, provided through for instance thermal fluctuations, a critical size nucleus will form. Contrary to nucleation, spinodal decomposition is not a thermally activated process. Instead, phase separation of an unstable mixture will occur through continuous change of composition.

So far in the description of two-component systems has been limited to describing systems where miscibility between the components only require a sufficiently high temperature, a critical upper temperature denoted T_U. However several polymer solvent mixtures exhibits phase diagrams in which there also exists another critical lower temperature, T_L[39,47,48]. Between T_L and T_U the system is fully miscible, but as the temperature is raised above T_L phase separation occurs[4,47]. Consequently there are two cloud point curves limiting miscibility region of the phase diagram of such a polymer-solvent system. A polymer known to exhibit a clouding compositions in solvents is HPMC[48].

The presence of an upper cloud point temperature has consequences for the dissolution of HPMC[49]. As the polymer matrix is hydrated during dissolution the compositions of the phase diagram between HPMC and the solvent is successively sampled. Phase separation of the polymer with the solvent will occur if clouding composition is reached at the temperature of the dissolution experiment.

5.5.2 Characterization of solid dispersions

DSC measurements of solid dispersions are routinely carried out to characterize the T_g of the system and to detect crystallization and melting of crystalline phases[50]. To predict the glass transition temperature of solid dispersions has been a long-term goal within the research field solid dispersions. A relation often used to estimate the glass transition of a two-component mixture is the Gordon Taylor equation given by

$$T_{g,mix} = \frac{[(w_1 T_{g,1}) + (K w_2 T_{g,2})]}{[w_1 + K w_2]}. \qquad (30)$$

The predicted glass transition of the system is computed using the weight fraction of each component w_i, and each components glass transition temperature $T_{g,i}$[50]. The

constant K is the ratio between the product of density, ρ_i, and the thermal expansitivity $\Delta\alpha_i$ of each component according to

$$K = \frac{\rho_1 \Delta\alpha_1}{\rho_2 \Delta\alpha_2}. \quad (31)$$

Alternatively the constant K is given by instead comparing the difference in heat capacity, or by simply relating the parameter K to the glass transition temperature of each of the single components

$$K = \frac{\rho_1 \Delta C_1}{\rho_2 \Delta C_2}, \qquad K = \frac{\rho_1 T_{g,1}}{\rho_2 T_{g,2}}. \quad (32)$$

The assumptions made when using the Gordon Taylor equation are that the components are fully miscible over the entire composition regime, and that there is ideal volume additive between the components in question[50]. These assumptions restrict the GT equation from being applied to mixtures that undergo phase separation at any point of the phase diagram.

The ability of equation **(30)** to successfully predict solid dispersion T_g is limited[50,51]. Extensions of the GT equation incorporating theory related to polymer solution theory has ben attempted[52]. To date there exists no totally predictive relation that is successfully able to predict the T_g of solid dispersions[50,52]. Apart from modeling the binary component system, there are experimental factors that complicate T_g determination in solid dispersions. Moisture, for instance, will plasticize the solid dispersion and depress T_g[26,50]. Additionally the DSC methods used to perform studies on T_g have different aims. Some studies are less interested in examining the state of the formulation after preparation. The sample may be cycled above its T_g in situ of the DSC equipment to determine T_g[51]. Other studies focus the attention to what T_g the preparation method of making amorphous solid dispersion gives rise to[22]. Studies also exist where the goal is to only study plasticized polymer T_g[53]. Consequently the large variations in ways of determining solid dispersion T_g makes comparison between studies difficult[51,53,54].

It has been proposed that a single T_g is descriptive of a homogenous solid dispersion[22]. Existence of multiple T_gs is attributed to heterogeneous structure, which may increase the risk of crystal nucleation due to API enriched domains. However the presence of one T_g may not necessarily mean that the solid dispersion is homogenous in structure. It has been shown using alternative methods to DSC such as Confocal Raman spectroscopy that materials that exhibit a single T_g may still display a high degree of heterogeneity.

Raman spectroscopy is a frequently used method of analyzing pharmaceutical systems[55,56]. Both chemical information such as composition, and the physical state of pharmaceuticals can be investigated using Raman spectroscopy[22]. Raman spectroscopy is non-invasive and does not significantly alter the state of the sample

provided that the laser intensity is adjusted to what system is investigated. Raman measurements in the wavenumber region of 10-400cm^{-1} is able to detect crystalline presence within the sample and has been utilized to detect crystalline API within solid dispersions[55]. Water does not give rise to intense Raman scattering, contrary to IR spectroscopy where the water content to a large extent will affect the quality of the spectrum. Raman spectroscopy measurements can even be performed on objects immersed in water[55]. This has been utilized to study dissolution mechanisms of felodipine amorphous solid dispersions. In addition of studying mechanisms of release, Raman spectroscopy has emerged as a tool for process analytical control. For instance in hot melt extrusion processes Raman spectroscopy has been utilized for in-line quality control[7].

5.5.3 Hot Melt Extrusion

Hot Melt Extrusion is a processing technique developed in plastics industry and with a history tracing back to 1930s[12]. Application of hot melt extrusion as a pharmaceutical processing technique has been an active area of research during the last two decades. Contrary to the traditional use of hot melt extrusion, the pharmaceutical hot melt extruder has a material feed that consists of pharmaceuticals mixed with polymers.

In hot melt extrusion the feed material is physically mixed within a barrel containing rotating screws[12]. The hot melt extruder also contains thermal elements that heat the barrel surrounding the screws. When the extruded material comes into contact with the surfaces within the hot melt extrusion barrel, it softens or melts. This facilitates mixing and processing of the material further. The result is solid dispersion where a high degree of mixing between the polymer and pharmaceutical is achieved. Additionally, the thermal heating provided in the process in constitutes a method of making amorphous solid dispersions. A schematic illustration of a hot melt extruder is shown in Figure 5.13.

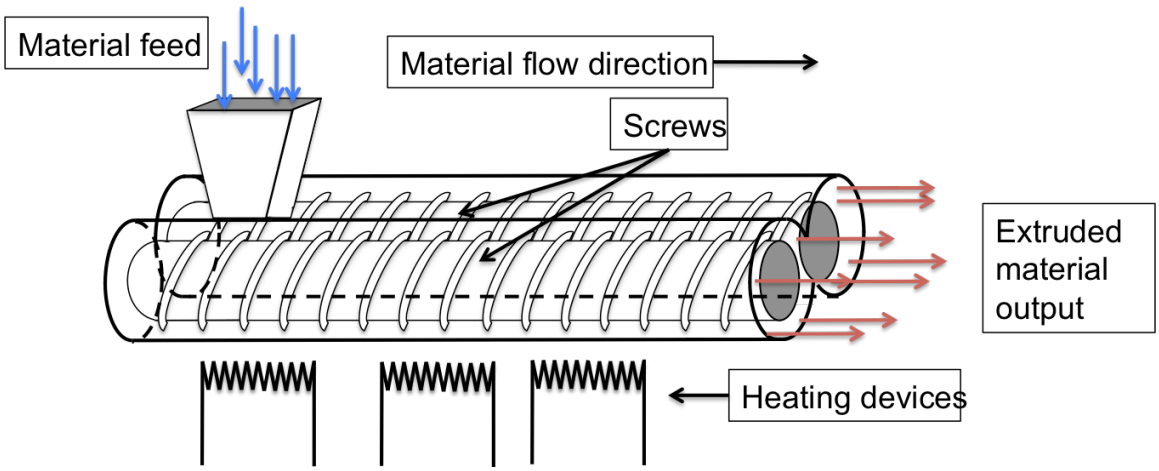

Figure 5.13. Schematic illustration of a hot melt extruder. The material is fed into the entrance of the extruder barrel. The material flows in the direction of the rotating screws. As the material flows through the barrel it is heated and softens or melts, increasing its plasticity.

As Figure 5.13 shows, the hot melt extrusion technique exposes the processed material to a combination of heat and shear force. Heat is applied to the extruded material through heat conduction that takes place when the extruded material is exposed to the barrel surface. One, or several, screws exert a shear force on the flowing material.

Hot melt extrusion has become a competitive processing technique for pharmaceuticals with respect to other techniques[7,12,18,57]. An advantage with hot melt extrusion is the possible reduction of processing steps, made possible since the material can be shaped to tablets immediately after exit. Thus compression and milling to achieve homogeneity of the material may not be required. In addition to immediate shaping of tablets, additional treatment of the tablets such as taste masking films may be added. Perhaps the primary advantage of hot melt extrusion is a solvent free method. Here mixing of the API with the polymer carrier is achieved without the use of volatile solvents, which is an environmentally an advantage. When preparing amorphous state formulations the possibility of residual solvents may compromise stability due to plasticizing effects. Hot melt extrusion also offers a convenient way of preparing amorphous state of the API. Within the hot melt extruder there is a melting of the API where amorphous state stabilization of the API within the polymeric carrier is possible. Consequently, hot melt extrusion has emerged as a promising processing technique compared to spray drying formulation technique and fluid bed coating which require solvents and several processing steps during the manufacturing process.

Limitations of hot melt extrusion technique is found in cases of APIs that may not withstand the heat treatment[18]. In such a case solvent-methods could provide a better method of incorporating the API within the matrix. In addition the polymer additives used need to display sufficient thermal stability[12]. The polymer additives should in general exhibit a suitable thermoplasticity, a property that relates to how easily a material deforms when exposed to heat[12,18].

5.5.4 Carriers polymer materials for solid dispersions

A wide range of polymers has been considered in amorphous solid dispersion and in hot melt extrusion research. Primarily three classes of polymer materials are identified as useful in controlled release formulations: Polyvinylactam polymers, polyethylene glycol, and cellulose derivatives[12]. All three classes of materials exhibit certain strengths and weaknesses. PEO, for instance, displays very good processability being thermoplastic, crush resistant, and with high swelling capacity[12]. In order to achieve sufficient performance plasticization with low molecular weight PEO, or using various additives, may be required. Polyvinyl lactam based polymers are synthetically prepared. This enables tailoring of solubility and processability needs. Most notable is the Soluplus polymer by BASF, that has been specifically manufactured for hot melt extrusion of amorphous solid dispersions shown to exhibit exceptional performance in raising solubility[12,58]. Cellulose derivatives are, naturally derived and functionalized to give desired amorphous solid dispersion matrix properties. In this thesis cellulose based products are considered as polymer matrix to make amorphous solid dispersions.

Cellulose is a crystalline material that is insoluble in water[59]. Upon chemical modification of cellulose, attaching hydrophobic substituent groups on the polymer backbone, the crystalline structure breaks down resulting in an amorphous material[59]. The properties of cellulose derivatives enable them to be considered in several pharmaceutical formulations. Since the 1980s the cellulose derivative hydroxyl propyl methylcellulose (HPMC) has been a key ingredient in successful pharmaceutical formulations[14]. HPMC is characterized by being non-toxic, easy to handle, cheap in relation to alternative materials, and a high drug dosage capacity[59]. Perhaps the most important property is the ability to swell upon solvent exposure which gives rise to a gel which act as a barrier between the exterior, bulk solvent, and interior of the dry tablet[59,60]. The gelling behavior of HPMC provides a way to control the rate at which the drug is released into the bulk solvent, achieving a controlled release profile. Another attractive property is the versatility in terms of manufacturing method for pharmaceutical formulations, including tablet compaction, solvent casting, and extrusion[12,14,59]. Even in non-oral formulation strategies it may be used as excipient material[3]. By further functionalization, i.e. adding different chemical groups, several useful cellulose derivatives have been invented[12]. The large diversity of hydrophilic matrices on the market generates large variability in properties[12,60]. Comparisons between manufacturers give rise to high variation. Even batch-to-batch variability exist between HPMC products which have been shown to result in large variations in both phase behavior, cloud point composition, and solubility properties of HPMC[59].

The variability of cellulose derivatives arises from lack of controlling the process of adding substituents to the polymer backbone[59]. Upon excessive substitution the polymer will be too hydrophobic to dissolve in aqueous systems[61]. Also the pattern of substituted groups achieved along the polymer backbone, substituent heterogeneity affects the polymer properties. Heterogeneously substituted

polymers display amphiphilic behavior, where regions that are highly substituted are hydrophobic, and regions of low substitution are hydrophilic. In aqueous solution this has the consequence of highly substituted regions of the polymer interacting with other hydrophobic polymer regions, or with drugs displaying low solubility. Heterogeneous substitution also gives rise to less robust tablet formulations displaying larger variations in release behavior[61]. If a drug with low solubility is incorporated into an HPMC matrix with heterogeneous substituent pattern, experiments has shown that the cloud point decreases further[62].

Some shortcomings of using HPMC in extrusion have been identified, e.g. lack of thermoplastic behavior and insufficient bioavailability enhancement in some cases[12]. New methods of substitution, to increase functionality and thereby performance has been investigated. In these methods other functional groups are attached to the cellulose polymer backbone. On the one hand this leads to improved dissolution behavior and potential to further increase bioavailability of the drug compounds. On the other hand, higher chemical complexity leads to lower thermal stability during extrusion. It is in general difficult to enhance both release performance and thermoplasticity. What is most common is trying to find a balance between extrusion and dissolution performance. In this respect HPMC AS shows a promising trade-off between thermoplasticity and dissolution making it a highly useful polymer in extrusion applications[12,63]. HPMC AS is a cellulose derivative that has been further chemically modified attaching acetyl and succinoyl functional groups onto the glucose backbone units. In addition HPMC AS has shown to be an effective crystallization inhibitor during storage.

5.5.5 Release mechanisms of dispersions

To describe dissolution of an amorphous solid we first consult a general case of dissolving a solid into a liquid, which involves two stages[4].

1. The first stage involves the phase change of molecules within the solid that migrate into solution. The molecules of the dissolving solid will saturate the solution in direct contact with the dissolving solid. The saturated concentration at the liquid-solid interface will equal C_S.
2. After entering the solution, transport into the bulk solvent of concentration C_{bulk} will occur. The transport of dissolved molecules into the bulk solution occurs by a combination of diffusion and convection. In close vicinity of the solid-liquid interface a so-called boundary layer where flow of liquid is slow, diffusion dominates the transport of dissolving species. Towards the edge of the boundary layer convective mass transport of the bulk liquid transport the molecules into the bulk solution.

Since solid-liquid dissolution contains more than one step, one of them will be rate limiting[4]. The first step, establishment of a solid-liquid interface occur almost immediately upon contact. The rate-determining step of solid-liquid dissolution is

therefore determined by the second step, i.e. by diffusion of molecules out of the static boundary layer. An illustration of a dissolving particle is shown in Figure 5.14.

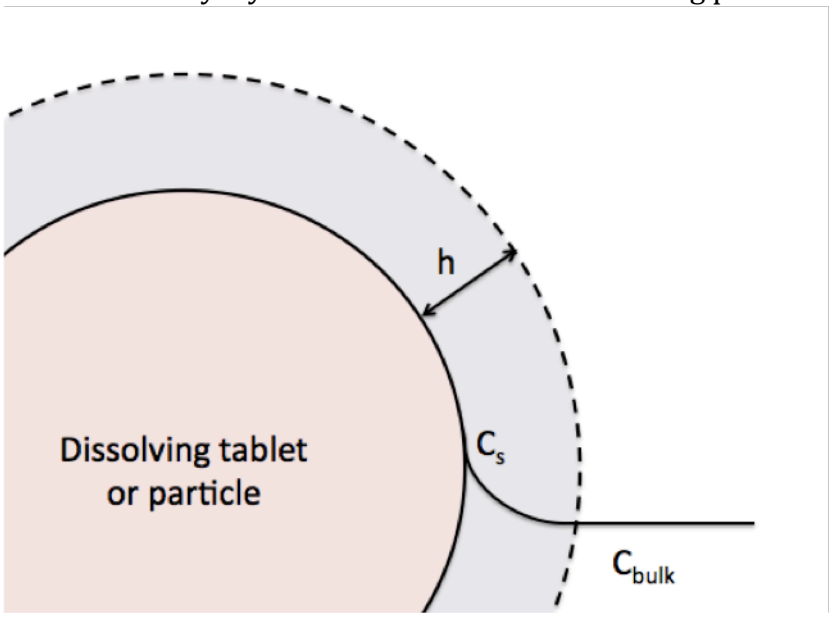

Figure 5.14. Illustration of a dissolving drug or dispersion particle within a liquid solution. Upon contact with the solvent a boundary layer with thickness, h, is established. The concentration at the immediate vicinity of the dissolving particle surface is the saturated solubility, C_s. The bulk concentration C_{bulk} is generally lower during dissolution due to the mass transport mechanisms diffusion and convective flow of the compound in the solvent bulk liquid.

Diffusion from a dissolving solid shown in Figure 5.14 follows Fick's law. Fick's law states that the rate of concentration change is proportional to the concentration gradient between the solid-liquid interface and the bulk solvent concentration. This relation, which is also referred to as the Noyes-Whitney equation is given by Equation **(33)**[2,4].

$$\frac{d\,C}{dt} = \frac{A \cdot D\,(C_s - C)}{h} \qquad (33)$$

The term $\frac{dC}{dt}$ describes the dissolution rate, $C_s - C$ is the concentration gradient, A is the exposed surface area, D is the diffusion coefficient, and h is the thickness of the boundary layer. From equation **(33)** it is clear that several factors affect the dissolution process. In Table 1 we can identify how the parameters of the Whitney Noyes equation, **(33)**, are influenced by different factors[4].

Table 1. Parameters of the Whitney-Noyes equation and factors that dissolution of a solid in liquid. Adopted with modifications from reference[4].

	Factors	Explanation
A	Size of particles	Smaller size of particles enables faster dissolution.
	Porosity of particles	Porosity of the individual particles increases surface exposure.

C_S	Temperature	Temperature strongly affects solubility and thereby saturated concentration value.
	Solid-liquid interactions	Compatibility between chemistry of solutes and solvent molecules.
	Solid state	Solid-state modifications affect the upper limit possible in terms of solution concentration.

C_{bulk}	Volume of solution	The volume available for dissolution varies during the Gastrointestinal transit.
	Accumulation over time	The time available for dissolving dictates to what extent the driving force, $C_s - C$, decreases.
	Removal of dissolved species	Various processes that remove the dissolved substance maintain the driving force for dissolution.

D/h	Thickness of boundary layer	The thickness of boundary layer is affected by the agitation that is present within the environment that the solid is dissolving in.
	Diffusion coefficient	The diffusive properties of the material depend on molecular size.

The Whitney-Noyes equation has some limitations to model solid-liquid dissolution applicable to a realistic gastrointestinal environment[2,4]. But it is a useful tool in explaining how different factors affect the dissolution process. As already mentioned in Section 5.4, solid-state modification rendering the dissolving material amorphous leads to increased solubility. However this is not the only limiting factor of the dissolution process. The volume of fluid in the gastrointestinal tract affects the concentration C, and thereby the rate at which dissolution can occur. The absorption of the dissolved drug in the intestine will act to continuously remove drug molecules from the solution. Hydrodynamic conditions within the intestines affect the boundary layer of the dissolving solid. The chemical composition of the gastrointestinal fluid, which is strongly affected by the food intake of the patient, will affect the diffusion coefficient and the chemical environment of the drug. The time spent within the gastrointestinal tract is limited; as a consequence the dissolution rate achieved under the circumstances must exceed the rate at which the tablet transit through the system.

The fundamental dissolution description given above is valid also for amorphous solid dispersions. The main difference however between an amorphous API particle dissolving, and an amorphous solid dispersion, is the presence of the polymer. As already pointed out, the polymers used for amorphous solid dispersions are swellable and hydrophilic. This affects the interface between the solid and the liquid. The boundary layer produced, rather than being a stagnant liquid layer is now composed of a hydrated, and as a consequence swollen, polymer network.

At some point during dissolution of an amorphous solid dispersion, the convective mass transport of the bulk solution is sufficiently large to dissociate the polymers from the gel network of the tablet surface. When amorphous solid dispersions molecules dissolve into an aqueous system various scenarios can occur. An illustration of how the API particles and polymer molecules are released into the gastrointestinal fluid from the amorphous solid dispersion is shown in Figure 5.15. In essence, it is the molecularly dissolved API, or nanometer scale particles that are able to penetrate into the epithelium cell layer, and enter the body achieving therapeutic effect[4].

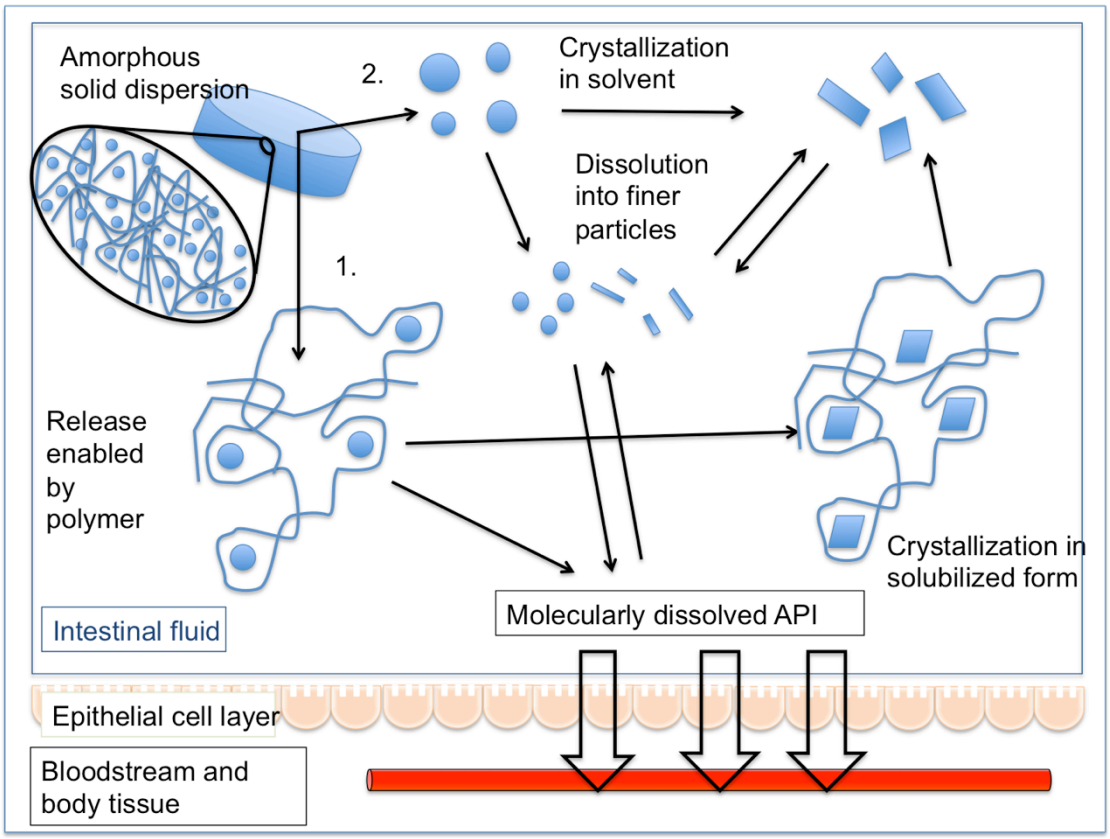

Figure 5.15. Illustration showing possible release mechanisms of API into solution from an amorphous solid dispersion. Amorphous drug particles release is coupled to the dissolution and disintegration of the polymer matrix, or the release rate is independent from the matrix. Dissolution of amorphous API particles eventually result in molecularly dissolved API, whereupon transfer into and through the epithelial cell layer is possible. Alternatively crystallization of the API may occur during dissolution.

The release of drug from the dispersion is primarily dictated by one of the following dissolution processes. The first mechanism of release is dictated by the polymer release into the solvent, see 1 in Figure 5.15. The swelling, dissolution, and erosion of the polymer carrier material determine at what rate the drug enters the solution. The drug being confined in the polymer matrix is hindered from moving into the solution even as the swelling polymer layer is hydrated, due to geometrical, intermolecular bonding, and/or viscosity constraints. The hydrated polymer layer effectively acts as a diffusion barrier of the drug into the solution. The second

mechanism of drug release is controlled by the diffusion of the drug itself, see 2 in Figure 5.15. Here the diffusion of the drug molecules within the hydrated matrix is decoupled from the polymer release into the solution.

By employing multiple analysis techniques able to quantify both API and polymer release the mechanisms of dissolution of a formulation can be elucidated. An example of a technique suitable for measuring both API and polymer release of solid dosage forms is UV spectroscopy combined with Size Exclusion Chromatography (SEC)[48,61]. UV spectroscopy method, as mentioned is able to determine API release, and SEC provides the polymer concentration in solvent.

6 Materials

6.1 Ibuprofen

Ibuprofen from Sigma Aldrich and Zhengzhou Chemicals Ltd. was one of the model drugs considered in this work. It was included due to its relatively simple molecular structure and extensive availability of literature references. This was exploited to model it as a compound with low solubility at low pH. It is a non-steroidal anti-inflammatory drug discovered in the 1960s[64]. It has since then become a widely used pharmaceutical substance. Ibuprofen chemical structure contains a carboxylic acid and an aromatic carbon ring as can be seen in Figure 6.1.

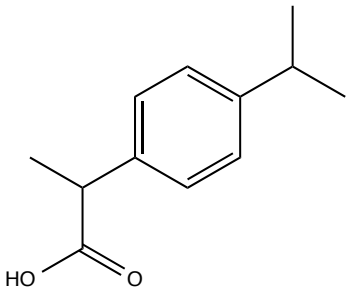

Figure 6.1. The chemical structure of ibuprofen.

Being an acid it has drastically lower solubility in acidic environment[65]. The pKa of ibuprofen has been determined to 4.4. Above the pKa ibuprofen dissolves readily in aqueous solutions. At a pH below the pKa the solubility decreases drastically. In the pH regime 1.2-3.85 the solubility lies between 0.053-0.062 mg mL^{-1}. In this report to ensure that ibuprofen displays low solubility the pH is kept at pH=1 to model an API with low solubility.

Table 2. Chemical data of ibuprofen taken from Shaw et al. the stated solubility value is for pH=1. In this pH regime the ibuprofen molecule is protonated and thus displays low solubility[65].

Chemical formula	$C_{13}H_{18}O_2$
CAS number	15687-27-1
Molecular weight [g/mol]	206.28
T_m [°C]	77
T_m [K]	248
Density [g/cm^3]	1.17
Solubility (pH=1) [mg/mL]	0.058

Ibuprofen and its solid state properties have been extensively studied[24,25,66]. Differential Scanning Calorimetry measurements of ibuprofen can be found in

numerous literature references. The T_g of ibuprofen determined by DSC lies at T=228K[67]. Dudognong et al. determined the most favorable nucleation regime of ibuprofen to be between 233-263K[67]. Johari et al have performed dielectric spectroscopy experiments on ibuprofen.[66], Brás et al.[25] and Adrjanowicz et al.[32], the main results of these studies are in close agreement with each other. Ibuprofen has a DS measured T_g at 225K, the VFT fit parameters D and T_0 are 4.2 and 181K respectively. The fragility of ibuprofen is determined to be m=87.

6.2 Felodipine

Felodipine, supplied by Astra Zeneca was the second model drug considered in this thesis. It is a calcium channel blocker with antihypertensive properties[68]. The chemical structure of felodipine is shown in Figure 6.2. As can be seen by the chemical structure, felodipine can hydrogen bond through its N-H group.

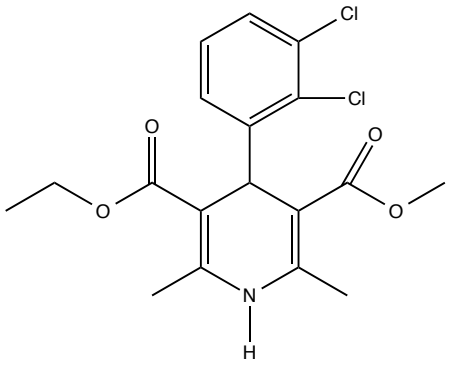

Figure 6.2. The chemical structure of felodipine.

Some chemical and physical properties of felodipine are presented in Table 3. The solubility values found in literature was only reported at T=37 °C and in phosphate buffer medium. A pKa value of felodipine could not be found in literature.

Table 3. Chemical data of felodipine. The data is taken from[10,46,51,54]

Chemical formula	$C_{18}H_{19}NO_4$
CAS number	72509-75-3
Molecular weight [g/mol]	384.25
T_m [°C] [69]	142
Density [g/cm^3] [51]	1.33
Aq. solubility [µg/mL] [46]	0.81

Felodipine display low solubility in water, 0.81 µg mL^{-1} [46]. In simulated gastrointestinal fluid, pH=6.8, the equilibrium solubility was determined to be 0.94±0.08 µg mL^{-1} [10]. Due to its low solubility felodipine has been a model drug compound in several solubility enhancement formulation studies[20,51,55,69-72]. Successful formulation methods in terms of raising the apparent aqueous solubility

has been liquid nanosuspensions[17,46,73], micelle suspensions[74] and nano-suspensions. Several of these formulation techniques have shown to enhance the solubility of felodipine by an order of magnitude. Felodipine has also been used as a model drug in solid dispersions in several studies[20,51,55,69-72].

6.3 Cilostazol

Cilostazol is the third API considered in this thesis. The manufacturer was Botai Chemicals. Cilostazol is a drug used to treat patients ischemic symptoms associated with peripheral arterial occlusive diseases[75]. The chemical structure of cilostazol differs from that of ibuprofen by being larger in size and containing nitrogen. Compared to felodipine it has a more rod like shape. Cilostazol can also hydrogen bond with a N-H group in its structure.

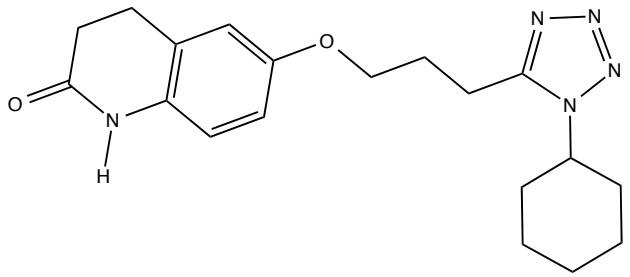

Figure 6.3. Chemical structure of cilostazol.

Some chemical and physical properties are presented in Table 4. Cilostazol displays three crystalline polymorphs, which distinguishes it from the other model drugs, considered.

Table 4. Chemical and physical properties of cilostazol. Data is taken from [75-77].

Chemical formula	$C_{20}H_{27}N_5O_2$
CAS number	73963-72-1
Molecular weight [g/mol]	369.46
T_m [°C] (Polymorph A)	159.0±0.5°C
T_m [K] (Polymorph A)	432±0.5°C
T_m [°C] (Polymorph B)	135.8±0.5°C
T_m [K] (Polymorph B)	408.8±0.2
T_m [°C] (Polymorph C)	146.8±0.5°C
T_m [K] (Polymorph C)	419.0±0.5
Aqueous solubility (w/v %)	
pH=7, T=25°C	3.12 x 10-4
Density [g/cm^3]	1.256

Stowell et al. investigated cilostazol using DSC[76]. They were able to obtain three unique melting endotherms by various thermal treatments of cilostazol. The melting temperatures of each of the endotherms are presented in Table 4. In the investigation no value of T_g was reported. In another study cilostazol solid dispersions with various polymer carriers were studied in terms of physical properties using DSC[75]. T_g determination of neat cilostazol could not be found in literature. However solvent casted cilostazol Kollidon VA64 dispersions resulted in DSC thermograms without a cilostazol melting peak. Release performance of various cilostazol dispersions in deionized water at T=37 °C did not show significant release enhancement relative to crystalline cilostazol. In vitro release methods containing surfactants (3 % SLS, Sodium Lauryl Sulfate) where cilostazol was dissolved under sink conditions resulted in enhanced release performance of several of the solid dispersions. Solubility of cilostazol was observed to show minor variations with pH within the range pH=2-7, around 3.12×10^{-4} (w/v %). To the best of the authors knowledge there is no available literature reference of an investigation of cilostazol using Dielectric spectroscopy.

6.4 Polymer excipient materials

In this thesis HPMC HME and HPMC AS manufactured by Dow Pharma & Food is used. The motivation for choosing HPMC HME is that it is a product specially developed for hot melt extrusion (HME) applications[26]. HPMC AS is a polymer known to effectively prevent re-crystallization of API in solid dispersions. It is also highly thermoplastic a property that makes HPMC AS suitable for hot melt extrusion applications[12].

The T_g of the HPMC variant used in this thesis differs from traditional T_g values that can be found in literature. The T_g of HPMC HME used in this study is significantly lower. The chemical structure of both polymers, HPMC HME and HPMC AS is shown in Figure 6.4.

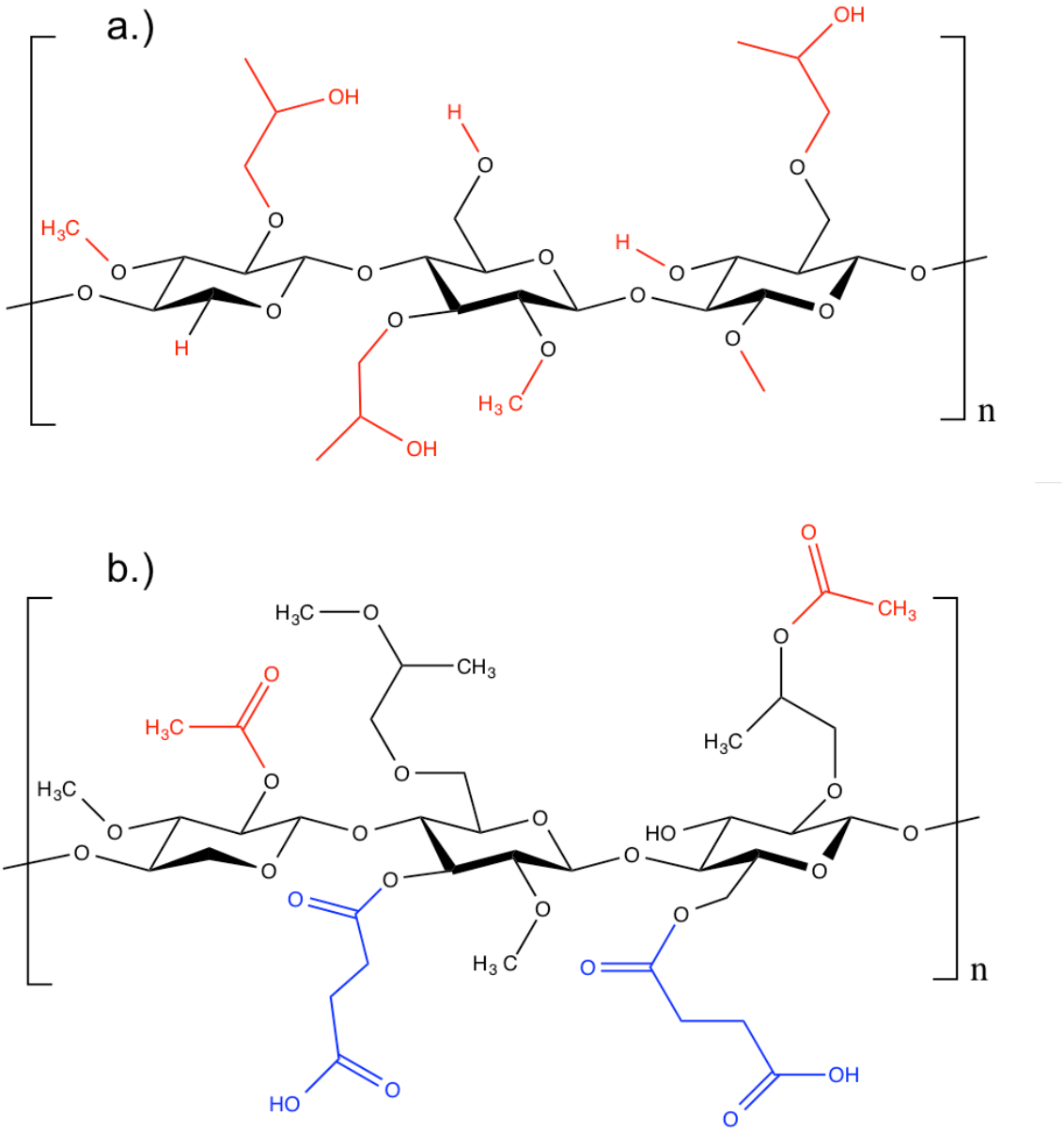

Figure 6.4. Chemical structure of a.) HPMC HME and b.) HPMC AS, adapted with modifications from[12,14,60].

The difference between HPMC HME and HPMC AS is readily observed by the color coding used in Figure 6.4. The functional groups of HPMC AS are different compared to HPMC HME. This will affect how these polymers interact with their surrounding and thereby their thermal properties and solubility.

7 Method

The method section is divided into three parts. The first part focus on material characterization methods, including a description of how each of the single components was analyzed but also how the binary blends in solid dispersion formulation were characterized. The second part describes the methods of making solid dispersions. The third part concerns the release experiments performed to evaluate dissolution performance of the amorphous solid dispersions.

7.1 Differential Scanning Calorimetry, DSC

DSC measurements were carried out using the Q1000 instrument from TA Instruments. A measured amount of sample was put in a hermetically sealed pan made of aluminum, which was sealed by using TA Tzero Press. The reference sample was composed of Indium. Liquid nitrogen was used for cooling. The purge gas used was helium at a flow of 25ml/min and nitrogen of 25ml/min. The samples were prepared in air and at room temperature. The presence, onset, heat of formation, onset, peak position, difference in heat capacity and midpoint location of eventual phase transitions and glass transitions was located and analyzed using TA instrument analysis software.

7.2 Dielectric Spectroscopy

A Novocontrol Dielectric Relaxation Spectrometer was used to measure dielectric spectra. The system was equipped with a Quatro Cryosystem with a temperature range of -160°C-400°C, an Alpha analyzer with a frequency range of 10^{-3}-10^{6}Hz, and a standard sample cell BDS 1200. To control the DS equipment WinDeta software was used.

Two types of experiments were performed in this study using DS. In the first method dielectric spectra at several different temperatures were collected to characterize relaxation processes within the material of interest. The second experiment focused on mapping the crystallization kinetics at one specific, fixed temperature over a period of time.

The first type of experiment aims to characterize the relaxation behavior over a broad temperature range below and above the glass transition temperature. The frequency range employed in these measurements was 10^{-2}-10^{6}Hz. In the experiment the sample was melted at 10°C above T_m for at least 1/2h, the temperature was then lowered below T_g. The temperature was then raised in steps recording the dielectric spectrum below and above the glass transition and relaxation processes were recorded. Data analysis of dielectric spectra was performed using either the software WinFit provided by the DS manufacturer Novocontrol, or by using MATLAB scripts written by the author of this thesis, utilizing the MATLAB least square non-linear optimization routine LSQNONLIN. In

all DS spectra presented in the Results section circles denote experimental data points. Solid curves are either drawn between data points as guide for the reader, or represents results obtained from fitting the spectrum using model functions. In cases where fitting of experimental data was performed, this is clearly stated. DS measurement and fitting was performed in duplicate to ensure reproducibility for all three API substances.

The second type of experiment aimed to study the re-crystallization process for ibuprofen, felodipine, and cilostazol. Two temperatures between the T_g and T_m were selected for investigation of re-crystallization kinetics. The choice of temperature interval was made to result in a reasonable induction time of crystallization. DSC results were used to select appropriate experiment temperatures. In the experimental procedure the sample holder was assembled with the material in the crystalline state and was then melted inside the DS equipment and kept 10°C above the melting temperature for 1h to ensure complete melting. After melting the temperature was lowered to T_{exp}. The dielectric spectrum was recorded between 10^1-10^6Hz resulting in approximately 1min measurement time of each individual spectrum. Dielectric spectra were then recorded every 600s. The total measurement time was 13.8h for all experiments performed unless stated otherwise. The Avrami and the Avramov methods were used to analyze crystallization kinetics of each material.

7.2.1.1 Sample preparation for dielectric spectroscopy

A gold plated Dielectric Relaxation Spectroscopy sample cell for liquids was used. The metal electrodes were polished prior to measurement. A Teflon spacer was used to separate the electrodes with thicknesses ranging between 50 to 200μm. The Teflon spacer thickness was adjusted for each material investigated to obtain a capacitance value within 30-200pF for the cell. The Teflon spacers used were 14mm in inner diameter. The Teflon ring sets the available sample volume for the substance in question.

In each sample preparation the amount of applied material was attempted to match the available sample volume as much as possible, to avoid getting insufficient signal strength by applying to little sample material, and to avoid leakage of out of the sample volume space when melting of the material occurs.

Disc samples for DS measurement were prepared using an evacuable KBr pellet die from International Crystal Laboratories along with an air powered 15-20 ton automated lab press, Air-EZ. A pressing force of 50kN was applied to the powder sample. The thickness of discs produced was recorded and a density value under the experimental circumstances was determined. If possible the disc was transferred to the DS sample holder and dielectric spectra were recorded. In a case where only brittle discs could be produced which was the case of all the API substances, the substance was inserted as powder. The thickness of the brittle discs upon 50kN pressing force could however be measured, and provided an upper estimate of how

much sample was needed to fill the available volume within the sample cell. For HPMC HME and HPMC AS pressed disc was transferred to the DS sample cell directly.

In the third type of experiment the dielectric spectrum of solvent-casted solid dispersions were recorded. The method of preparing films is described in Section 7.7 below. Using a punch, circular films of uniform thickness were cut out and transferred into a DS liquid sample holder. The film was sealed around Teflon ring and sandwiched between the gold electrodes for the DS measurement.

7.3 Thermal Gravimetry Analysis

Thermal gravimetric measurements were conducted using a NETCHT Thermal Gravimetry Analyzer. A sample size of ca. 5mg was used. The Purge gas used was air (80/20) mixture. The flow rate was set to 50ml/min. For each experiment a correction run that served as a baseline was performed with an empty aluminum crucible. The weight loss was recorded as a function of temperature. A weight loss exceeding 1% was used to identify the onset of thermal degradation within the sample material.

7.4 Raman Spectroscopy

A Confocal Raman Spectrometer, Dilor Labram, was used to study pure substances and binary mixtures. The laser wavelength used was 632nm. When recording the spectrum of powder crystalline API, melt quenched API, polymers or solid dispersions the spectrum was recorded in ten cycles of duration 60s. For each substance of mixture investigated several measurements were performed to ensure representative results.

To systematically characterize the homogeneity and to look for compositional changes as a function of the spatial position a Raman mapping of solvent-casted felodipine HPMC AS solid dispersion was performed. The material was selected due to its uniform thickness facilitating data analysis since the background was expected to not vary significantly, contrary to extruded solid dispersion surfaces. Raman spectra within an area of 250×100μm were collected with steps of 25 and 50μm respectively. The confocal hole size was set to 500μm, the acquisition time was 20 seconds and was repeated three times.

7.5 Cloud point measurement of HPMC and HPMC AS

A Mettler Toledo cloud point temperature instrument was used to measure the cloud point temperature. Polymer solutions were prepared by weighing a sample amount corresponding to 0.25mg polymer. The polymer powder was transferred to

a 25 mL glass vial. The vial was placed on a scale and phosphate buffer, pH=6.8 and 0.1M, was added to the vial until the polymer amount corresponded to 1% (w/w) of the added liquid. The sample was put on magnetic stirring for at least 24h. Once no trace of polymer powder could be observed cloud point samples were prepared. A minor amount of liquid was transferred to a glass pipe. The pipe was cleaned with ethanol and inserted to the cloud point measurement apparatus. A temperature ramp of 0.1°C/min between 25-65°C was used and the measured was light transmittance of the solutions. For each type of polymer the experiment was performed in triplicate.

7.6 Hot Melt Extrusion

A HAAKE MiniLab II Compounder was used to prepare Hot Melt Extruded solid dispersions. The barrel temperature was set to exceed the glass transition temperature of the polymer to enable a flow and softening of the extruded material. The temperature was also adjusted with respect to the pharmaceutical. To prepare an amorphous solid dispersion the extruder operating temperature was set to exceed the melting temperature of the API ensuring that it melted during extrusion. The operating temperature of the extruder was set between the glass transition temperature T_g, and degradation temperature T_{deg} of the polymers extruded.

A sample amount of around 5 g was weighted and inserted manually into the HME. To avoid sudden increase of torque the material was feed into the barrel in steps and under t_{feed}=2:00 min. The rpm chosen was 100min^{-1}. The time of exposure was set to t_{circ}=5:00 min after finishing feeding all the material. This was to ensure sufficient time for melting of the API, softening of the polymer, and homogenous mixing of the API and polymer. After 5 min of cycling the material the material was flushed out of the extruding chamber for a period of t_{flush}=1-2 min. After flushing the chamber was reopened and the circulation chamber strip material was extracted from the equipment.

While the material was still hot tablets were punched out of the strip shaped object using a circular 8mm wide punch. Before the dispersion temperature dropped below T_g and solidified, 3-5 tablets were prepared with 1 mm thickness and 8 mm diameter. The approximate weight of a tablet of this size was 100mg, depending on drug content. Additional extruded material was pelletized. All the extruded material was stored in a desiccator with dry silica until further analysis.

7.7 Solvent-casting

Film casted solid dispersions were prepared by dissolution of the API in a 1:1 (v/v) mixture of dichloromethane and ethanol. Two different polymers were used, HPMC HME 100cP and HPMC AS. The polymer was added to the solution under magnetic stirring. The applied amount of polymer varied depending on solubility within the solvent mixture usually 1-2 % (w/v). The solution was kept stirring for several

hours until the polymer was completely dissolved, and was then casted onto a shallow glass plate. The solvent was evaporated overnight in a fume hood. The remaining solid dispersion was dried in vacuum oven at T=60°C for at least 6 hours. Upon extraction from the vacuum oven the temperature was brought to above the API T_m, once the film had been exposed to the $T>T_m$ for 10 minutes the film taken out of the vacuum oven and equilibrated to RT. The film was then removed from the glass surface.

7.8 Release performance evaluation of amorphous solid dispersions

The method used to evaluate API release behavior and amorphous solid dispersion performance was USP II with paddle stirring and a basket sample holder according to Figure 7.1.

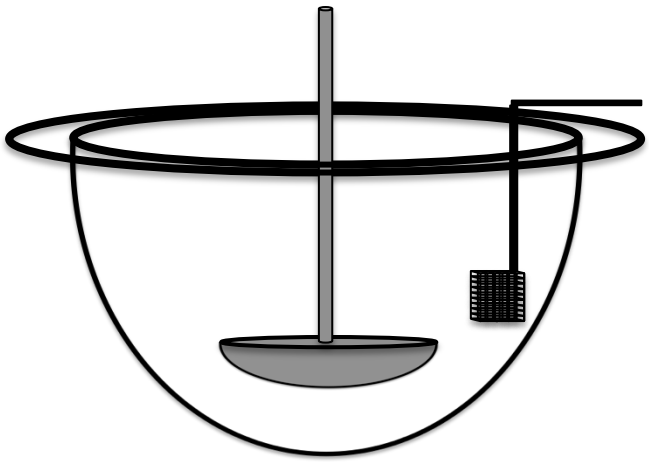

Figure 7.1. USP 2 setup with paddle stirring and basket sample holder.

Using a paddle and a basket ensures that the position of the tablet within the vessel is fixed throughout the whole experiment, and that the entire tablet is exposed to the solvent. A disadvantage of using a basket can be that the basket mesh interferes with the swelling of the polymer at the surface of the tablet[48].

A water bath surrounding the outside of the vessel controlled the temperature of the dissolution bath. The temperature was set to 37±0.5°C. The paddle speed was set to 50 rpm. A dissolution vessel equipped with an inward pointing dent located at the bottom of the vessel was used, so called Peak-vessels.

To quantify the presence of dissolved API within the release medium either an in-situ UV measurement fiber probe, or sampling of release medium and external measurement was employed. The choice of using in-situ or external measurement tools depended on the ability of the in-situ UV-measurement to successfully detect the API within the solution. If the concentration of API within the release medium

was too low external HPLC-UV measurements were carried out on samples taken at predefined time points of the release experiment.

If in situ UV-probes were used to quantify API release the dissolution medium was degassed using a SOTAX instrument. The primary reason for degassing the medium was to avoid bubble formation in the vicinity of the probe tip, which would potentially scatter light and interfere with the measurement.

Prior to measuring API release within the selected release medium a reference solution was prepared. API was dissolved in methanol and diluted with release medium achieving a known concentration of API within the prepared solution. The UV signal at this concentration was recorded and used as a reference in later measurements of the tablet release experiments.

7.8.1 Release performance testing of Ibuprofen:HPMC HME dispersions

Ibuprofen release from HPMC 100cP was evaluated in 0.1 M HCl with pH=1. Crystalline ibuprofen displays solubility of 0.06 mg mL^{-1} in these conditions. In-situ UV-probes were capable of detecting ibuprofen in reference solution of S=0.03 mg mL^{-1} and this method was therefore used to quantify the API release into the release medium. Measurements were carried out every 30 min for a total of 24 h. To prepare standards ibuprofen was dissolved in methanol. The solution was diluted by HCl such that the total methanol contribution was 5 % (v/v). Methanol in 5 % concentration within HCl was shown to give no significant UV-absorption.

7.8.2 Release performance testing of felodipine:HPMC HME and felodipine:HPMC AS dispersions

Felodipine concentrations in aqueous system could not be detected using in-situ UV probes (S=0.0005 mg mL^{-1}). Agilent UPLC-UV equipment was instead used to quantify felodipine release. Standard solutions of the API were prepared in a 50:50 mixture of acetonitrile and deionized water. Four standards of different concentrations ranging between 0.05-1 µg mL^{-1} were prepared. A few mg of felodipine was weighted and mixed with a few drops of HPLC grade ACN. When crystalline particles disappeared ca. 25mL ACN:H_2O mixture was applied to the beaker. The solution was put in an ultrasound bath for 30min, thereafter diluted further to 50mL. By further dilutions four solutions covering the intended concentration range were prepared. The experiment was performed in triplicate ensuring that the method provides consistent results. The standard solution was run along with the experimentally gathered samples in UPLC, a standard calibration curve was made using Empower software. The RSD was inspected to ensure acceptable consistency of the calibration.

In addition to taking samples to quantify felodipine, samples were taken to detect polymer presence in solution. At each time point samples for SEC, Size Exclusion

Chromatography was collected. Sampling consisted of extracting ca. 1mL of medium liquid from each vessel. No filtering was carried out. The samples were put in refrigerator for storage until analysis was carried out.

8 Results and discussion

The presentation of results will first focus on the physical properties of each material. In the second part of the results section results are presented concerning solid dispersions in terms of physical properties and dissolution behavior. The last section of results concern release properties of hot melt extruded solid dispersions.

8.1 Physical properties of single components

This section is divided into the three methods used to characterize each single material. The first sections treats DSC and TGA results, the second the Dielectric spectroscopy results providing an insight to relaxation processes of each API material, and in the last part of this section Raman spectroscopy results are reported, which offer a non-invasive and rapid investigation of the state of the APIs.

8.1.1 Phase behavior of APIs and polymers

A summary of DSC results obtained for each compound is given in Table 5, for examples of DSC thermograms and how T_g was determined see Supplementary Figure S1.1. For each compound reported Glass transition temperatures, melting temperatures, and crystallization temperatures are presented.

Table 5. Values for glass transition T_g, melting temperatures T_m, crystallization temperature T_c and degradation temperature T_{deg} of each component determined by DSC. * ibuprofen from Sigma Aldrich ** ibuprofen from Zhengzhou Chemicals. n=3. Reference values found from literature for the GT, melting temperatures, crystallization temperatures, and degradation temperatures are also presented.

Substance	T_g [°C]	T_m [°C]	T_c [°C]	T_{deg}[°C]
Felodipine	45 ± 2	142 ± 4	87	-
Ibuprofen*	−44 ± <1	75 ± 1	53 ± 6	-
Ibuprofen**	−44 ± 1	76 ± <1	56 ± 3	112
Cilostazol	32 ± <1	135 ± 1, 158 ± <1	108 ± 9	-
HPMC HME	96 ± 3	-	-	175
HPMC AS	118 ± 2	-	-	194

Substance	T_g [°C]	T_m [°C]	T_c [°C]	T_{deg}[°C]
Felodipine[9,72]	46	142-147	-	-
Ibuprofen[9,67,24]	-45	76-77	27-70	130-140
Cilostazol[76]		159,146,136	~108	-
HPMC HME[26]	113	-	-	200
HPMC AS[12,26]	119	-	-	~180

The experimental results presented in Table 5 can be compared with literature references provided. The determined T_g and T_m for ibuprofen, felodipine, correspond closely to literature values. Cilostazol T_m also agrees well with reference

values. No T_g could be found in literature of Cilostazol. The T_g value observed in this study was found to be reproducible.

The polymeric materials are completely amorphous and thus exhibit no melting endotherm, this agrees previous studies of HPMC HME and HPMC AS[26]. A minor weight decrease of HPMC HME, see Supplementary Figure S1.26. This plateau feature of the TGA scan arise due to water loss[26]. Water is known to plasticize glasses giving rise to a lowering of T_g[50]. Consequently, a lower T_g was found in the case of HPMC HME. No moisture was detected in HPMC AS, see Supplementary Figure S.1.27. The T_g of HPMC AS also agrees well with literature references[12,26].

8.1.2 Relaxation processes of APIs

Figure 8.1 shows a Dielectric spectroscopy measurement of felodipine at T=67 °C. The dielectric spectrum, real a) and imaginary b), parts are shown as functions of frequency.

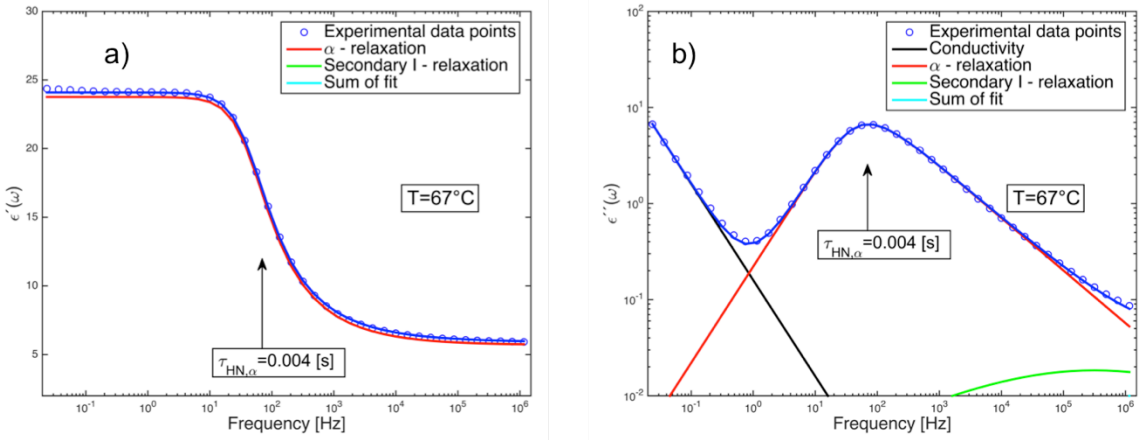

Figure 8.1. Dielectric spectrum of felodipine at 67 °C. The dielectric functions, real part a), and imaginary part b) are shown as functions of frequency. Solid lines represent curve fitting results using model functions.

Felodipine at T=67 °C exhibits a relaxation process with relaxation time $\tau = 0.004$ s as indicated in Figure 8.1. Felodipine at T=67 °C is a supercooled liquid according to DSC results, T_g=45 °C, see Table 5. Consequently the α-relaxation of felodipine at T=67 °C should be faster than $\tau_\alpha = 100$ s. The relaxation process observed in Figure 8.1 does indeed satisfy these conditions. Several measurements performed at different temperatures presented in Figure 8.2 show how the relaxation process shifts as a function of temperature. Higher temperature leads to shorter relaxation time and faster dynamics. The relaxation time of felodipine at T=47 °C, near T_g, (Figure 8.2), correspond to a relaxation time of $\tau = 7$ s. There is a clear resemblance of the detected relaxation process with the α-relaxation since the relaxation time approaches 10^2 s as the temperature approaches the T_g. Consequently, the relaxation process indicated with arrows in Figure 8.1 and Figure 8.2 is the α-relaxation.

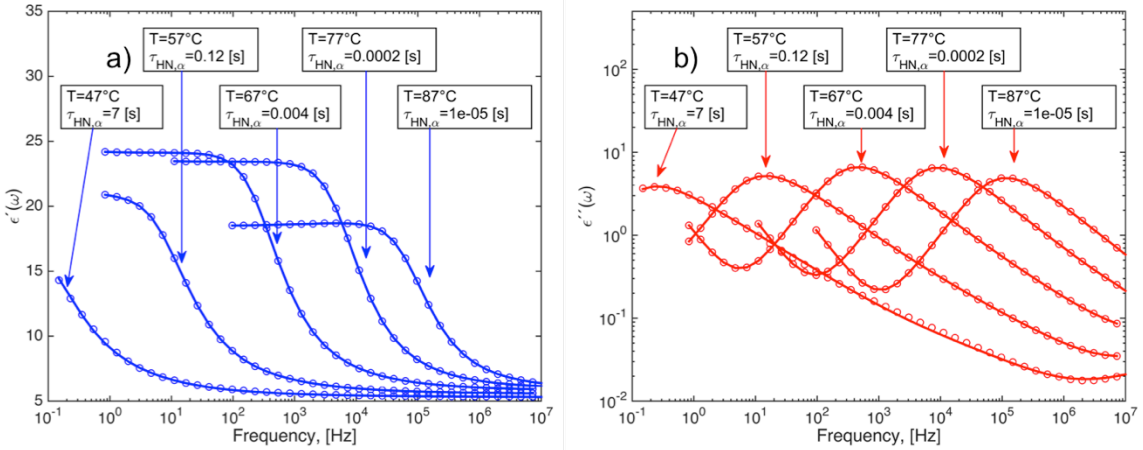

Figure 8.2. Real (blue) and imaginary (red)parts of the dielectric function of felodipine shown as a function of frequency and for temperatures 47-87 °C. The experimental data points are shown as circles. The data fit result obtained through optimization using model functions is shown as solid lines.

A common way of visualizing the α-relaxation time and its temperature dependence, along with other detected relaxation processes is a relaxation map. In a relaxation map the relaxation processes on a $\log_{10}$ scale are visualized as functions of inverse temperature. A relaxation map of felodipine is shown in Figure 8.3. Additional figures related to the fitting of felodipine experimental data are presented in Supplementary Figures S1.3-5.

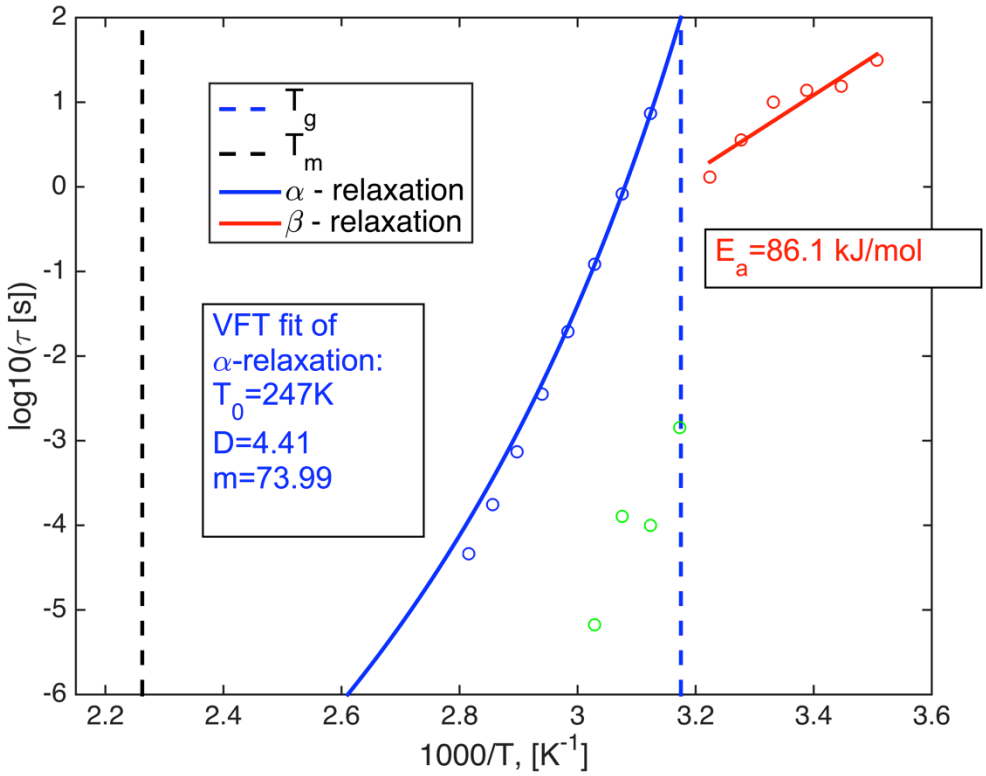

Figure 8.3. Relaxation map of felodipine. The relaxation time of each detected process is plotted as a function of inverse temperature. Data points of the relaxation time for each temperature measurement

are shown as circles. VFT fit of the α-relaxation is shown in blue. Secondary relaxations detected below and above the T_g of felodipine are displayed in red and green circles respectively. The T_g and T_m of felodipine are shown as dashed lines, blue and black respectively.

In Figure 8.3 the α-relaxation of felodipine is shown in blue. The VFT model fit is shown as a solid blue line. Secondary relaxations are also indicated in Figure 8.3. A slow secondary relaxation was detected below T_g, with activation energy 86.1 kJ/mol (red color in Figure 8.3), and above T_g another faster secondary relaxation was observed, (green in Figure 8.3, see also Supplementary Figure S1.2). Although no relaxation map for felodipine could be found in literature, similar secondary relaxation dynamics has been observed in several glass forming liquids[24,30,32,33,78]. Due to its general appearance in molecular glass formers, even in molecules that have no internal rotational degree of freedom, this secondary relaxation is considered to be of fundamental importance to the glass transition[30]. In recent years, several studies of this slow relaxation, also called the Johari-Goldstein relaxation (JG-relaxation) has been proposed to play a role in glass stability and re-crystallization[24,30,32]. It should be stressed that the identity of the slow secondary relaxation presented here has not strictly been determined. This study only identified considerable similarities of the JG-relaxation in other glasses with those observed here in felodipine[24,32,78].

There is one previous study where Dielectric spectroscopy measurements on felodipine within the temperature interval 45-65 °C[79]. The α-relaxation time reported there differs from the results obtained in this study by one order of magnitude. Some shortcomings of that work can be identified. For instance, a definition of what relaxation time corresponds to the T_g was not given and a Dielectric spectroscopy determined T_g is absent[79]. Furthermore it was claimed that the Dielectric spectroscopy measurements were carried out above T_g=45 °C of felodipine, however at the measurement performed at T=45 °C, the reported α-relaxation was $\tau_\alpha = 255$ s.

The analysis of felodipine α-relaxation is presented in terms of T_g, fragility (m), and the VFT parameters in Table 6. The results obtained for ibuprofen and cilostazol are also presented in this table.

Table 6. Fragility (m), D, T_0, and the glass transition temperature T_g determined by Dielectric spectroscopy for each of the API considered in this study.

	Cilostazol	Felodipine	Ibuprofen
m	98	74	85
D	3.1	4.4	3.7
T_0 [K]	253	249	184
T_g [°C]	30	42	-47

All three substances were determined to be fragile[9]. Determination of T_g using Dielectric spectroscopy result in similar values as those obtained using DSC, see Table 5. The obtained T_g=-47 °C and fragility of 85 for ibuprofen corresponds closely

to what is reported in other studies[24,25]. The close agreement of ibuprofen VFT parameters, fragility and T_g values with previous reports contribute to verify that the methodology used here is accurate.

A comparison of the relaxational behavior and the fragility can be made using an Angell plot. The Angell plot visualizes the α-relaxation times of the APIs as a function of scaled temperature, T_g/T. An Angell plot based on the results obtained for each API is shown in Figure 8.4. Clearly the viscous liquid behavior of all APIs fall into the same category of fragile liquids, see Figure 5.2. The behavior seen in Figure 8.4 is typical of molecular liquids. Molecular liquids are loosely packed, and minor thermal fluctuations result in structural rearrangement within the liquid resulting in a strongly non-exponential relaxation time-temperature behavior[8].

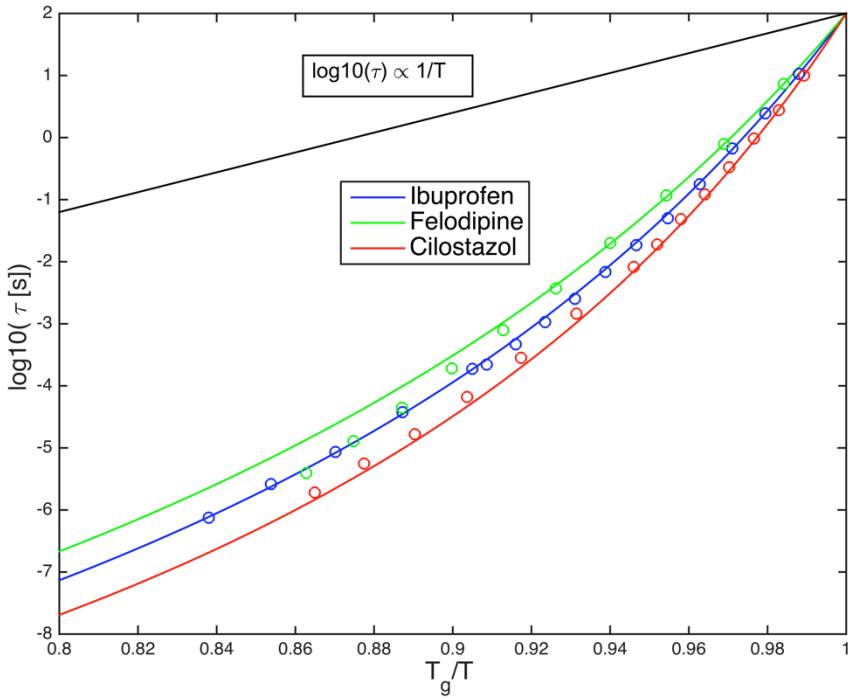

Figure 8.4. Angell plot of the three APIs, ibuprofen, felodipine and cilostazol. The α-relaxation time, τ (s), is shown as a function of scaled temperature (Tg/T),. The solid curves are fit to experimental data points, circles, using the empirical VFT function. The fit of ibuprofen relaxation time is accurate, while felodipine data fit deviates from the data points.

The Angell plot show that although the behavior of all APIs are similar, the degree to which the VFT model fits the experimental data varies. The VFT model of the felodipine α-relaxation, green solid line in Figure 8.4, clearly display some deviation from the experimental values. A possible reason for the deviation from the VFT model is sensitivity of the fitting procedure near T_g, where minor differences in the relaxation time affects the shape of the VFT curve to a large extent. The other two APIs, ibuprofen and cilostazol the VFT α-relaxation fits the data points to a higher degree.

A comparison of the dielectric function of liquid felodipine and ibuprofen is shown in Figure 8.5. The dielectric spectrum of ibuprofen, differ from felodipine since it contains two separated relaxation processes. The α-relaxation process is indicated by arrow in Figure 8.5 b). The additional structural relaxation with lower characteristic frequency is the so-called Debye-relaxation.

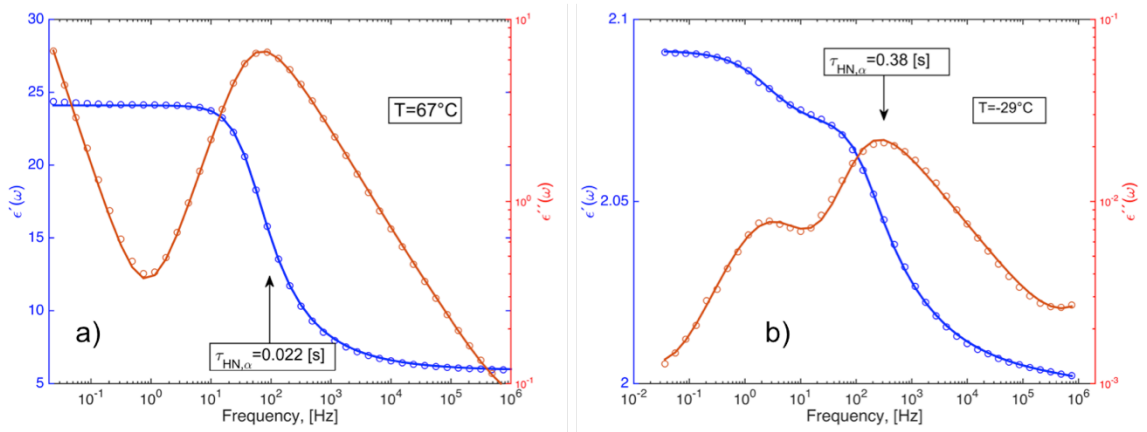

Figure 8.5. Comparison of the dielectric functions (red=imaginary, blue=real) as a function of frequency of felodipine at T=67 °C a), and ibuprofen at T=-29 °C b).

As stated in Section 5.2.2.2, the presence of the Debye-relaxation within ibuprofen liquid has been entitled to ibuprofens ability to form hydrogen bonds. The felodipine molecule also contains an N-H functional group that enables it to form hydrogen bonds, see Figure 6.2. However this ability does not give rise to a Debye-relaxation in the dielectric function, see Figure 8.5 a). The lack of a Debye-relaxation within felodipine may either be due relatively weak-hydrogen bonding dynamics present within felodipine compared to its structural relaxation process, or that it does not occur in molecules that form hydrogen-bonds form N-H functional groups.

The relaxation map obtained from ibuprofen corresponds closely to literature references, see Figure 8.6[24,25]. Apart from the α-relaxation, a Debye-relaxation, and two secondary relaxations were detected.

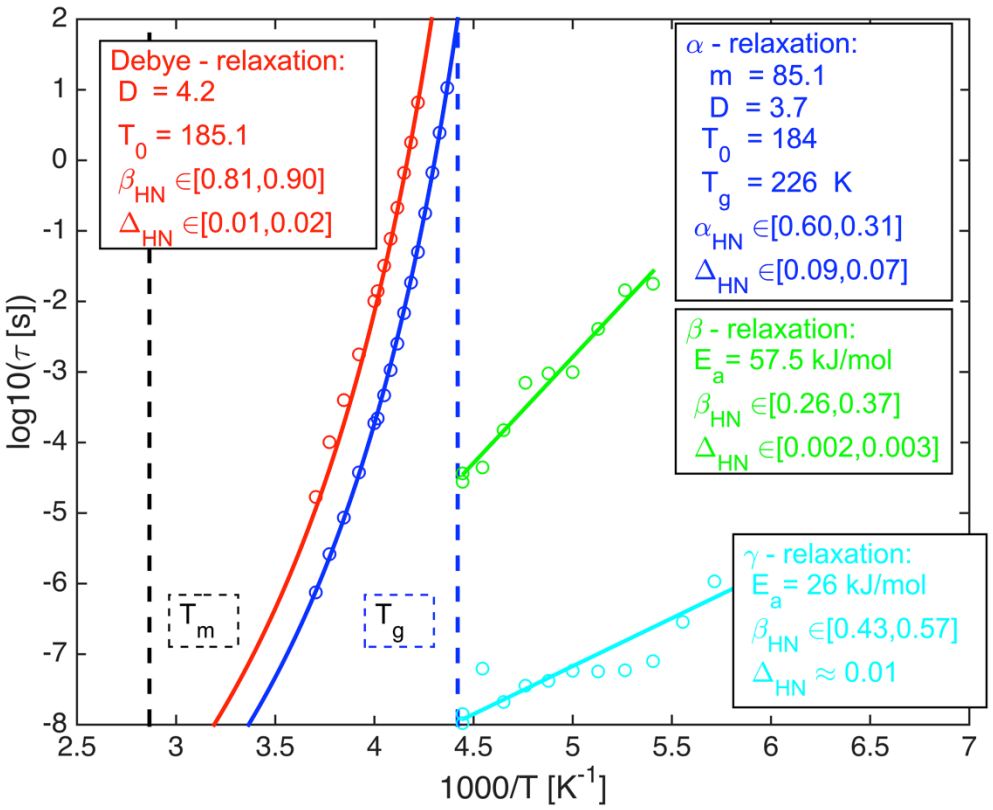

Figure 8.6. Relaxation time shown as a function of inverse temperature of ibuprofen. The relaxation time of each detected process is plotted as a function of inverse temperature. Data points of the relaxation time for each temperature measurement are shown as circles and data fit is shown in solid curves. T_m and T_g are shown as dashed lines.

The slower secondary relaxation activation energy was determined to be 57.5 kJ/mol, and the faster secondary relaxation to be 26 kJ/mol, both values are in agreement with previous studies[24,25]. The slower secondary relaxation process has previously been identified as the J-G-relaxation[25,64]. The faster secondary relaxation process has been connected to intramolecular dynamics related to motion of the carboxylic acid group of ibuprofen, see Figure 6.1[25]. Additional figures related to the fitting of ibuprofen to experimental data are presented in Supplementary Figures S1.6-S1.8.

Similar to felodipine, a relaxation map of cilostazol could not be found in literature. The relaxation map of cilostazol obtained from DS measurements and fit to data of these is given in Figure 8.7.

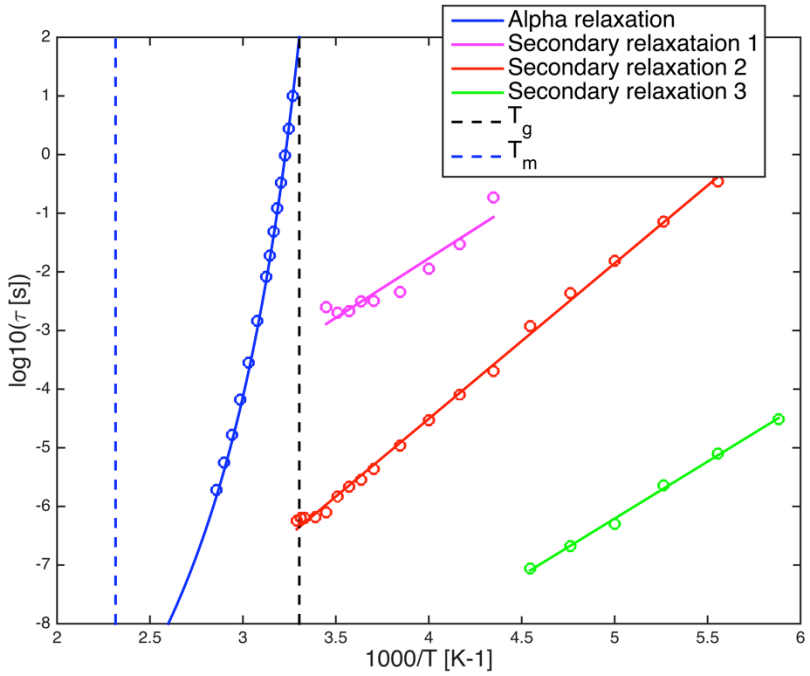

Figure 8.7. Relaxation time is shown as a function of inverse temperature of cilostazol. The relaxation time of each detected process is plotted as a function of inverse temperature. Data points of the relaxation time for each temperature measurement are shown as circles and data fits as solid curves. T_m and T_g are shown as dashed lines.

Cilostazol exhibits three secondary relaxations below T_g. The different dynamics of cilostazol compared to felodipine and ibuprofen is better understood by comparing their molecular structures, Figure 6.1 and Figure 6.2 with Figure 6.3. Due to its rod shaped structure the cilostazol molecule could possibly possess higher degrees of intramolecular rotational freedom. Fast secondary relaxations, such as the red and green data points, are in general related in intramolecular dynamics of the molecule[23,30,32]. The relaxation map indicates that cilostazol indeed exhibit at least two intramolecular secondary relaxations, red and green. The third secondary relaxation resembles the JG-relaxation of cilostazol similar to the JG-relaxation observed for ibuprofen. Additional figures that resulted from the fitting of the cilostazol dielectric spectrums are presented in Supplementary Figures S1.9-S1.11.

8.1.3 Crystallization kinetics of API melts

Felodipine crystallized when kept at constant temperature of T=92 °C over the timescale of 13.8 h, see Figure 8.8 a.). The dielectric strength of the α-relaxation decreased by roughly one order of magnitude. Cilostazol crystallized when kept at T=67 °C for 13.8h, a complete disappearance of the α-relaxation was observed, see Figure 8.8 b.). Additional dielectric spectrums obtained from crystallization experiments are presented in Supplementary Figure S1.12.

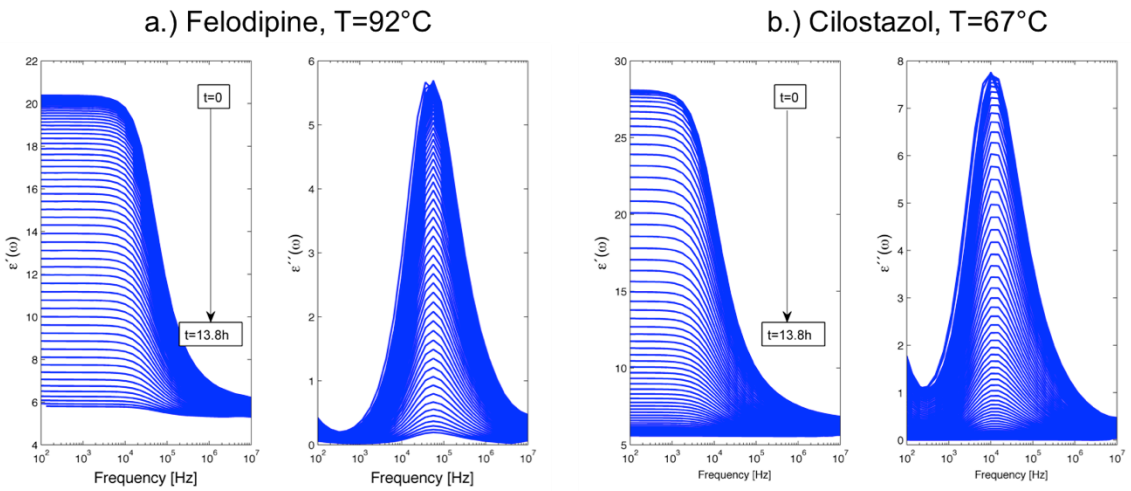

Figure 8.8. Real and imaginary part of the dielectric spectra of felodipine during crystallization monitored at T=92 °C on a timescale of 13.8 h. The dielectric strength of the α-relaxation decreases by an order of magnitude during the period of the measurement.

The onset of felodipine crystallization at T=92 °C is visualized in Figure 8.9. At the chosen frequency, f=133 Hz, the real dielectric spectra strength is shown as a function of time. The induction time, t_0 indicated in Figure 8.9, marks the initial decrease in dielectric strength marking the onset of crystallization.

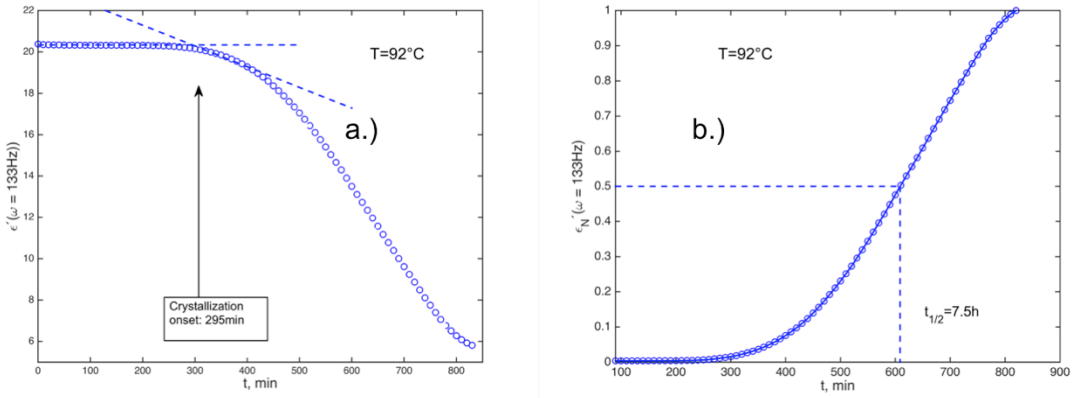

Figure 8.9. Crystallization of felodipine at T=92 °C, f=133 Hz. a.) Onset determination, t_0, is indicated in the figure. b) Normalized dielectric strength, ε_N. The crystallization half time corresponding 50% crystallization is indicated.

A similar induction time, similar to Figure 8.9 a), of 253 min was determined for felodipine at T=82 °C, however crystallization experiment performed on felodipine at 109 °C resulted in no detected crystallization, see Supplementary Figure S1.13. An additional experiment performed at below 82 °C would be of interest to observe if the induction time of felodipine decreases further, or if the system becomes kinetically hindered by viscosity increase. See Supplementary Figure S1.14 for induction time determination of cilostazol and ibuprofen.

The normalized dielectric signal, degree of crystallinity, obtained using equation **(22)** show that felodipine crystallization process is a symmetric process. The curvature of growth initially is similar to the curvature of the final phase of

crystallization. This was not always the case, and affects the values of parameters n and τ_{cryst} as will be shown in Table 7. For additional normalized, real, dielectric spectra, see Supplementary Figures S1.15.

Characterization of felodipine crystallization kinetics using the Avrami method resulted in an approximately linear behavior of double logarithmic normalized dielectric strength as a function of logarithmic time could be obtained, see Figure 8.10.

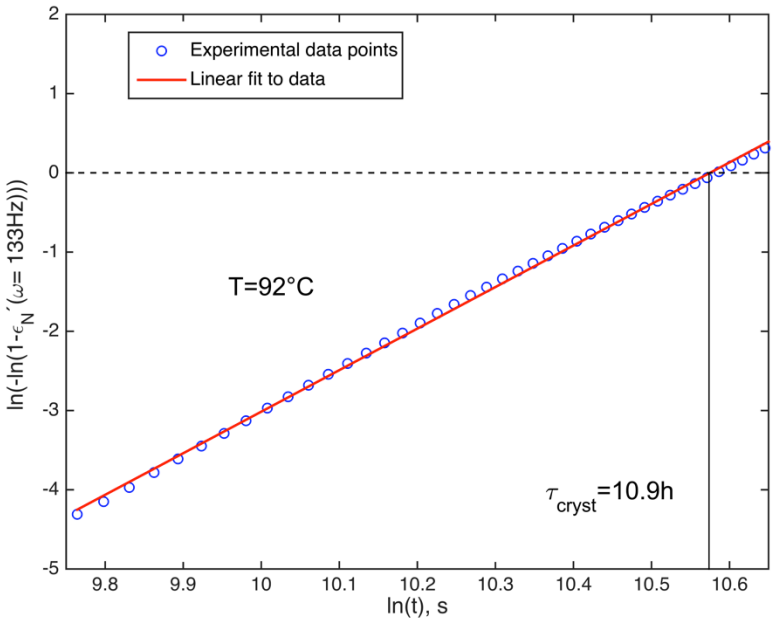

Figure 8.10. Avrami fit of felodipine crystallization kinetic experiment data, T=92 °C and f=133 Hz. The double logarithm of the normalized dielectric function is shown as a function of logarithmic time. A near linear behavior within the investigated time window is achieved.

The crystallization timescale, τ_{cryst}, indicated in Figure 8.10 differ from the value determined using the Avramov method, Figure 8.11. This is expected since the Avramov method takes into account the induction time while the Avrami method does not[43].

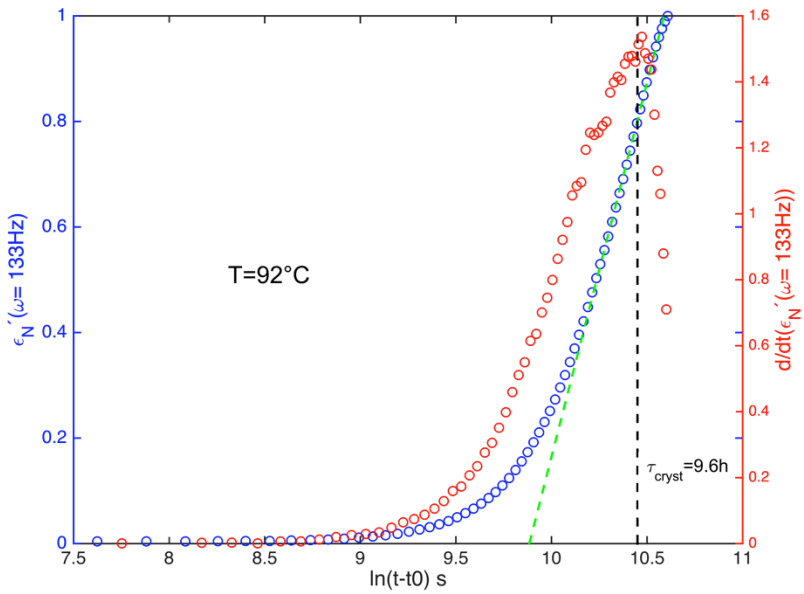

Figure 8.11. Avramov analysis of felodipine at T=92 °C, ω=133 Hz. The normalized dielectric permittivity and its derivative are shown as a function of the logarithm of time adjusted by induction time t_0, in seconds. The timescale of crystallization is marked by the red dashed line. The tangent marking the maximum rate of crystallization is shown by the green dashed line.

Crystallization kinetics parameters obtained by analysis of experimental data using Avrami and Avramov methods are summarized in Table 7. The crystallization kinetics was studied for at least one temperature for each material where model parameters n and k could be estimated using both the Avrami and Avramov method.

Table 7. Results from crystallization experiments and Avrami and Avramov analysis.

		Avrami		Avramov				
	T [°C]	n	ln(k)	n	τ_c [h]	t_0 [h]	$t_{1/2}$ [h]	k [s]
Felodipine	82	4.95	-52.30	2.85	6.97	4.22	5.86	3.15E-13
	92	5.42	-57.22	3.86	9.60	2.60	7.65	5.46E-18
Ibuprofen	-1	1.90	-19.68	2.07	10.19	1.50	5.93	7.88E-10
	-11	0.96	-10.52	-	-	1.30	9.53	3.12E-05
Cilostazol	57	2.99	-31.07	1.96	6.76	2.60	5.29	2.97E-09
	67	2.03	-18.05	1.69	3.34	0.83	3.06	9.93E-08

In a previous study of ibuprofen $n = 2.2 - 2.3$ was reported using both Avramov and Avrami method[64]. The results presented here for ibuprofen are slightly lower, and show larger variation between two methods. In both experiments the experimental time was not sufficient to fully crystallize the liquid. This most probably contributes to the deviation compared to literature values. For felodipine and cilostazol, close to, or complete crystallization was observed during the timescale of the experiment. Felodipine displays a high n=4-5 which can be interpreted as crystal nucleation and growth occurring as three-dimensional

spherulite [38]. Cilostazol was found to have a lower n =2, similar to ibuprofen, corresponding to two-dimensional crystal growth in disc. However, for all compounds however there are some variations in the determined n, both between different temperatures and between the Avrami and Avramov methods. Previously published work performed on molecular crystallization kinetics show only a slight variation in n between the Avrami and Avramov methods[43,64]. Additional experiments where full crystallization is always observed should produce more reliable results. Repeated measurements to validate the determined n are also required. Finally, the source of the API sample, i.e. manufacturer, and sample purity, may also result in different crystallization kinetics due to heterogeneous nucleation. In addition the nucleation rate depends on the absolute size of the sample. Additional data with Avrami and Avramov analysis are presented in Supplementary Figures S1.16-17.

The analysis of cilostazol crystallization kinetics at T=67 °C and the resulting fit to experimental data is shown in Figure 8.12. The parameters obtained from the Avrami and Avramov analysis, from Table 7, were inserted into equation **(20)** and compared directly with the experimental data (real part of the dielectric function).

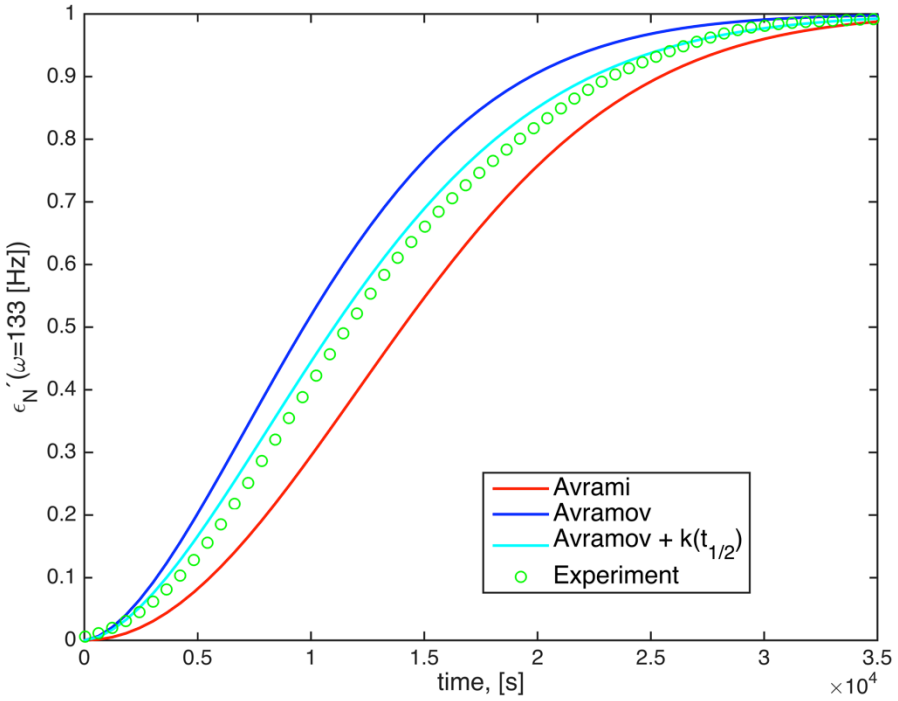

Figure 8.12. Dielectric strength (real part) as a function of time at 133 Hz during crystallization of cilostazol at T=67 °C. A comparison is made between the ability of the Avrami and Avramov methods to describe the experimental data.

Figure 8.12 shows that both the Avramov and Avrami method deviate from experimental data. However, the crystallization rate, k, computed using equation **(26)**, together with the determined Avramov coefficient n, resulted in a reasonably

good fit to experimental data. Close fits to experimental data using k and Avramov n was obtained also in other crystallization experiments, see Supplementary Figures S1.18.

8.1.4 Non-invasive study of API glasses and crystals

Amorphous melt-quenched felodipine is readily distinguished from crystalline felodipine by comparison of the Raman spectra, see Figure 8.13. Crystallized felodipine gives rise to sharp and well defined bands. The Raman bands from amorphous felodipine are broader, and diffuse. Also, the bands are slightly shifted to higher wavenumbers. In particular the Raman band at 100cm^{-1} enables the detection of crystalline felodipine.

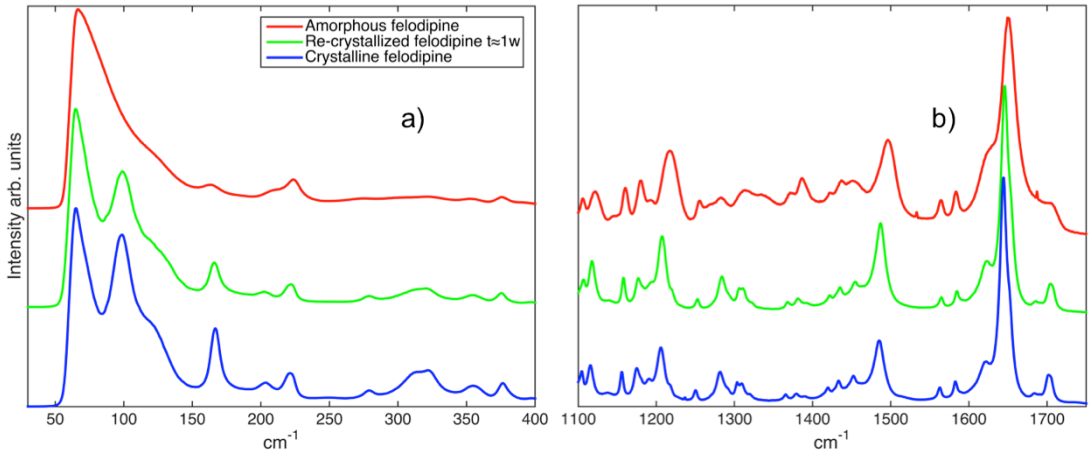

Figure 8.13. Raman intensity as a function of wavenumber, cm^{-1} in a) phonon region (30-400cm^{-1}), and b) fingerprint region (1100-1750cm^{-1}). Spectra shown correspond to crystalline, re-crystallized and amorphous felodipine.

Similar to felodipine separation of amorphous and crystalline cilostazol is possible using Raman spectroscopy, see Figure 8.14.

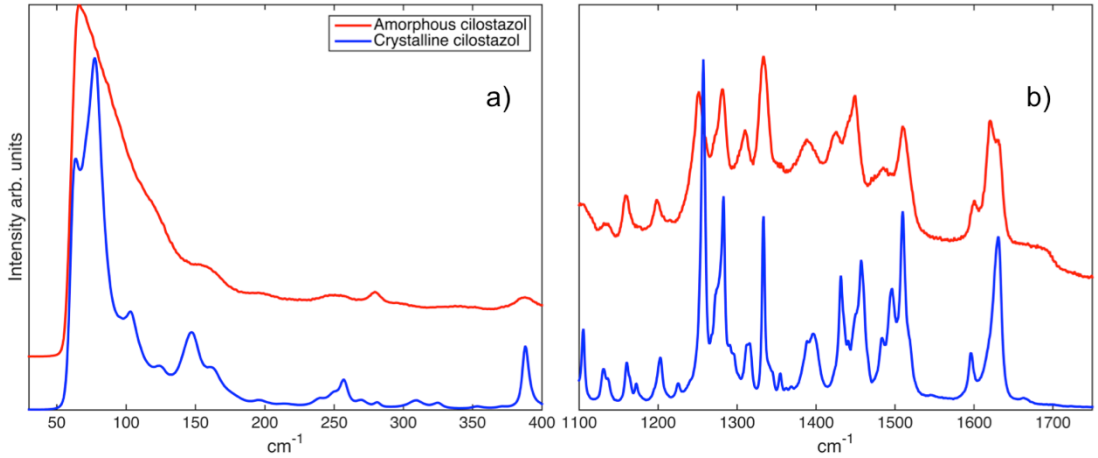

Figure 8.14. Raman intensity as a function of wavenumber, cm^{-1}. In a) phonon region (30-400cm-1), and b) fingerprint region (1100-1750cm^{-1}).

The Raman spectra in Figure 8.13 and Figure 8.14 are of great utility when studying the state of pharmaceuticals. The neat API spectra provide the basis for interpretation of the API state within the solid dispersions. As mentioned in section 5.5.2, the phonon region 30-400cm^{-1} is sensitive to the crystalline or amorphous state of the API. This is clearly observed in Figure 8.13 a.) and Figure 8.14 a.).

8.2 Solid dispersion physical properties evaluation

The results obtained when characterizing the physical properties of the single components in Section 8.1 served as a basis for preparing amorphous solid dispersions. In this section results related to the evaluation of amorphous solid dispersions prepared by solvent casting or hot melt extrusion are presented.

8.2.1 Summary and overview

The progress made in in terms of making amorphous solid dispersions is summarized and presented in

Table 8. The results of each manufacturing technique and material combination tested are discussed in detail in the following subsections.

Table 8. Summary of amorphous solid dispersions prepared and tested. *Ibuprofen:HPMC in high dosage form crystallized over the course of 1 month but was initially amorphous. **Cilostazol exhibits cold-crystallization during DSC measurement but is amorphous at RT.

API:	**POLYMER:**	Ibuprofen			Felodipine			Cilostazol		
Method:	**API:POL**	+	0	-	+	0	-	+	0	-
Extrusion	HPMC HME	v	o	v	v	v	v	v**	o	v
	HPMC AS	x	o	x	v	o	v	o	o	o
Film-casting	HPMC HME	v*	o	v	v	o	o	o	o	o
	HPMC AS	o	o	o	v	o	v	o	o	o

Table 8 is interpreted by consulting Table 9 where the significance of each symbol is explained.

Table 9. Explanation of symbols used in

Table 8.

Legend	
Symbol	**Significance**
v	Successfully produced Solid dispersion
o	Not tested
x	Attempted but without success
+	High concentration

0	Medium concentration
-	Low concentration
v	No crystallinity of API detected in DSC
v	Crystallinity of API detected in DSC

Two observations can be made based on the summary in

Table 8: From an API point of view felodipine is the API that is most readily incorporated and easiest to stabilize in the amorphous state in a solid dispersion. A second observation is the capability of HPMC HME in stabilizing all APIs in hot melt extruded amorphous solid dispersions.

8.2.2 Felodipine solid dispersions

Felodipine amorphous solid dispersions were successfully prepared using both solvent-casting and hot melt extrusion. Hot melt extrusion was performed using both HPMC HME polymers and HPMC AS polymers. Solvent-casted solid dispersions of felodipine and HPMC AS were prepared.

Hot melt extruded felodipine HPMC HME was found to contain only amorphous felodipine within the composition range 10-30 wt.% API, see Figure 8.15.

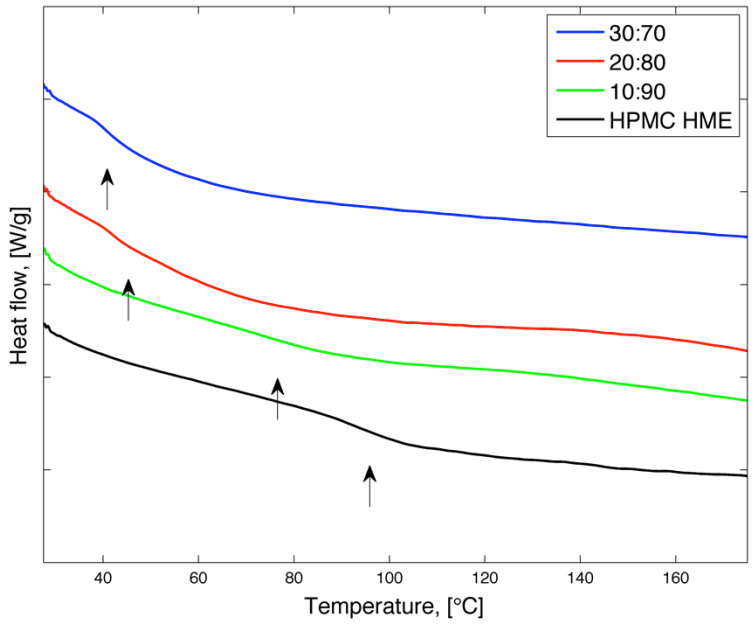

Figure 8.15. MDSC results for 10-30 wt. % felodipine within HPMC HME. A thermogram of neat HPMC HME is shown for comparison. The heat flow signal is in arbitrary scale.

The lack of melting endotherms or re-crystallization and the presence of a glass transitions means that the formulation suppresses crystallization of felodipine even

when exposed to temperatures above T_g. The reversing heat flow shown in Figure 8.15 contains several glass transition-like features and are marked with arrows in Figure 8.16. Felodipine HPMC HME 4000cP with 10 wt.% API exhibits multiple glass transition events, indicating a heterogeneous structure.

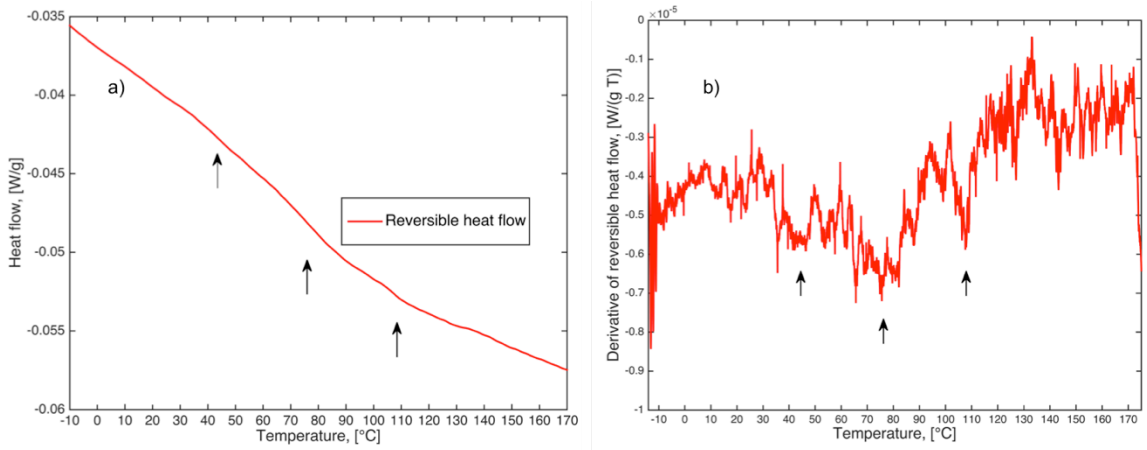

Figure 8.16. Modulated DSC data from 10wt. % felodipine HPMC HME solid dispersion. Black arrows are used to mark glass transitions like features. a) Reverssing heat flow shown as a function of temperature. b) Derivative with respect to temperature of the reversing heat flow. The glass transition temperatures were assigned to the local minima in the derivative of the heat flow.

Incomplete mixing of API and carrier matrix within the extruder, resulting in a heterogeneous structure, is a probable explanation for the observed behavior. Alternatively the mixing of felodipine with HPMC HME polymer could result in phase separation.

Hot melt extruded felodipine HPMC AS solid dispersions gives rise to a glass transition that is more easily detected in DSC, see Figure 8.17. On the one hand, felodipine and HPMC AS containing 30 wt.% API displayed only one T_g intermediate between neat felodipine, and neat HPMC AS and is consistent with Gordon-Taylor (equation **(30)**) prediction of T_g. On the other hand, the 10 wt.% solid dispersion displayed two T_gs, one indicative of neat HPMC AS, and one at intermediate temperature.

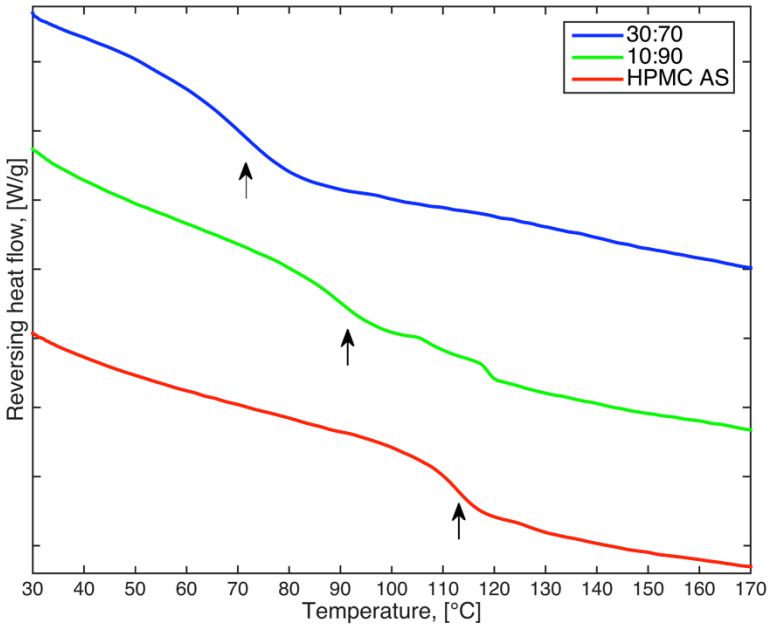

Figure 8.17. Comparison of modulated DSC experiments on felodipine HPMC AS dispersions. The composition range investigated is 10-30 wt. % of felodipine. Thermogram for neat HPMC AS is shown for comparison.

Multiple T_gs in some hot melt extruded solid dispersions indicates a heterogeneous structure. The absence of felodipine melting endotherm indicates that there is no bulk crystalline felodipine within the dispersion, which agrees with previously reported results[10].

Figure 8.18 shows the comparison of the dielectric spectra of neat felodipine and solvent-casted HPMC AS with 40 wt.% of felodipine at T=80 °C. The relaxation process detected within the solid dispersion has a similar relaxation time as the α-relaxation of neat felodipine, compare blue and red curves in Figure 8.18. However the shape of the relaxation peak of the solid dispersion (blue) shown in Figure 8.18 is broader compared to neat felodipine (red).

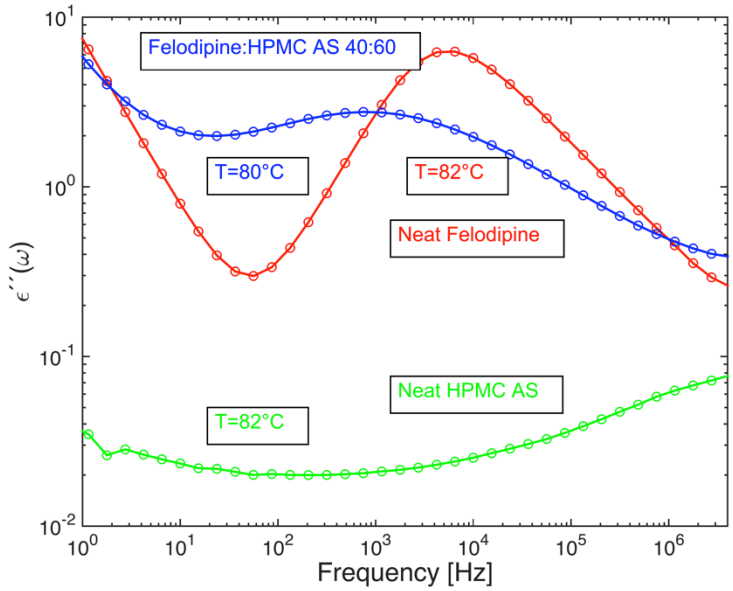

Figure 8.18. Imaginary part of dielectric spectra at T=80°C as a function of frequency for felodipine HPMC AS dispersion with 40wt.% felodipine, and for neat felodipine at T=82 °C.

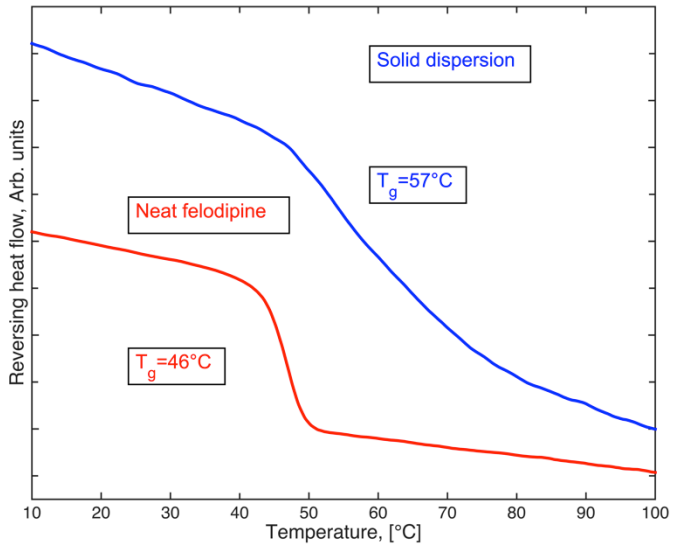

Figure 8.19. Heat flow as a function of temperature of neat felodipine and felodipine within HPMC AS matrix containing 40 wt. % felodipine.

MDSC measurements reveal that the solid dispersion undergoes a glass transition at $T_{g,disp}$=57 °C, compared to neat felodipine which has a $T_{g,neat}$=46 °C, see Figure 8.19. The glass transition of the solid dispersion detected by DSC in Figure 8.19 is broader compared to neat felodipine. Figure 8.20 further compares the α-relaxation of neat felodipine (red curve) with the α-relaxation detected within the solid dispersion (blue curve) as functions of inverse temperature. In addition other relaxations were detected (blue crosses and triangles) in the solid dispersions. These additional

relaxations detected are compared with relaxations found in neat HPMC AS, see green data points in Figure 8.20.

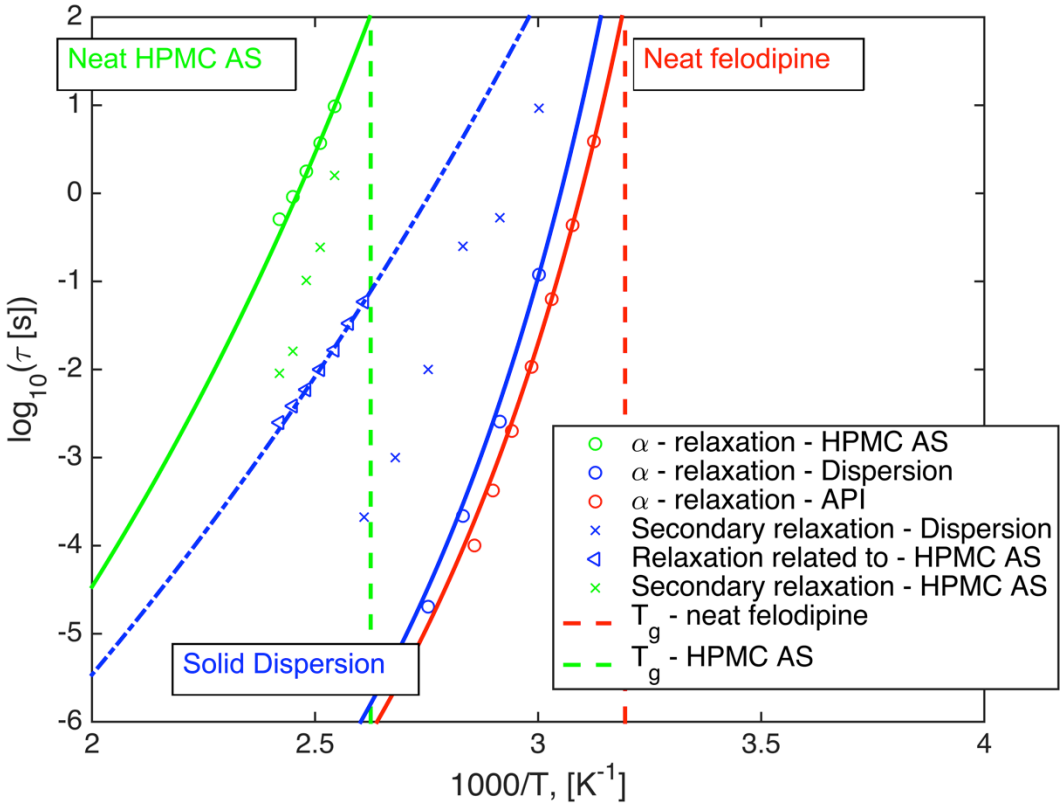

Figure 8.20. Relaxation time as a function of inverse temperature for felodipine HPMCAS solid dispersion (blue), neat HPMC AS (green), and neat felodipine (red). The data points corresponding to the α-relaxations of each material are shown in circles. Secondary relaxations are marked with crosses.

Three relaxation processes were detected in the DS measurement of the solid dispersion, see Figure 8.20, and spectra in Supplementary Figure S1.19. The fastest relaxation process (blue circles), can be assigned to the α-relaxation of neat felodipine by the high similarity between the calculated VFT fit parameters, T_g, and fragility of the fast solid dispersion relaxation and the neat felodipine α-relaxation presented in Table 10. These results indicate that the confinement effect exerted by the HPMC AS matrix has minor effect on felodipine liquid dynamics.

The slowest of the three relaxation processes detected in the solid dispersion (blue triangles) resembles the α-relaxation (green circles) in neat HPMC AS, Figure 8.20. Comparing these two relaxation processes shows that the HPMC AS matrix is affected by the presence of felodipine. The fragility, D, and T_g is different in the solid dispersion compared to neat HPMC AS. Consequently the felodipine plasticizes the HPMC AS matrix lowering its T_g.

The intermediate relaxation process detected in the DS measurement (blue crosses) resembles the secondary relaxation detected in neat HPMC AS (green crosses). The

secondary relaxation within neat HPMC AS is most likely due to side-chain dynamics, see Figure 6.4. Similar dynamics has been observed and attributed to side chain dynamics in other cellulose derivatives[80]. However, the secondary relaxation detected in the solid dispersion does not display the same behavior as in neat HPMC AS. The secondary relaxation process of the dispersion dynamics is less coupled to the HPMC AS α-relaxation and is instead more closely coupled to the felodipine α-relaxation (blue circles) confined in the polymer. This indicates that there is a substantial interaction between the felodipine and HPMC AS, most likely through hydrogen bonding since both felodipine and HPMC AS has the ability to hydrogen bond.

Table 10. T_g, VFT parameters (D, T_0) and fragility (m) for the fast and the slow relaxation processes detected in Dielectric Spectroscopy measurement of felodipine HPMC AS solid dispersion with 40wt. % API. Corresponding values for neat HPMC AS and neat felodipine are shown for comparison.

	SD fast relaxation process	Neat felodipine
T_g [°C]	45	41
D	4,2	4,2
T_0 [K]	253	248
m	77	77
	SD slow relaxation process	Neat HPMC AS
T_g [°C]	62	108
D	20	14
T_0 [K]	148	206
m	29	35

It should be noted that no clear glass transition at T_g=45°C or T_g=62°C could be detected in the DSC measurement of the solid dispersion. The T_g detected in DSC is however very broad with an onset at T=46 °C, endpoint at T=68°C, and midpoint at T=57°C. It is therefore most likely that DSC detects an intermediate of the two relaxation processes observed in Dielectric spectroscopy.

Results from crystallization kinetics experiment results are shown in Figure 8.21. They indicate that the felodipine within the HPMC AS dispersion is stable on a timescale of 20h at 92°C, in contrast with the behavior of neat felodipine. The stable dielectric signal strength in Figure 8.21 b) on a timescale of 20h show that crystallization of felodipine is effectively suppressed within the solid dispersion of HPMC AS, despite favorable conditions for crystallization exhibited by neat felodipine, Figure 8.21 a).

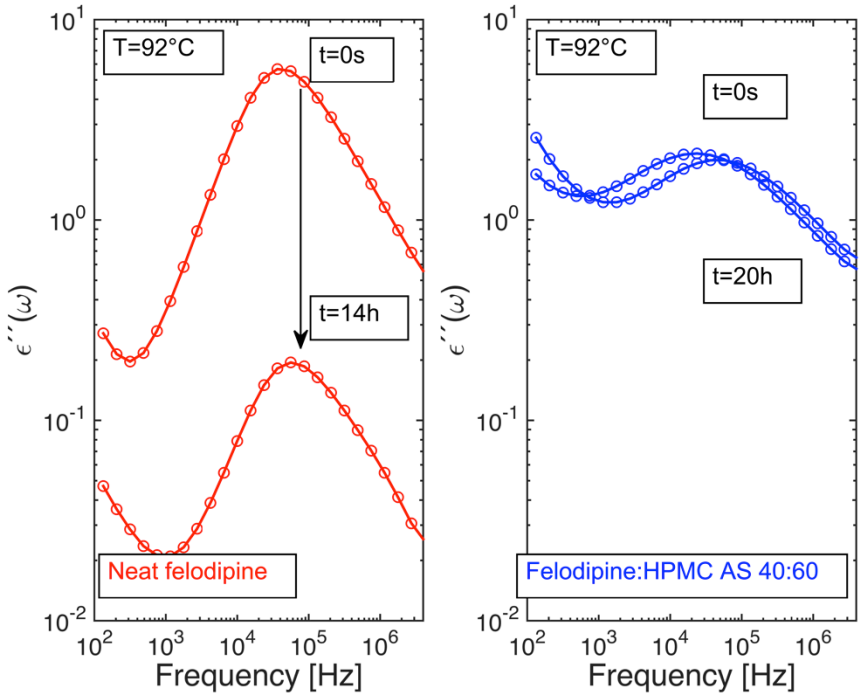

Figure 8.21. Crystallization kinetics experiments at T=92°C for a) neat felodipine and b) felodipine HPMC AS solid dispersion (40 wt.%). The imaginary dielectric function is shown as a function of frequency.

As indicated by the results on the relaxational dynamics and on crystallization kinetics intermolecular interactions between the felodipine and HPMC AS polymer may be present within the solid dispersion. Indeed, Raman spectroscopy results indicate that the frequency of the carbonyl bands around 1650cm^{-1} of felodipine shift within the substance incorporated in the HPMC AS matrix, see Figure 8.22. Furthermore, the shape of the solid dispersion carbonyl band is similar to the shape of amorphous felodipine, confirming the presence of amorphous felodipine within the solvent-casted material. Raman spectroscopy measurements of neat felodipine and solvent-casted felodipine HPMC AS solid dispersions are shown in Figure 8.22.

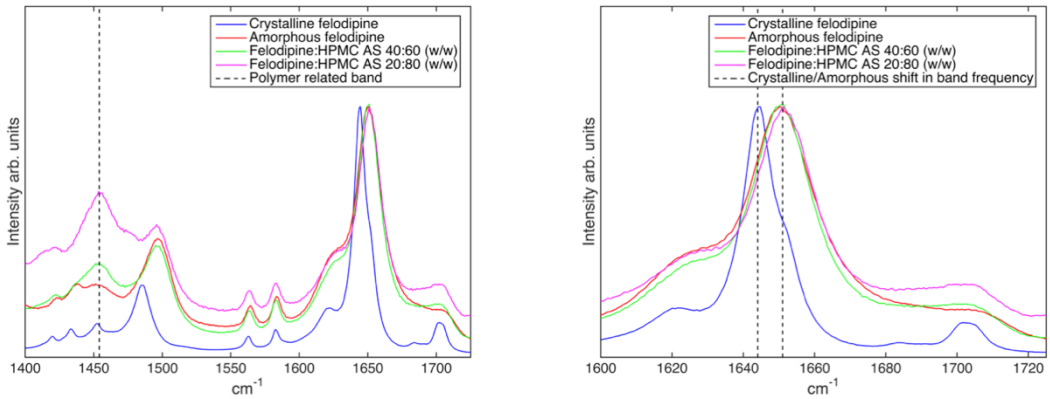

Figure 8.22. Raman spectra of solvent-casted felodipine:HPMC AS solid dispersions with felodipine concentration of 20 and 40 wt.%. Neat felodipine Raman spectra are shown as comparison. The carbonyl

group band at 1650cm^{-1} indicates that felodipine is amorphous within the solid dispersions. The band at 1450cm^{-1} increases with HPMC AS content.

The solvent-casted material had a uniform in thickness. Thus, contrary to extruded material it was possible to collect Raman spectra with similar intensity at several different positions on the sample without adjusting the focus, which enabled the use of Raman mapping, result is shown in Figure 8.23.

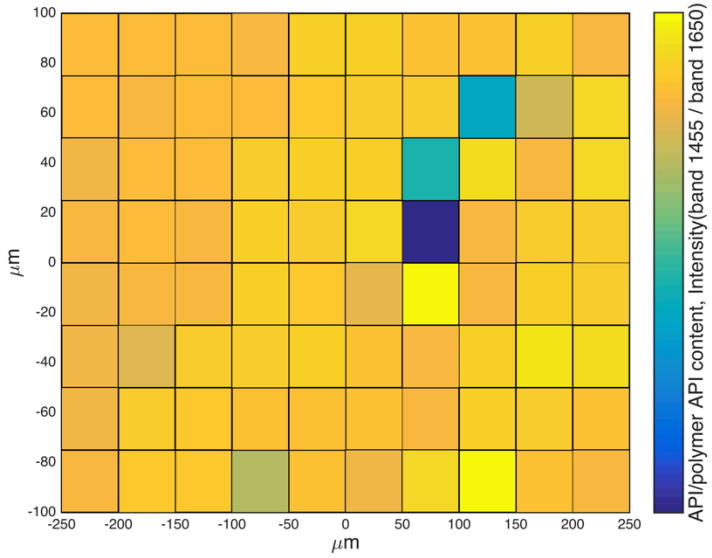

Figure 8.23. Raman mapping in the fingerprint region of felodipine:HPMC AS. Variations in the quotient value between an HPMC AS band (1455cm-1 in Figure 8.22), with the felodipine band (1650cm-1 in Figure 8.22) is shown in color scale as a function of spatial position (x and y) of the film.

The Raman map of felodipine:HPMC AS 20:80 (w/w) shown in Figure 8.23 indicates spots where the API concentration is lower with respect to polymer. The data in Figure 8.23 is normalized with respect to the felodipine band at 1650cm^{-1} and the HPMC AS band at 1455cm^{-1}. Background contributions from the HPMC AS matrix complicate analysis and affects individual spectra. An alternative normalization procedure of the data taking background into account may be needed to improve the result. One approach would be to use z-position autofocus with respect to the laser beam intensity. This way material with less uniform surface texture such as the hot melt extruded solid dispersions may also be examined.

Since the material in solvent-casted is completely dissolved within the solvent mixture during the sample preparation the material should in theory be homogenous. The thermal treatment during preparation ensuring melting of the API could however give rise to phase separation between the API and polymer creating API and polymer enriched domains respectively. Apart from four spots indicated in the Raman mapping of Figure 8.23, the signal shows only minor variations and based on this Raman mapping it is difficult to tell if the sample is completely homogenous. As shown in Supplementary Figure S1.20, the DSC measurement on this sample indicates two T_gs, one at 47 °C and one at 140°C. Although the highest T_g

exceeds what is found in both neat felodipine and neat HPMC AS, see Table 5, multiple T_g generally indicate the presence of multiple phases within the sample.

The primary motivation for using Raman mapping in discovering concentration variations is the possible comparison which can be used to compare the two preparation methods, hot melt extrusion and film-casting. Due to the less uniform surface texture of hot melt extruded material a Raman mapping of hot melt extruded solid dispersion could not be performed.

8.2.3 Ibuprofen solid dispersions

Solvent-casted solid dispersions of ibuprofen and HPMC HME were successfully prepared in a solvent mixture of dichloromethane and ethanol. The concentration of ibuprofen within the dispersion was 40 wt.%. Dielectric spectroscopy measurements performed at T=-13°C of the solvent-casted dispersion and of neat ibuprofen are shown in Figure 8.24 a) and DSC measurement of the same materials are shown in Figure 8.24 b).

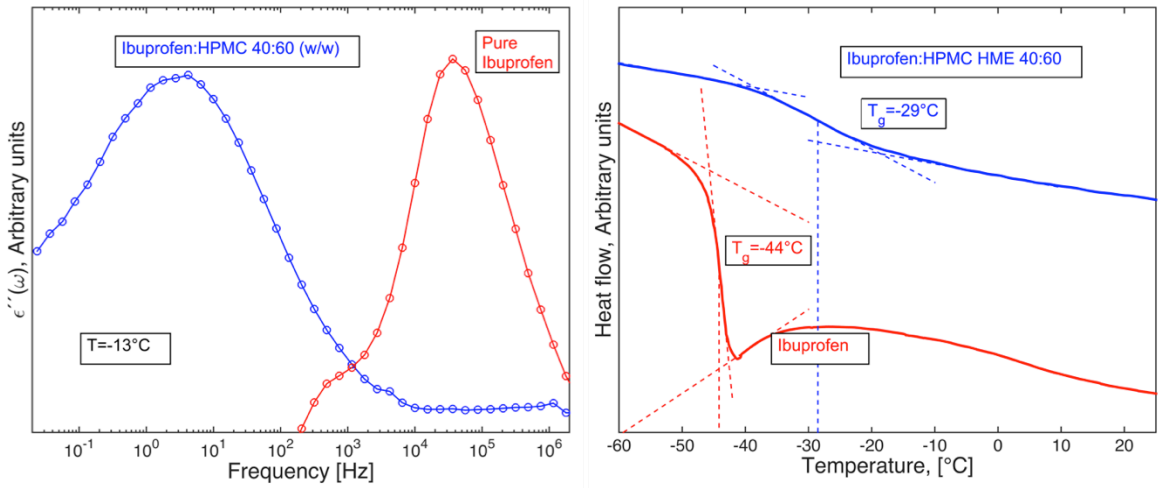

Figure 8.24. a) Comparison of the structural relaxation loss peaks of ibuprofen confined within an HPMC polymer and of neat ibuprofen at T=-13 °C. The characteristic peak frequency of the structural relaxation is clearly shifted to lower frequencies (slower motion), when ibuprofen is confined within the HPMC polymer. b) DSC results of ibuprofen:HPMC HME dispersion and neat ibuprofen.

The presence of a structural relaxation process of neat ibuprofen in Figure 8.24 a) shows that it is liquid at the temperature of the measurement, T=-13°C. In the case of the ibuprofen:HPMC HME dispersion there is also a relaxation loss peak. The DSC measurement in Figure 8.24 b) shows a glass transition at T_g=-29 °C within the solvent-casted dispersion. Both these observations, DSC and DS, indicates that the drug is liquid also within the solvent-casted dispersion at -13°C. The relaxation process within the solvent-casted solid dispersion is traceable back to the T_g detected by DSC, see Figure 8.25 b). The peak maxima of the T=-23 °C correspond approximately to the glass transition relaxation time of 100 s. The results obtained

are consistent with each other which enable a treatment of the observed relaxation loss peak of Figure 8.25 a) as a α-relaxation within the solvent-casted dispersion.

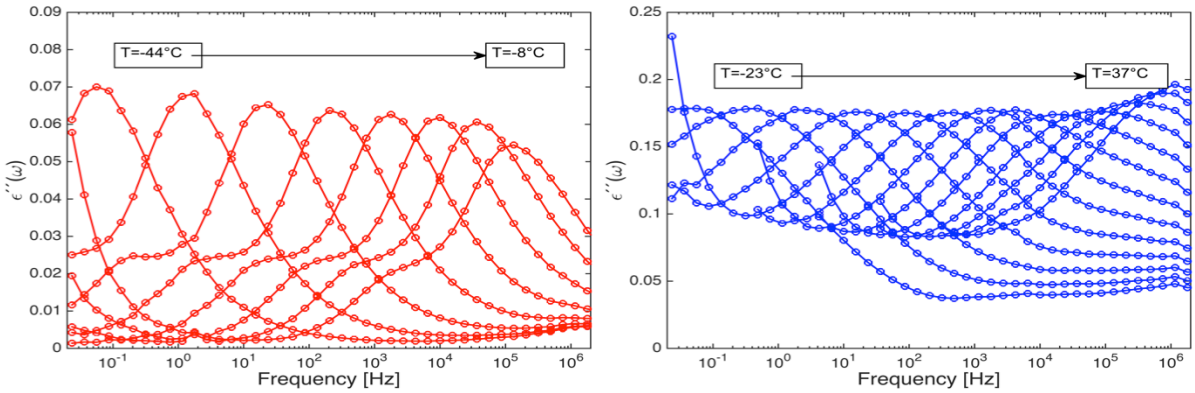

Figure 8.25. Dielectric spectroscopy spectra of neat ibuprofen (left) and of 40 wt.% ibuprofen within HPMC (right) over temperature ranges -44 °C to -8 °C and -27 °C to 37 °C respectively.

The presence of a relaxation process in a dielectric spectra of a multicomponent system is in general difficult to attribute to a single component of the system[23,37]. In the case of HPMC and the solvent-casted dispersion the relaxations were found to be well separated in frequency, see Supplementary Figure S1.23 for a further comparison. In addition neat HPMC HME display a glass transition at T_g=97 °C and neat ibuprofen at T_g=-44 °C. Consequently it appears that within the dispersion there are ibuprofen enriched liquid domains, displaying significant confinement effect based on the change of relaxation loss peak position and shape in Figure 1 a), and comparing Figure 8.25 a) with b). The change in the relaxation behavior is detected by an elevation of the glass transition temperature of ibuprofen in confinement within the solvent-casted dispersion, T_g=-29 °C, compared to neat ibuprofen, T_g=-44 °C.

The Dielectric spectroscopy spectra of the solvent-casted dispersion is compared to the neat ibuprofen spectrum in Figure 8.25. In the case of neat ibuprofen shown in Figure 8.25 b) one observes a decrease in dielectric strength of the relaxation loss peak, signaling crystallization. However, in the spectra of the solid dispersion, Figure 8.25 b) the dielectric strength of the relaxation loss peak is preserved within the whole temperature range investigated (which is also much larger). This indicates that crystallization of ibuprofen is suppressed in the solvent-casted solid dispersion with respect to neat ibuprofen.

To further characterize the change of the dynamics of ibuprofen related α-relaxations within confinement of HPMC HME, the relaxation loss peak data shown in Figure 8.25 was fit using an empirical model function, equation **(15)**. The procedure used is similar to a method developed when characterizing dynamics of polycarbonate within a polymer matrix PMMA (poly(methyl-methacrylate)[27]. The use of equation **(15)** is motivated since it has been shown to provide fits of equal or

better accuracy than the HN function[27,81]. A comparison of the α-relaxation time of confined and neat ibuprofen as a function of inverse temperature is shown in Figure 8.26.

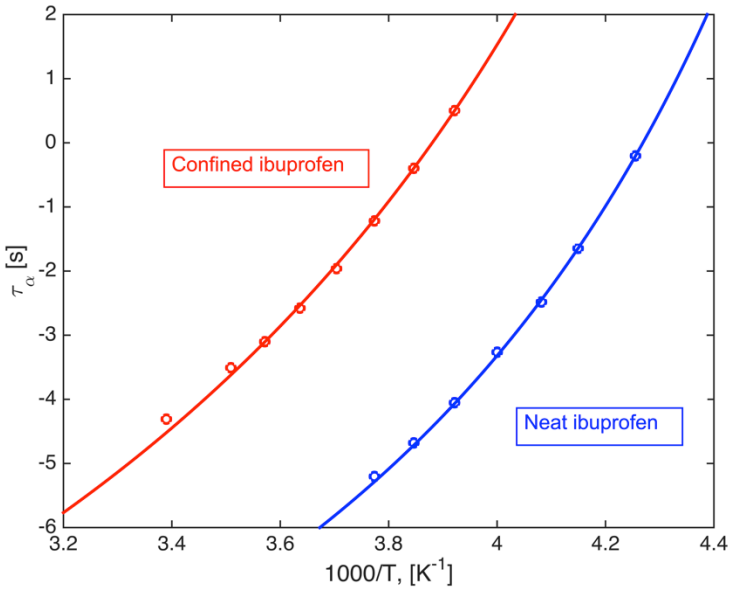

Figure 8.26. Relaxation time as a function of inverse temperature obtained from fitting dielectric spectra from neat ibuprofen and ibuprofen in a solvent-casted solid dispersion.

The relaxation time as a function of inverse temperature clearly shows how the dynamics of ibuprofen is slower upon confinement in the polymer. The solid lines of Figure 3 are fits to the empirical VFT function, equation (2). The parameters obtained from the fits are presented in Table 11.

Table 11. VFT parameters obtained from curve-fit analysis of neat ibuprofen and ibuprofen confined within HPMC HME.

	Neat Ibuprofen α-relaxation	Confined ibuprofen α-relaxation
T_g [°C]	-45	-25
m	82.2	58.0
D	3.87	6.10
T_0 [°C]	184.0	179.0

The glass transition temperatures obtained by evaluating the results from Dielectric spectroscopy in Table 11 display the same trend as is observed in the DSC experiments. There is an increase in T_g, which is consistent with slower α-relaxation dynamics within the solvent-casted dispersion compared to neat ibuprofen.

The shape of the structural relaxation process of the neat ibuprofen liquid, Figure 8.25 a) and ibuprofen within the HPMC polymer matrix, Figure 2b), show significant differences. In the neat liquid state a Debye peak, attributed to hydrogen bonding, is clearly visible whereas it is lacking in the spectra from the dispersion. Thus, upon confinement within the HPMC the hydrogen bonding behavior of ibuprofen is clearly altered, most likely due to interaction with the HPMC HME.

When stored at ambient temperature and in dry atmosphere, in a desiccator with dry silica, solvent-casted ibuprofen dispersions crystallize over time. DSC results in Figure 8.27 show a melting endotherm of the solvent-casted ibuprofen HPMC HME solid dispersion. Compared to the solvent-casted material of the same composition there is a much smaller, but similar, melting endotherm of the hot melt extruded dispersions. The hot melt extruded solid dispersions also seem to exhibit a small cold-crystallization peak at 60°C. In addition, there is no change in state over the timescale of 1 month, verified by comparing DSC thermograms obtained directly after extrusion, and after 1 month storage time, see Supplementary Figure S1.24. High surface area of solvent-casted dispersions could give rise to a rapid crystallization due to nucleation of ibuprofen at exposed surfaces. Another possibility is crystallization induced by residual solvents left within the solvent-casted dispersions.

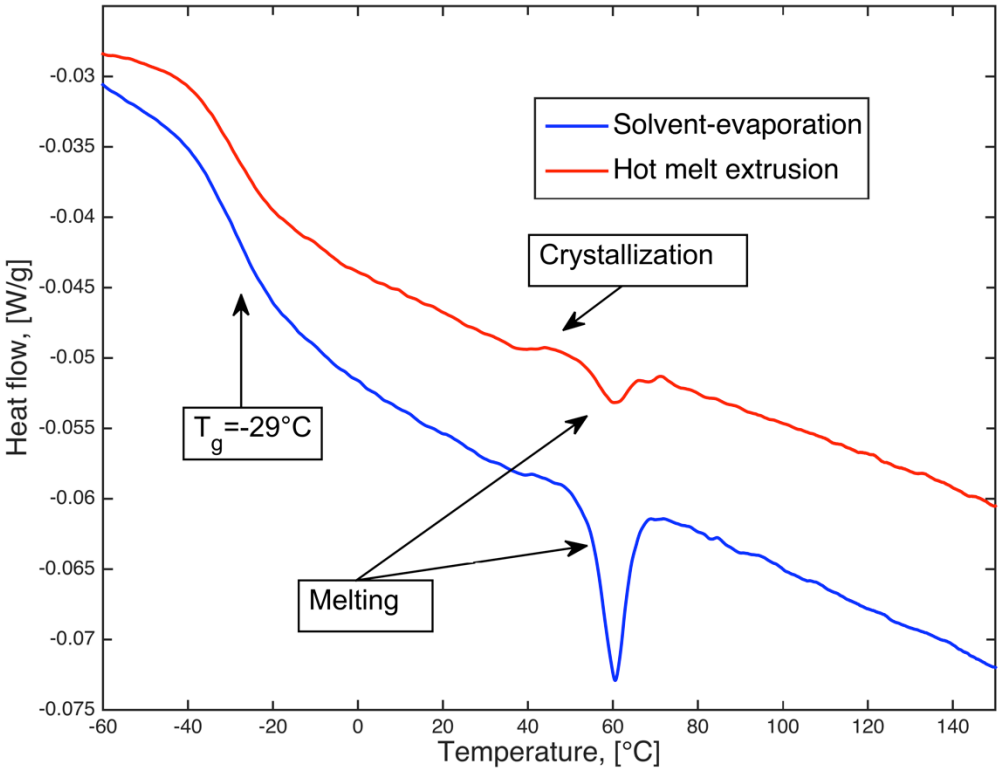

Figure 8.27. DSC thermogram of hot melt extruded and solvent-casted ibuprofen:HPMC HME 40:60(w/w) solid dispersions stored for 1 month. The total heat flow indicates melting endotherms positioned at T_m=60°C.

Figure 8.27 shows that ibuprofen under confinement occur at T_g=-29 °C regardless of preparation method. Also, melting of ibuprofen occur at $T_{m,conf}$=60 °C in both hot melt extruded and solvent-casted solid dispersions. Melting of neat ibuprofen occur at $T_{m,neat}$=77 °C. Thus, there is a significant depression of T_m of ibuprofen upon confinement, which was also observed in systems with less ibuprofen content, see Figure 8.28.

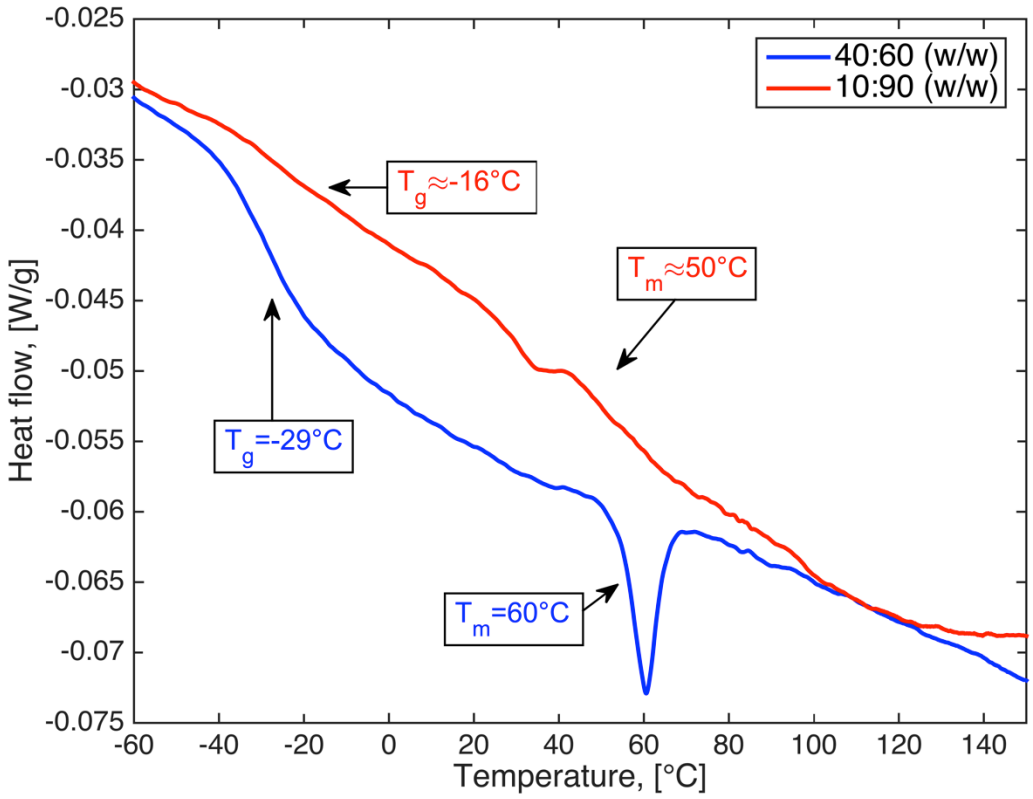

Figure 8.28. Heat flow as a function of temperature shown for solvent-casted solid dispersions of different ibuprofen content, 10 wt.% and 40 wt.%. The concentration of ibuprofen within the polymer matrix affects the T_g and T_m observed.

Glass transition temperatures of around T_g≈-20 °C was obtained for solvent-casted ibuprofen HPMC HME dispersion with 10 wt.% ibuprofen, similar values were found for hot melt extruded dispersions of corresponding composition. An exact value of T_g was difficult to determine due to a weak signal in the MDSC measurement. A possible melting endotherm was also observed for dispersions of 10 wt.% ibuprofen content, at T_m≈50 °C. At high concentrations 40 wt.%, the solid dispersion gives rise to a clear step-like change in heat flow, Figure 8.28. However for lower concentrations this signal is much weaker.

8.2.4 Cilostazol solid dispersions

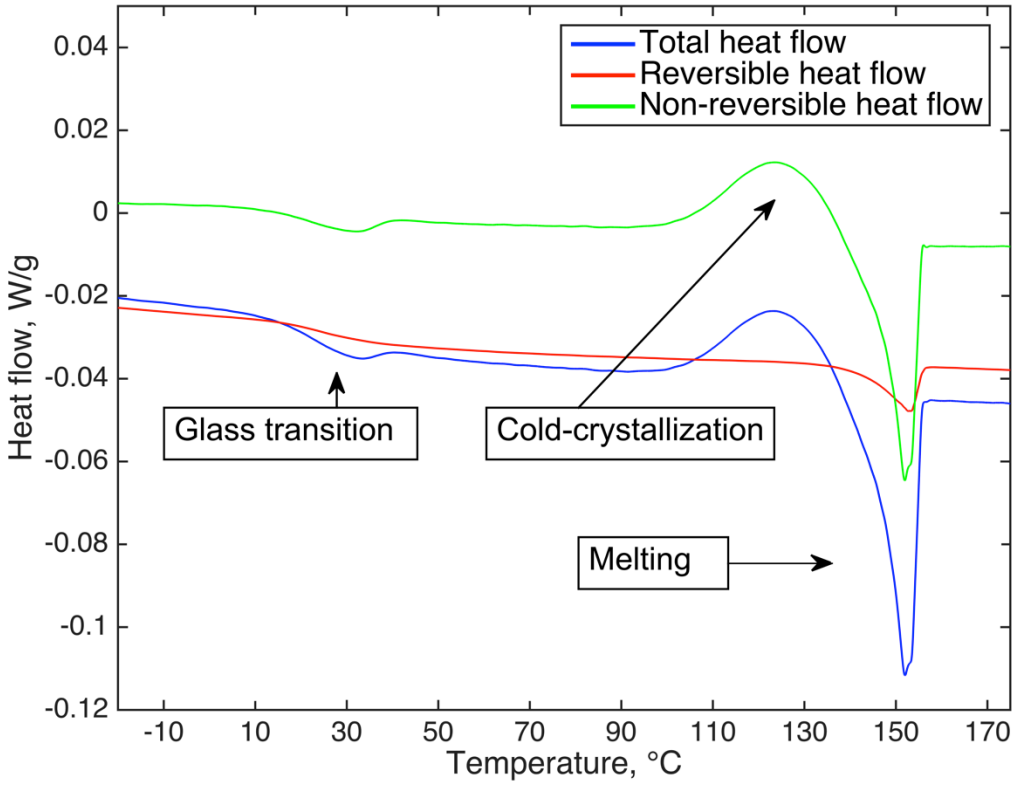

Figure 8.29. DSC results of cilostazol HPMC HME solid dispersion. A glass transition is detected at T_g=25°C, cilostazol crystallizes during the experiment which is followed by melting at T_m=155 °C.

DSC results for hot melt extruded 30 wt.% cilostazol in HPMC HME solid are shown in Figure 8.29. A glass transition at T_g=25 °C is found followed by a cold-crystallization at elevated temperatures, T_c≈120 °C. It is interesting to evaluate is if it is likely that there was significant amounts of crystalline API material within the as prepared solid dispersion before the experiment. To evaluate this the heat flow peak related to crystallization can be integrated with respect to temperature and compared with the corresponding melting peak. If the heat released on crystallization equals the heat absorbed on melting then it is safe to assume that there was no or minor crystallinity in the as prepared material. Indeed, cilostazol was calculated to be amorphous in the as prepared solid dispersion. It is interesting that the T_g of the system lies below the T_g of neat cilostazol and at room temperature. Lower concentrations of cilostazol at 10 wt.% resulted in a T_g=67 °C, see Supplementary Figure S1.25. A trend of T_g depression with increased cilostazol concentration within the dispersion is the opposite of what is observed in the ibuprofen:HPMC system.

8.3 Solid dispersion release performance evaluation

Release experiment results for felodipine HPMC AS and HPMC HME dispersions and ibuprofen HPMC HME dispersions are presented in this section. The main results

obtained are the release concentration profiles as a function of time. Photographs of the tablets dissolving as a function of time will be used to describe the observed release profiles and can be found in the Supplementary material section. DSC and RAMAN spectroscopy results obtained from solid dispersion material remaining after the release experiment, and Raman spectroscopy measurements performed on solid dispersions in aqueous systems will also be presented.

8.3.1 Felodipine solid dispersions

Two types of felodipine release experiments were performed. The first experiment presented aimed to compare the solubility enhancement effect by the type of polymer carrier used to prepare amorphous solid dispersions whereas the second experiment aimed to compare felodipine HPMC HME 100cP solid dispersions that have been extruded above and below the melting temperature of the API.

8.3.1.1 Comparison of HPMC AS & HPMC HME

The effect of polymer type upon dissolution of amorphous solid dispersions into phosphate buffer at pH=6.8 is reported in this section. The two types of polymers compared were HPMC HME and HPMC AS. Both types of dispersions were extruded at the same conditions and contained a felodipine dose of 20 wt.%. Figure 8.30 shows the felodipine release profiles measured using UPLC with and without filtering of the samples (0.22 μm PTFE filters). The details of the release experiment are presented in Section 7.8.2.

The equilibrium solubility of felodipine in phosphate buffer has been reported to be 0.94μg/mL. A similar value, 0.81μg/mL, has been reported felodipine aqueous solubility, pH=7, [10,46]. Measured felodipine concentrations of dissolving felodipine HPMC AS solid dispersions exceeded the crystalline equilibrium solubility regardless if filtering of the sample solution was performed or not. Consequently amorphous solid dispersions of felodipine HPMC AS resulted in supersaturated concentration of felodipine. In contrast, the concentration of felodipine released from the felodipine HPMC HME dispersion did not exceed felodipine solubility throughout the time of the experiment, regardless if the sample aliquots were filtered or not. The equilibrium solubility of felodipine in phosphate buffer is shown for comparison in Figure 8.30 as a dashed black line.

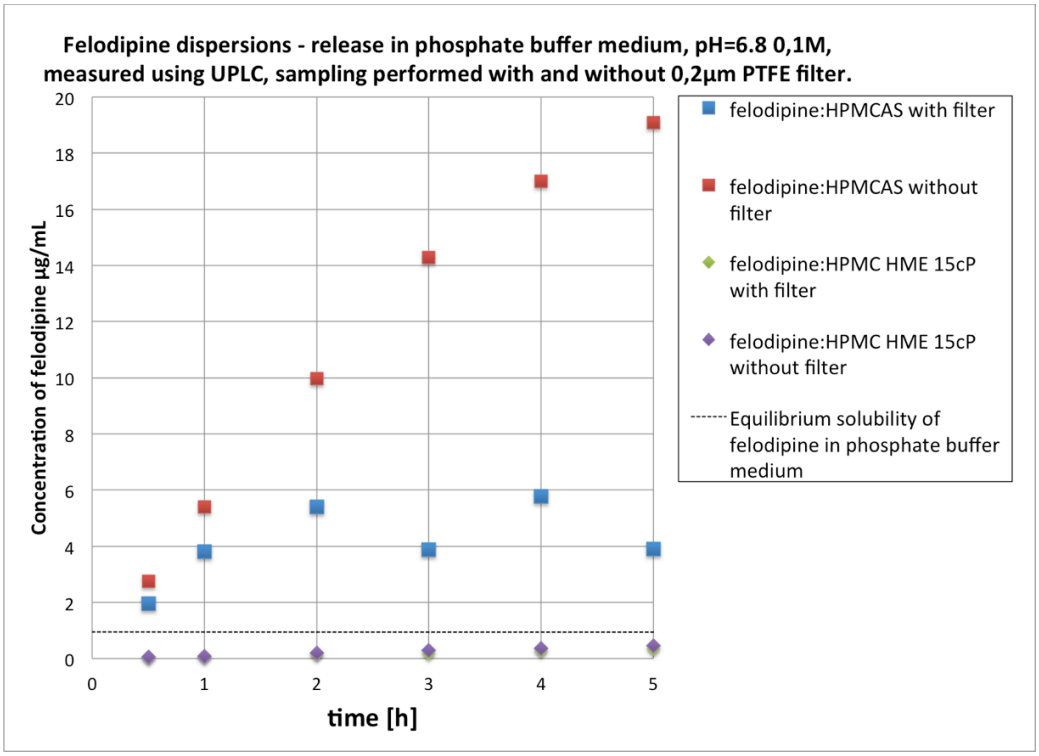

Figure 8.30. Concentration of felodipine as a function of time during release experiments of 20 wt.% felodipine HPMC AS and felodipine HPMC HME solid dispersions. Release experiment conditions were, T=37 °C, rpm=50, I=0.1M, pH=6.8.

The dissolution profile of felodipine HPMC AS solid dispersions has been investigated in previous studies[10]. The results obtained here confirm the capability of HPMC AS to supersaturate felodipine. The release behavior is shown in photographs taken during the release experiments, see Supplementary Figure S1.30. It is interesting to observe that the release medium turns milky and white 3-5h into the experiment. However, after 24h the experiment the liquid has turned clear again and in addition precipitated material can be spotted on the tablet holder basket. Cloud point measurement shows that HPMC AS is miscible in the phosphate medium at all concentrations exceeding those within the release vessel, >2 wt.% see Supplementary Figure S1.31. The precipitated material observed after 24h is therefore believed to be primarily precipitated crystals of felodipine. This tells us that there is a temporary supersaturation of felodipine within the release medium over the course of 24h.

It is also of interest to study not only the felodipine release, but also the polymer release from the solid dispersions. This way the mechanism of release and the contribution of the polymer in raising felodipine solubility can be deduced. The release in terms of percentage of released of felodipine is shown in Figure 8.31, in the same graph the release profile of HPMC AS, measured using SEC, is reported.

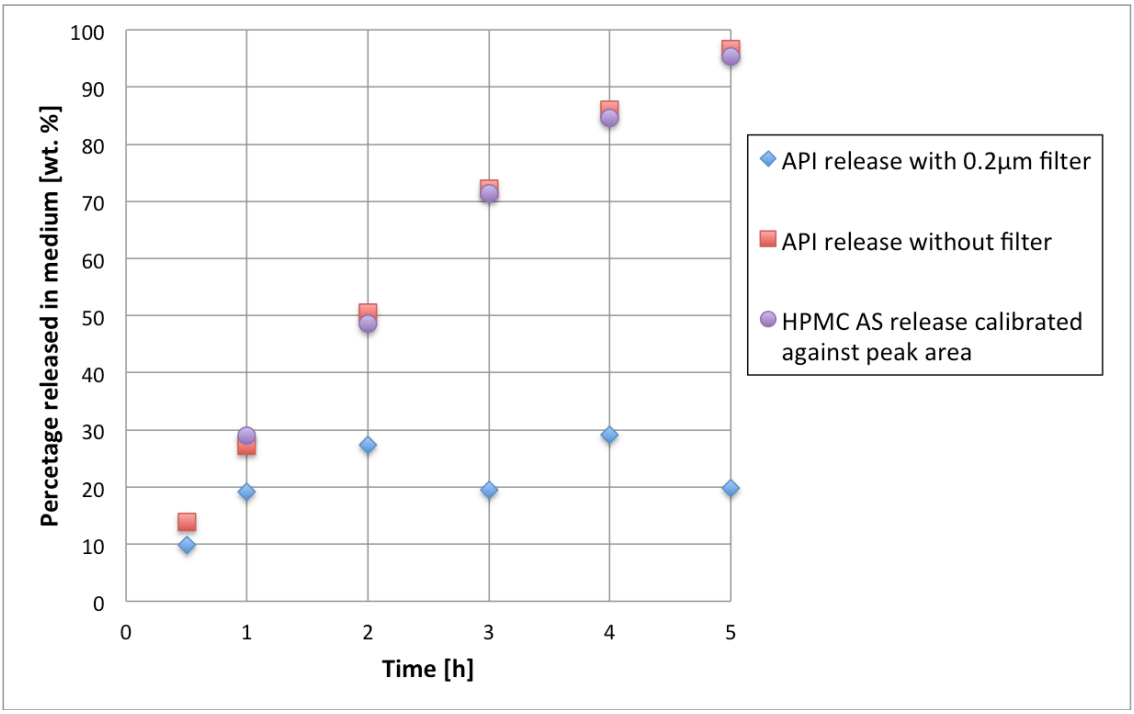

Figure 8.31. Release concentration of felodipine and of HPMC AS as a function of time. The release experiment conditions were, T=37 °C, rpm=50, I=0.1 M, pH=6.8. Felodipine release was measured using UPLC and polymer release was measured using SEC.

The release concentration profile in Figure 8.31 tells us that the unfiltered API release is closely coupled with the HPMC AS release. This indicates that the polymer dictates the release of felodipine. At full dissolution of the tablet, the unfiltered concentration of felodipine within the release medium corresponds to 14,3 mg. This amount of felodipine corresponds to 19% of the solid dispersion weight prior to the release experiment. The UPLC calibration curve displayed an RSD value of 5%, which is one source of error. Adhesion of felodipine on the beaker and syringe surfaces is another source of experimental error. However, these results indicate that the composition of the hot melt extruded amorphous felodipine HPMC AS dispersions are of the same composition as the feed material composition. This show both that the material is sufficiently homogenously mixed within the extruder, and that neither felodipine nor HPMC AS seems to have affinity for the extruder interior surfaces, which could result in an altered composition of the solid dispersions produced. The use of SEC to measure polymer concentration is also an accurate method of quantifying the release of polymer in solution, since the method result in a close to 100% release when the tablet is fully dissolved. It should be noted that there was a minor tablet residue left within the release chamber at t=5 h. A repeated measurement after 5h may have resulted in an even closer release to 100% of both UPLC (felodipine) and SEC (HPMC AS).

Filtration of the aliquots collected when sampling the dissolution medium clearly affect the concentration of felodipine measured in the UPLC instrument. It is difficult to prove if the filter is correctly saturated when preparing the UPLC samples or if it absorbs an excess of molecularly dispersed felodipine within the solution. The fact

that the solution is supersaturated and susceptible to crystallization adds to the uncertainty in the filtered data points, which contribute to the data points fluctuating during the 2-5 h measurements. Another issue related to the filtering is what the particles of sizes larger than 0.22 μm are composed of. These particles may be amorphous and dissolving, but most likely felodipine particles within the 37 °C phosphate buffer will crystallize rapidly. A last, probable explanation, could be agglomerates of HPMC AS and felodipine particles.

Regardless of what is removed when filtering using 0.22 μm, felodipine concentration 4 to 6 times higher than the crystalline equilibrium solubility of felodipine is still accomplished in dissolution experiments of felodipine HPMC AS dispersions. The concentration of felodipine after filtering corresponds to molecularly dissolved felodipine, or felodipine particles of size 0.22 μm or less. Particle reduction on a micrometer range generally results in significant increase in dissolution rate and thereby increased bioavailability[2,4]. The reproducibility has not been thoroughly tested, however the results of Figure 8.30 and Figure 8.31 correspond closely to previous studies of felodipine HPMC AS system solid dispersions[10].

8.3.1.2 Comparison of extrusion temperature

Felodipine HPMC HME solid dispersions were prepared, at two different temperatures, T=135°C, and T=150°C. Apart form the operating temperature of the extruder all other parameters were kept the same. The release of felodipine reveals that the concentration of felodipine in solution is below the equilibrium solubility limit in phosphate buffer of 0.94μg mL^{-1} over the course of 6h, see Figure 8.32.

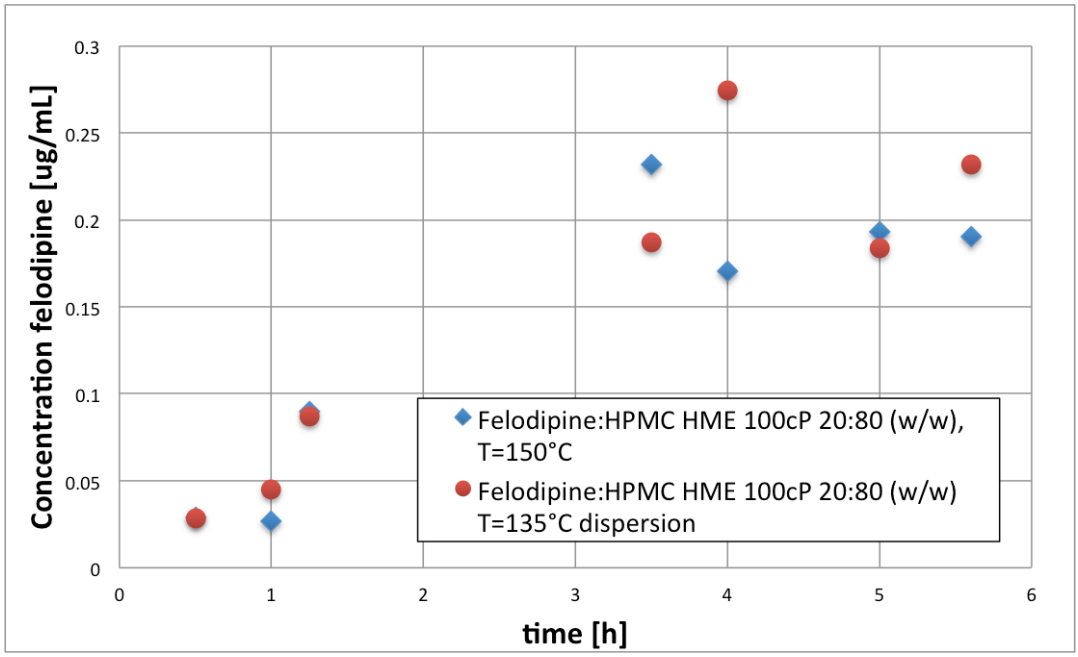

Figure 8.32. Release profile where concentration in is shown as a function of time. Solid dispersions extruded below and above the T_m of felodipine were tested felodipine and HPMC HME 100cP with 20 wt. % drug doses.

Due to less dissolution of tablet material over the course of 6 h supersaturated concentrations (>0.94µg mL^{-1}) were not observed. However, sampling of the medium after 72h into the experiment resulted in a concentration of 1.95µg mL^{-1}. This demonstrates that the prepared solid dispersions can generate supersaturation of felodipine above the equilibrium solubility limit. Due to the similarity in concentration profile, the extrusion temperature used to prepare the felodipine:HPMC HME 100cP dispersions seems to play a minor role in terms of solubility enhancement. A visual comparison of the tablets show that both tablets retain their appearance throughout the course of 7h, see Supplementary Figure S1.31. The similarity between the two tablets during dissolution suggests that extrusion below T_m of felodipine might not result in a crystalline felodipine solid dispersion.

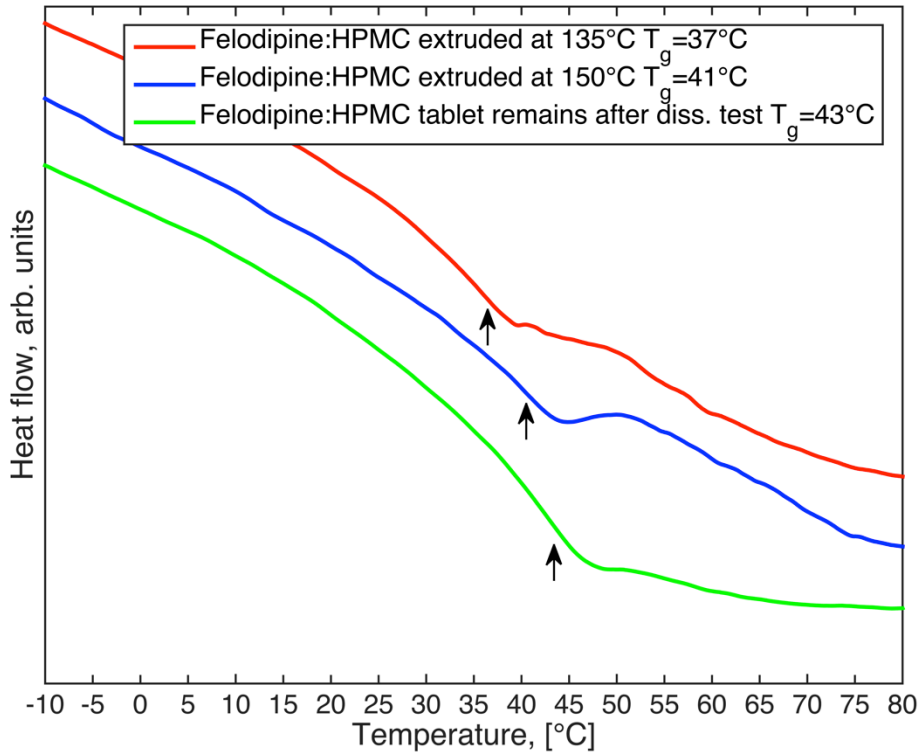

Figure 8.33. Comparison of DSC thermograms of felodipine HPMC HME solid dispersion extruded at two temperatures, 135°C and 150°C and tablet remains retrieved after a dissolution experiment.

To investigate the effect of extrusion temperature further DSC measurement of each of the solid dispersions were performed. In addition, dried tablet remains after dissolution experiment was investigated. The DSC traces from all three samples show a T_g, see Figure 8.33 and there is no melting endotherm present in the DSC traces of the solid dispersion extruded at T=135°C. Thus, extruding felodipine below its T_m together with HPMC HME did not result in crystalline felodipine within the polymer matrix. These results may be explained by insufficient temperature control of the extrusion equipment. Raman spectroscopy confirms the presence of amorphous felodipine in all three samples tested in Figure 8.33, see Supplementary Figure S1.22.

Another interesting observation was made when analyzing tablet remains from dissolution experiments using Raman spectroscopy. A Raman spectra from dried tablet remains after dissolution test experiment is shown in Figure 8.34 together with the Raman spectra obtained from the dry dispersion prior to dissolution experiment.

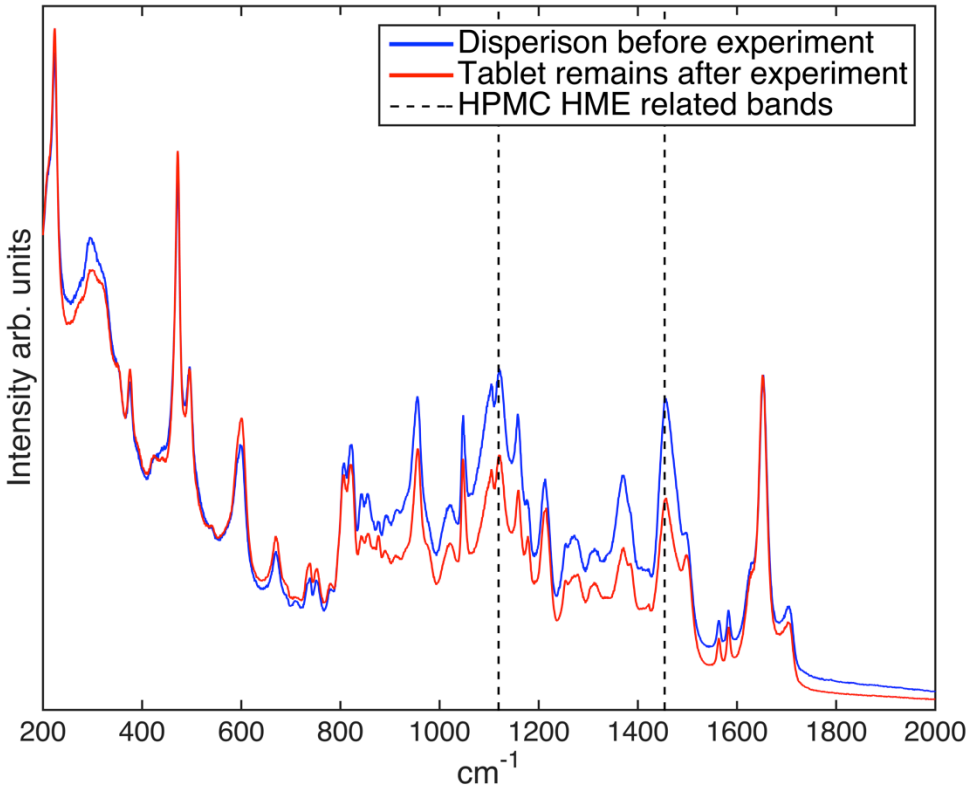

Figure 8.34. Comparison of normalized Raman spectra of felodipine HPMC HME dispersions before and after a dissolution experiment. The spectra are normalized with respect to the 1650cm^{-1} bands.

Clearly the spectra differ in intensity within the region, 800-1400cm^{-1}, but not to the same extent in the lower and higher wavenumber intervals. This indicates composition differences between the material before and after the dissolution experiment. Neat HPMC HME spectra display high intensity in the 800-1400cm^{-1} region, see supplementary Figure S1.22 for comparison of neat felodipine, neat HPMC HME and felodipine HPMC HME dispersions. The comparison shows that bands associated with HPMC HME have lower intensity after the dissolution experiment, suggesting that polymer is released into the medium at a higher rate than the API.

A striking observation made in Figure 8.33 and Figure 8.34 is the well-preserved state of felodipine HPMC HME dispersions despite exposure to the phosphate buffer solvent for in over 72h. Considering the instability of many pharmaceutical glasses when exposed to humidity and water, the behavior of felodipine HPMC HME system is highly resilient toward crystallization based on the measurements presented here. Despite low solubility of felodipine, Figure 8.32, the system exhibits an extended release profile where after 72h supersaturation two times its equilibrium solubility of felodipine is found.

8.3.2 Ibuprofen solid dispersions

Ibuprofen display a relatively high solubility at neutral pH[65]. Release experiments performed at pH=6.8, such as those performed on felodipine, would not result in restricted solubility. A different buffer medium of lower pH was used here, to model a drug of low solubility. In addition, this gives the possibility to observe eventual solubility enhancement of the hot melt extruded solid dispersions.

The release medium used was 0.1M HCl with pH=1 and 0.1M, see Section 7.8.1 for a more detailed description of the method. In a solution of pH=1 ibuprofen displays low solubility[65]. Photos taken during the release experiment are shown in Supplementary Figure S1.32. Ibuprofen release from HPMC 100cP with drug concentration 40:60 (w/w) prepared by extrusion dissolved very slowly (+113h). Similar behavior was observed in the two other doses tested, 30:70 and 20:80. A fully dissolved tablet was not observed in any of the experiments, and the concentration of ibuprofen in solution did never exceed the equilibrium solubility of ibuprofen[65]. A summary of the tablets tested and the concentration of ibuprofen reached within the release medium is given in Table 12.

Table 12. Release data of ibuprofen from solid dispersions with different weight loadings of ibuprofen in relation to HPMC.

	Ibuprofen:HPMC HME 100cP dispersions		
Drug load in wt. %	40	30	20
Total weight of tablet [mg]	98,7	107,3	98,9
Total estimated ibuprofen mass [mg]	39,4	32,2	19,8
Percentage of ibuprofen dissolved (24h)	17,1	20,5	34,2
Absolute amount dissolved, [mg] (24h)	6,75	6,60	6,76
Concentration [mg/mL] (24h)	0,01	0,01	0,01
% of ibuprofen dissolved (113h)	45,1	-	89,6
Absolute amount dissolved, [mg] (113h)	17,81	-	17,73
Concentration [mg/mL] (113h)	0,04	-	0,04

The concentration achieved in the release medium after 24h was, approximately 20% of the solubility limit of ibuprofen in HCl and pH=1, S=0.06mg/mL[65]. After 113h the concentration was estimated to lie at about half of the solubility limit. The almost identical concentration of ibuprofen within the release medium for all three solid dispersions, with different drug load, at t=25h, indicates that the drug load does not affect the release into the solution, see Table 12. Additional UV-vis measurement performed after 113h of exposure of the 20 and 40 wt. % tablets display the same values, again indicating that the drug load has no effect on the release. The strikingly similar release profiles are shown in Figure 8.35. There was no precipitated tablet material on the bottom of the release vessels, indicating that all dissolved ibuprofen stayed within the bulk fluid.

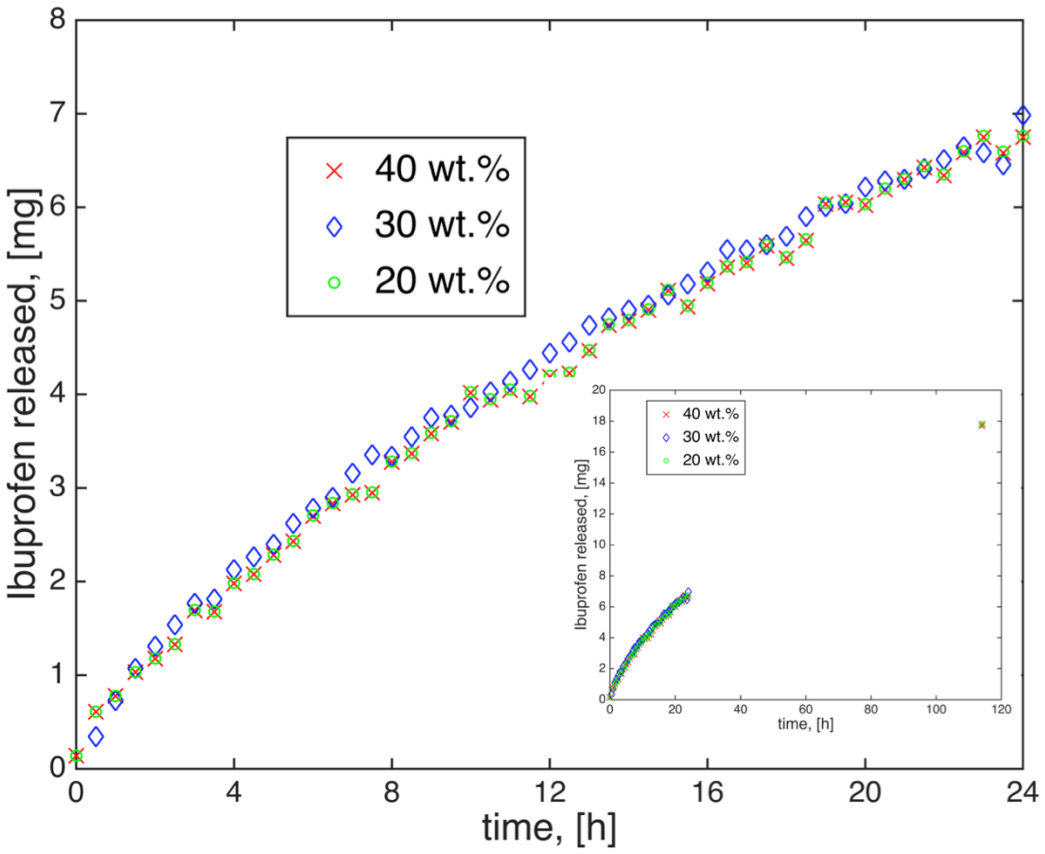

Figure 8.35. Ibuprofen concentration in mg present within the bulk medium measured as a function of time using on-line UV-vis spectrophotometer.

The delayed dissolution observed is thought to be due to the limited driving force of ibuprofen to enter the solution. It is observed in Supplementary Figure S1.32 that there is no transparent film forming at the edge of the tablet. It is generally acknowledged that neat HPMC forms a transparent film when dissolving in aqueous systems[82] and also solid dispersion systems of HPMC have shown to create transparent films on the edge of the tablet during dissolution. It should be noted that the creation of a transparent film when a solid dispersion dissolves implies that also the dispersed substance dissolves, and not only the HPMC. The transparent film is a consequence of the outer shell of the polymer matrix becoming successively hydrated by water penetration[82]. Neat extruded HPMC HME tablets prepared in the same way as ibuprofen HPMC HME dispersions dissolve in the same medium within 16h, a transparent film forms upon surface exposure, see Supplementary Figure S1.33.

The observation that neat HPMC dissolves more rapidly than ibuprofen HPMC solid dispersions suggests some interaction between the drug and the polymer, which delays the dissolution of the tablet as a whole. An alternative explanation related to the absence of transparent film formation is crystallization of ibuprofen within the film. Crystallization within the film could impede the release of ibuprofen and HPMC

HME into solution, resulting in an ibuprofen crystalline interface in contact with the bulk solution.

To explore these hypotheses the intrinsic dissolution rate of crystalline ibuprofen is compared with the dissolution rate of ibuprofen in the solid dispersions. The intrinsic dissolution rate of ibuprofen, at pH=6.8, I=0.05M, and 50rpm, is $DR_{intrinsic}$=0.28 mg×min^{-1}×cm^{-2}.[65] The equilibrium solubility difference between ibuprofen at pH=6.8, is approximately $S_{pH6.8}$=27,51 mg×mL^{-1}, compared with the equilibrium solubility at pH=1 which is $S_{pH1.0}$=0.06mg×mL^{-1}.[65] The dissolution rate of ibuprofen solid dispersions in Figure 8.35 was computed to be between DR_{disp}=0.002-0.001 mg×mL^{-1}. There is a difference between $DR_{intrinsic}$ and DR_{disp} of order 10^2. However since $DR_{intrinsic}$ is evaluated at pH=6.8 and ibuprofen is more soluble at these pH this could be expected. It is interesting to note that there is a corresponding difference of about 10^2 in solubility, S, between pH=7 and pH=1.

From Whitney Noyes equation we know that saturated solubility affects the dissolution rate, equation **(33)**[4]. The difference by two orders of magnitude between dissolution rates obtained from our experiment and literature, scales with the equilibrium crystalline solubility of ibuprofen between pH=1, and pH=7. This similarity of scaling are based on estimates and cannot be used to claim that the ibuprofen solid dispersions dissolve at the rate at which crystalline ibuprofen dissolves at pH=1. However it provides an indication is that there could be crystallized ibuprofen at the interface of the dispersion, which controls the rate at which ibuprofen enters the solution. In fact, an excellent way of testing this would be to perform intrinsic dissolution testing at pH=1 of ibuprofen, and to perform additional release experiments at pH=6.8. Also, it would be important to use the same ionic strength of the buffer solution as quoted in literature. These experiments could be used to determine if the solid dispersions dissolve at the rate comparable to the intrinsic rate of crystalline ibuprofen.

Ibuprofen within HPMC HME is liquid. Compared to the polymer matrix the dynamics of the drug are several orders of magnitudes faster. The possible formation of crystalline ibuprofen at the surface of the tablet during dissolution could be explained by the inability of the matrix to control the release of ibuprofen into solution. Contrary to the case of felodipine HPMC AS solid dispersions where felodipine is in the glass state, ibuprofen in the HPMC HME matrix is in the liquid state, ibuprofen will therefore have a much more rapid diffusion within the solid dispersion. This diffusion which gives rise to crystallization at the surface of the solid dispersion upon solvent exposure.

9 Conclusion

The conclusions section is divided into three parts. The first part addresses the solid state properties, the second part focus upon the release experiments results, and finally an outlook of what further investigations within the field of amorphous solid dispersions could focus upon is presented.

9.1 Dry properties of APIs and solid dispersions

The dynamics of all three model drugs considered in this work was successfully studied using both DSC and Dielectric spectroscopy. The glass properties were characterized and all three APIs were determined to be fragile glass formers. Ibuprofen dynamics could be effectively compared with literature references, which turned out to agree well with the results obtained here. Based on the success in reproducing literature values of ibuprofen, the same characterization was carried out for felodipine and cilostazol resulting in relaxation maps for felodipine and cilostazol covering a broad frequency and temperature ranges.

Using DS solid dispersions properties were studied. The felodipine HPMC AS solid dispersion effectively suppressed crystallization of the drug. Dielectric spectroscopy measurements on solvent-casted felodipine HPMC AS solid dispersions show that crystallization is suppressed on a timescale of 20 hours at T=92 °C, which are conditions where neat felodipine fully crystallizes within 14 hours.

Dielectric spectroscopy performed on solvent casted solid dispersions was not only an illustrative method of comparing neat and confined API crystallization kinetics. This work shows that the structural relaxation and features of the dielectric spectrum related to hydrogen bonding is significantly changed when an API is confined within a polymer matrix. Changes in liquid behavior could be studied in both felodipine HPMC AS solid dispersion and in ibuprofen HPMC HME solid dispersions. The change in dynamics was most striking in the case of ibuprofen HPMC HME where apart from changes in the peak shapes, an increase of T_g and a corresponding shift in the α-relaxation time was observed.

9.2 Release properties in solution of solid dispersions

Solubility of felodipine in a hot melt extruded amorphous solid dispersion with HPMC AS as polymeric carrier resulted in a six-fold increase compared to the crystalline equilibrium solubility. The solid dispersion was fully dissolved within five hours, and the enhanced solubility effect was observed on a timescale exceeding four hours. The properties of HPMC AS makes it a potentially useful polymer carrier for delivery in small intestines.

The release experiments conducted on ibuprofen:HPMC HME 100cP and felodipine:HPMC 100cP/15cP systems showed very slow dissolution. These solid

dispersions did not demonstrate any enhancement in solubility of the APIs. The failure in producing crystalline solid dispersion to be used as comparison with the amorphous solid dispersion made it difficult to de-convolute the role of amorphous state API in terms of raising solubility. The slow dissolution of these dispersions is considered to be due to insufficient polymer release. As pointed out in previous studies, the very low solubility of felodipine makes it reliant on the presence of a polymer carrier to enter the solution[55]. In this case 20 wt.% API load may be too high in terms of aiding dissolution. The potential of the felodipine:HPMC HME system of achieving supersaturation is however noted by the UPLC measurement of the release medium after 72h.

The release mechanisms of amorphous solid dispersions were found to depend primarily on the polymer additive choice. The HPMC polymer studied in this thesis differs from those typically found in literature. The low T_g enabled extrusion at exceptionally low temperatures without addition of plasticizer. The enhanced processabillity comes to the price of altered phase behavior in the solvent. HPMC HME was observed to have a low upper cloud point temperature across all viscosity grades tested. It is believed that this phase behavior is further enhanced upon the addition of an API with low solubility making the dispersion virtually insoluble over the course of a few hours, and to retain tablet body integrity over several days of solvent exposure.

The fact that the solid dispersions based on HPMC HME retain the physical form in solvent leads to low concentrations of API in the solution. This was observed in both ibuprofen and felodipine based HPMC HME tablets. These results may appear discouraging in terms of achieving supersaturation in solution and for amorphous solid dispersion use. However the results do not necessarily mean that they are useless for pharmaceutical applications. The fact that felodipine within HPMC HME remained amorphous despite extensive exposure to water is remarkable. Several examples in literature show that some formulations suffer from crystallization within the tablet during dissolution[10,55]. In fact the felodipine HPMC AS dissolution experiments conducted in this thesis resulted in crystal precipitation within 24h. Understanding the high stability of amorphous felodipine within the HPMC HME matrix during dissolution may provide tools for generating more stable amorphous solid dispersions during dissolution. Similarly, an understanding of the HPMC AS polymer and how it is able to generate release profiles resulting in such high API concentrations will surely contribute to development of effective supersaturating drug delivery systems.

Another aspect of the release experiments study worth discussing is the effect of preparation method. The hot melt extruded solid dispersions were formed at high-pressure gradients, $\Delta P \approx 60$ bar. Contrary to tablet punching in which some elasticity related to the tablet punch impact may be encountered; solid dispersions were formed under high and constant pressure for several minutes[4]. The preparation state has been shown to affect the release behavior in other studies, where hot melt extruded tablets maintain their tablet form for longer time in

solution than what is found other manufacturing methods, such as tablet compaction[12]. Within the scope of this thesis a comparison of punched tablets with equivalent solid dispersions was not tested, however such a study would assist in de-convoluting the release effect of preparation method, and the release effect as a result of the polymer and API materials.

9.3 Outlook

The methodology developed in this thesis is summarized in Figure 9.1. It enables a systematical method of identifying suitable API and polymer carrier candidates for hot melt extrusion of amorphous solid dispersions as formulation method. By implementing Dielectric spectroscopy, as a tool for characterization solid dispersions it would be possible to determine what dynamics in solid dispersions that result in stabilized amorphous state. This thesis considers preparation of solid dispersions on a small batch scale. Further work should consider how successful results on small-scale could be translated to larger scale.

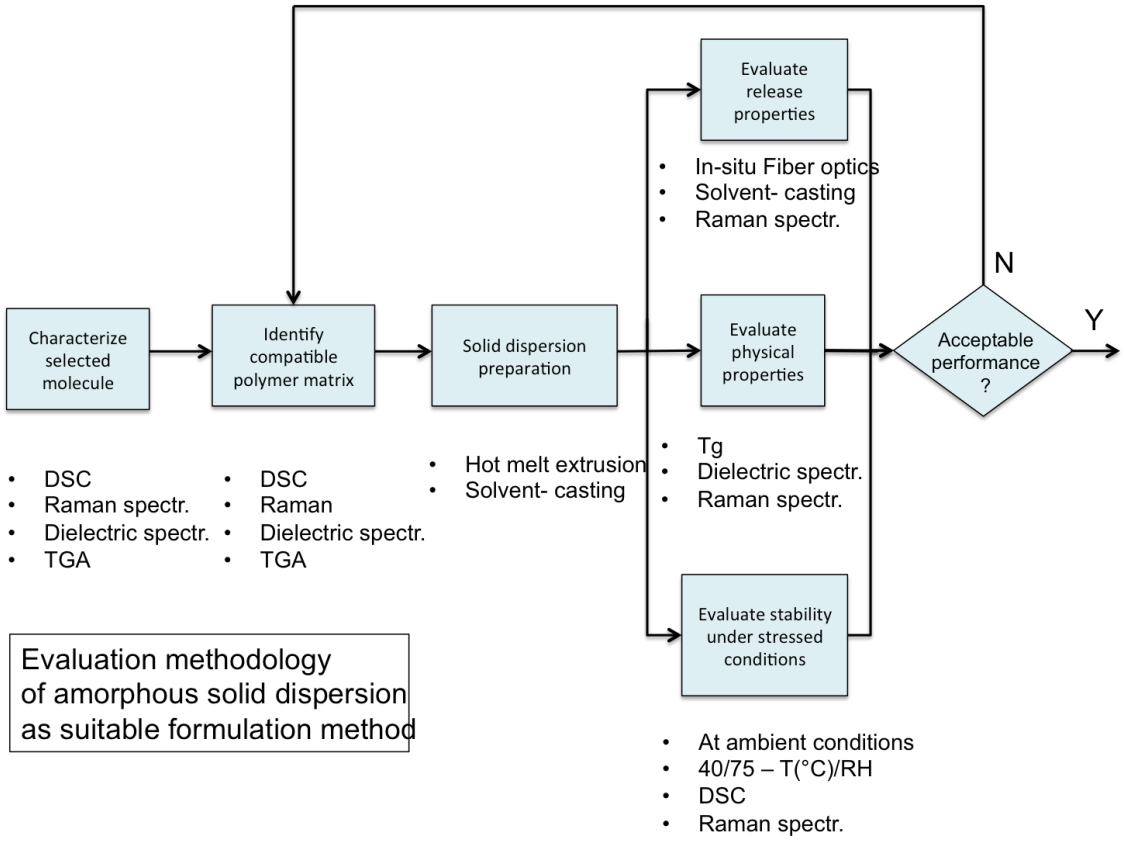

Figure 9.1. Methodology developed to evaluate amorphous solid dispersion properties and performance. Dielectric spectroscopy plays a central role in determining how the dynamics of the drug and polymer are changed in the solid dispersion. Both physical properties and release performance was tested in this thesis.

It is possible to study the dynamics of an API confined within a polymer carrier matrix. It is possible to study how the dynamics is altered upon confinement compared to the neat API state. According to the author this is the primary contribution of this thesis to the field of pharmaceutical research. Instead of only characterizing the neat API relaxations, this work goes one step further and tries to understand API relaxations within solid dispersions. Further interpretation of how small molecule dynamics changes upon confinement is from a fundamental science point of view also an important problem to address. The study of confinement within inorganic matrices has been thoroughly studied. The polymer matrix approach however has important applications not least in pharmaceutical sciences.

Development of the methodology described in this thesis could improve characterization of amorphous solid dispersions from dry state and single components, to formulation and dissolution. It is emphasized that both physical stability properties and dissolution performance is tested within the scope of one project. Further efforts to cover both physical characterization and release performance may facilitate identification of common denominators between preparation method and release functionality.

10 References

1 Lipinski, C. A. Drug-like properties and the causes of poor solubility and poor permeability. *Journal of Pharmacological and Toxicoloical Methods* **44**, 235-249 (2000).

2 Hywel D. Williams *et al.* Strategies to Address Low Drug Solubility in Discovery and Development. *Pharmacological Reviews* **65**, 315-499 (2013).

3 Mitragotri, S., Burke, P. A. & Langer, R. Overcoming the challenges in administering biopharmaceuticals: formulation and delivery strategies. *Nature reviews. Drug discovery* **13**, 655-672, doi:10.1038/nrd4363 (2014).

4 Aulton, M. E. *Pharmaceutics The Science of Dosage Form Design Second Edition*. (2002).

5 Traverso, G. & Langer, R. Special delivery for the gut. *Nature* **519**, S19 (2015).

6 Adrjanowicz, K. *et al.* Dielectric relaxation studies and dissolution behavior of amorphous verapamil hydrochloride. *J Pharm Sci* **99**, 828-839, doi:10.1002/jps.21877 (2010).

7 Shah, S., Maddineni, S., Lu, J. & Repka, M. A. Melt extrusion with poorly soluble drugs. *Int J Pharm* **453**, 233-252, doi:10.1016/j.ijpharm.2012.11.001 (2013).

8 Angell, C. A. Formation of Glasses from Liquids and Biopolymers. *Science* **267**, 1924-1935 (1995).

9 Jared A. Baird, Bernard Van Eerdenbrugh, a. & Taylor, L. S. A Classification System to Assess the Crystallization Tendency of Organic Molecules from Undercooled Melts. *Journal of Pharmaceutical Sciences* **99**, 20 (2010).

10 Konno, H., Handa, T., Alonzo, D. E. & Taylor, L. S. Effect of polymer type on the dissolution profile of amorphous solid dispersions containing felodipine. *European Journal of Pharmaceutics and Biopharmaceutics* **70**, 493-499 (2008).

11 Repka, M. A. *et al.* Melt extrusion: process to product. *Expert Opinion Drug Delivery* **9**, 105-125 (2012).

12 Repka, M. A., Langley, N. & DiNunzio, J. (eds Michael A. Repka, James DiNunzio, & Nigel Langley) (Springer New York Heidelberg Dordrecht London, 2013).

13 Staff, W. H. O. (World Health Organization (WHO), Switzerland, 2003).

14 Peter Timmins, Samuel R. Pygall & Melia, C. D. (eds Peter Timmins, Samuel R. Pygall, & Colin D. Melia) (Springer, Springer New York Heidelberg Dordrecht London, 2014).

15 Dyre, J. Colloquium: The glass transition and elastic models of glass-forming liquids. *Reviews of Modern Physics* **78**, 953-972, doi:10.1103/RevModPhys.78.953 (2006).

16 Hancock, B. C. & Parks, M. What is the True Solubility Advantage of Amorphous Pharmaceuticals. *Pharmaceutical Research* **17**, 397-404 (2000).
17 Lindfors, L. *et al.* Amorphous Drug Nanosuspensions. 1. Inhibition of Ostwald Ripening. *Langmuir : the ACS journal of surfaces and colloids* **22**, 906-910 (2006).
18 Demuth, B. *et al.* Downstream processing of polymer-based amorphous solid dispersions to generate tablet formulations. *Int J Pharm* **486**, 268-286, doi:10.1016/j.ijpharm.2015.03.053 (2015).
19 Leuner, C. & Dressman, J. Improving drug solubility for oral delivery using solid dispersions. *European Journal of Pharmaceutics and Biopharmaceutics* **50**, 47-60 (2000).
20 Marsac, P. J., Shamblin, S. L. & Taylor, L. S. Theoretical and practical approaches for prediction of drug-polymer miscibility and solubility. *Pharm Res* **23**, 2417-2426, doi:10.1007/s11095-006-9063-9 (2006).
21 Zhang, J. *et al.* The stability of solid dispersions of felodipine in polyvinylpyrrolidone characterized by nanothermal analysis. *Int J Pharm* **414**, 210-217, doi:10.1016/j.ijpharm.2011.05.037 (2011).
22 Qian, F. *et al.* Is a distinctive single Tg a reliable indicator for the homogeneity of amorphous solid dispersion? *Int J Pharm* **395**, 232-235, doi:10.1016/j.ijpharm.2010.05.033 (2010).
23 Kramer, E. & Schönhals, A. (Springer-Verlag Berlin Heidelberg, 2003).
24 Adrjanowicz, K. *et al.* Dielectric Relaxation and Crystallization Kinetics of Ibuprofen at Ambient and Elevated Pressure. *Journal of Physical Chemistry B* **114** (2010).
25 Brás, A. R. *et al.* Molecular Motions in Amorphous Ibuprofen As Studied by Broadband Dielectric Spectroscopy. *Journal of Physical Chemistry* **112**, 11087-11099 (2008).
26 K. P. O'Donnell & Woodward, W. H. Dielectric spectroscopy for the determination of the glass transition temperature of pharmaceutical solid dispersions. *Informa Healthcare*, 1-10 (2014).
27 C. Svanberg, R. Bergman, P. Jacobsson & L. Börjesson. (ed Department of experimental and applied physics at Chalmers University of Technology) (SE-412 96 Göteborg, Sweden, 2000).
28 Elliott, S. R. *Physics of amorphous materials*. Second edition edn, (Longman Scientific & Technical, 1990).
29 Mattson, J. *Glass Transition Dynamics in Soft Condensed Matter* Ph.D thesis, Chalmers University of Technology, Göteborg University, (2002).
30 Ngai, K. L. (Springer New York Dordrecht Heidelberg London, 2011).
31 Williams, R. O. (eds Alan B. Watts & Dave A. Miller) (Springer New York Dordrecht Heidelberg London, 2012).
32 Wojnarowska, Z. *et al.* Broadband Dielectric Relaxation Study at Ambient and Elevated Pressure of Molecular
Dynamics of Pharmaceutical: Indomethacin. *The journal of physical chemistry. B* **2009**, 12536-12545 (2009).

33 Schneider, U., Brand, R., Lunkenheimer, P. & Loidl, A. Excess Wing in the Dielectric Loss of Glass Formers: A Johari-Goldstein beta Relaxation? *Physical Review Letters* **84** (2000).
34 Kaminski, K., Kaminska, E., Paluch, M., Ziolo, J. & Ngai, K. L. The True Johari-Goldstein ß-Relaxation of Monosaccharides. *The journal of physical chemistry. B* **110**, 25045-25049 (2006).
35 Gainaru, C. *et al.* Shear-Modulus Investigations of Monohydroxy Alcohols: Evidence for a Short-Chain-Polymer Rheological Response. *Physical Review Letters* **112**, doi:10.1103/PhysRevLett.112.098301 (2014).
36 Affouard, F. & Correia, N. Debye Process in Ibuprofen Glass-Forming Liquid: Insights from Molecular Dynamics Simulation. *Journal of Physical Chemistry* **114**, 11397-11402 (2010).
37 Svanberg, C., Bergman, R., Jacobsson, P. & Börjesson, L. Restricted dynamics of a supercooled liquid in a polymer matrix. *Physical Review B* **66**, doi:10.1103/PhysRevB.66.054304 (2002).
38 Jones, R. A. L. *Soft Condensed Matter*. (Oxford University Press, 2002).
39 Cowie, J. M. G. & Arrighi, V. *Polymers: Chemistry and Physics of Modern Materials*. Vol. Third Edition (CRC Press, Taylor & Francis Group, 2008).
40 Turnbull, D. & Fisher, J. C. Rate of Nucleation in Condensed Systems. *The Journal of Chemical Physics* **17**, 71, doi:10.1063/1.1747055 (1949).
41 Zanotto, E. D. & James, P. F. Experimental Tests of the Classical Nucleation Theory for Glasses. *Journal of Non-Crystalline Solids* **74**, 373-394 (1985).
42 Weinberg, M. C. A few topics concerning nucleation and crystallization in glasses. *Journal of Non-Crystalline Solids* **255**, 1-14 (1999).
43 Napolitano, S. & Wübbenhorst, M. Monitoring the cold crystallization of poly(3-hydroxy butyrate) via dielectric spectroscopy. *Journal of Non-Crystalline Solids* **353**, 4357-4361, doi:10.1016/j.jnoncrysol.2007.01.082 (2007).
44 Wanapun, D., Kestur, U. S., Kissick, D. J., Simpson, G. J. & Taylor, L. S. Selective Detection and Quantitation of Organic Molecule Crystallization by Second Harmonic Generation Microscopy. *Anal. Chem.* **82**, 5425-5432 (2010).
45 Eerdenbrugh, B. V. & Taylor, L. S. Influence of Particle Size on the Ultraviolet Spectrum of Particulate-Containing Solutions: Implications for In-Situ Concentration Monitoring Using UV/Vis Fiber-Optic Probes. *Pharm Res* **28**, 1643–1652, doi:10.1007/s11095-011-0399-4 (2011).
46 Lindfors, L. *et al.* Amorphous Drug Nanosuspensions. 2. Experimental Determination of Bulk Monomer Concentrations. *Langmuir : the ACS journal of surfaces and colloids* **22**, 911 (2006).
47 Holmberg, K., Jönsson, B., Kronberg, B. & Lindman, B. *Surfactants and Polymers in Aqueous Solution Second Edition*. (John Wiley & Sons, Ltd., 2002).
48 Anna Viridén, S. A.-A., Bengt Wittgren and Anette Larsson. (ed Chalmers University of technology SE-412 96 Gothenburg Department of Biological Engineering, Sweden, Astra Zeneca R&D, SE-431 83 Mölndal, Sweden) (2011).

49 Viriden, A., Larsson, A. & Wittgren, B. The effect of substitution pattern of HPMC on polymer release from matrix tablets. *Int J Pharm* **389**, 147-156, doi:10.1016/j.ijpharm.2010.01.029 (2010).
50 Baird, J. A. & Taylor, L. S. Evaluation of amorphous solid dispersion properties using thermal analysis techniques. *Advanced drug delivery reviews* **64**, 396-421, doi:10.1016/j.addr.2011.07.009 (2012).
51 Konno, H. & Taylor, L. S. Influence of Different Polymers on the Crystallization Tendency of Molecularly Dispersed Amorphous Felodipine. *Journal of Pharmaceutical Sciences* **95**, 2692-2705 (2006).
52 Kalogeras, I. M. A novel approach for analyzing glass-transition temperature vs. composition patterns: application to pharmaceutical compound+polymer systems. *European journal of pharmaceutical sciences : official journal of the European Federation for Pharmaceutical Sciences* **42**, 470-483, doi:10.1016/j.ejps.2011.02.003 (2011).
53 Brabander, C. D., Mooter, G. V. D., Vervaet, C. & Remon, J. P. Characterization of Ibuprofen as a Nontraditional Plasticizer of Ethyl Cellulose. *Journal of Pharmaceutical Sciences* **91** (2002).
54 Marsac, P. J., Konno, H. & Taylor, L. S. A comparison of the physical stability of amorphous felodipine and nifedipine systems. *Pharm Res* **23**, 2306-2316, doi:10.1007/s11095-006-9047-9 (2006).
55 Tres, F. *et al.* Real time Raman imaging to understand dissolution performance of amorphous solid dispersions. *Journal of controlled release : official journal of the Controlled Release Society* **188**, 53-60, doi:10.1016/j.jconrel.2014.05.061 (2014).
56 Thomas Dieing, Olaf Hollricher & Toporski, J. in *Springer Series in Opical Sciences* (ed W. T. Rhodes) (Sprigner Verlag, Springer Heidelberg Dordrecht London New York, 2010).
57 Roblegg, E. *et al.* Development of sustained-release lipophilic calcium stearate pellets via hot melt extrusion. *European journal of pharmaceutics and biopharmaceutics : official journal of Arbeitsgemeinschaft fur Pharmazeutische Verfahrenstechnik e.V* **79**, 635-645, doi:10.1016/j.ejpb.2011.07.004 (2011).
58 Kolter, K., Karl, M. & Gryckze, A. in *Extrusion Compendium 2nd Revised and Enlarged Edition* (BASF The Cehmical Company, BASF SE
Pharma Ingredients & Services 67056 Ludwigshafen, Germany, 2012).
59 Viriden, A., Wittgren, B. & Larsson, A. Investigation of critical polymer properties for polymer release and swelling of HPMC matrix tablets. *European journal of pharmaceutical sciences : official journal of the European Federation for Pharmaceutical Sciences* **36**, 297-309, doi:10.1016/j.ejps.2008.10.021 (2009).
60 Siepmann, J. & Peppas, N. A. Modeling of drug release from delivery systems based on hydroxypropyl methylcellulose (HPMC). *Advanced drug delivery reviews* **48**, 139-157 (2001).
61 Viriden, A., Wittgren, B. & Larsson, A. The consequence of the chemical composition of HPMC in matrix tablets on the release behaviour of model drug substances having different solubility. *European journal of*

pharmaceutics and biopharmaceutics : official journal of Arbeitsgemeinschaft fur Pharmazeutische Verfahrenstechnik e.V **77**, 99-110, doi:10.1016/j.ejpb.2010.11.004 (2011).
62 Viriden, A., Wittgren, B., Andersson, T. & Larsson, A. The effect of chemical heterogeneity of HPMC on polymer release from matrix tablets. *European journal of pharmaceutical sciences : official journal of the European Federation for Pharmaceutical Sciences* **36**, 392-400, doi:10.1016/j.ejps.2008.11.003 (2009).
63 William Curatolo, James A. Nightingale & Herbig, S. M. Utility of Hydroxypropylmethylcellulose Acetate Succinate (HPMCAS) for Initiation and Maintainance of Drug Supersaturation in the GI Milieu. *Pharmaceutical Research* **26**, 1419-1431 (2009).
64 Adrjanowicz, K., Grzybowski, A., Kaminski, K. & Paluch, M. Temperature and volume effect on the molecular dynamics of supercooled ibuprofen at ambient and elevated pressure. *Molecular pharmaceutics* **8**, 1975-1979, doi:10.1021/mp200211w (2011).
65 Shaw, L. R., Irwin, W. J., Grattan, T. J. & Conway, B. R. The effect of selected water-soluble excipients on the dissolution of paracetamol and Ibuprofen. *Drug development and industrial pharmacy* **31**, 515-525, doi:10.1080/03639040500215784 (2005).
66 Johari, G. P., Kim, S. & Shanker, R. M. Dielectric relaxation and crystallization of ultraviscous melt and glassy states of aspirin, ibuprofen, progesterone, and quinidine. *J Pharm Sci* **96**, 1159-1175, doi:10.1002/jps.20921 (2007).
67 Dudognon, E., Danede, F., Descamps, M. & Correia, N. T. Evidence for a new crystalline phase of racemic Ibuprofen. *Pharm Res* **25**, 2853-2858, doi:10.1007/s11095-008-9655-7 (2008).
68 Blychert, E., Edgar, B., Elmfeldt, D. & Hedner, T. A population study of the pharmacokinetics of felodipine. *Br. J. clin. Pharmac.* **31**, 15-24 (1991).
69 Won, D. H., Kim, M. S., Lee, S., Park, J. S. & Hwang, S. J. Improved physicochemical characteristics of felodipine solid dispersion particles by supercritical anti-solvent precipitation process. *Int J Pharm* **301**, 199-208, doi:10.1016/j.ijpharm.2005.05.017 (2005).
70 Konno, H., Handa, T., Alonzo, D. E. & Taylor, L. S. Effect of polymer type on the dissolution profile of amorphous solid dispersions containing felodipine. *European journal of pharmaceutics and biopharmaceutics : official journal of Arbeitsgemeinschaft fur Pharmazeutische Verfahrenstechnik e.V* **70**, 493-499, doi:10.1016/j.ejpb.2008.05.023 (2008).
71 Marsac, P. J., Konno, H., Rumondor, A. C. F. & Taylor, L. S. Recrystallization of Nifedipine and Felodipine from Amorphous Molecular Level Solid Dispersions Containing Poly(vinylpyrrolidone) and Sorbed Water. *Pharmaceutical Research* **25**, 647-655 (2007).
72 Marsac, P. J., Konno, H. & Taylor, L. S. A Comparison of the Physical Stability of Amorphous Felodipine and Nifedipine Systems. *Pharmaceutical Research* **23**, 2306-2318 (2006).
73 Lindfors, L., Skantze, P., Skantze, U., Westergren, J. & Olsson, U. Amorphous Drug Nanosuspensions. 3. Particle Dissolution and Crystal

Growth. *Langmuir : the ACS journal of surfaces and colloids* **23**, 9866-9874 (2007).
74 Zadymova, N. M. & Ivanova, N. I. *Colloid Journal* **75**, 159-169 (2012).
75 Chen, Y. C., Ho, H. O., Chiou, J. D. & Sheu, M. T. Physical and dissolution characterization of cilostazol solid dispersions prepared by hot melt granulation (HMG) and thermal adhesion granulation (TAG) methods. *Int J Pharm* **473**, 458-468, doi:10.1016/j.ijpharm.2014.07.043 (2014).
76 Stowell, G. W. *et al.* Thermally-Prepared Polymorphic Forms of Cilostazol. *Journal of Pharmaceutical Sciences* **91**, 2481-2488 (2002).
77 Schimizu, T., Osumi, T., Niimi, K. & Nakagawa, K. Physiochemical Properties and Stability of Cilostazol. *Drug Res.* **35**, 1117-1123 (1985).
78 Lunkenheimer, P. & Loidl, A. Dielectric spectroscopy of glass-forming materials: a-relaxation and excess wing. *Chemical Physics* **284**, 205-219 (2002).
79 Bhugra, C., Shmeis, R., Krill, S. L. & Pikal, M. J. Different measures of molecular mobility: comparison between calorimetric and thermally stimulated current relaxation times below Tg and correlation with dielectric relaxation times above Tg. *J Pharm Sci* **97**, 4498-4515, doi:10.1002/jps.21324 (2008).
80 Sousa, M. *et al.* Dynamical Characterization of a Cellulose Acetate Polysaccharide. *The journal of physical chemistry. B* **114**, 10939-10953 (2010).
81 Bergman, R. General susceptibility functions for relaxations in disordered systems. *Journal of Applied Physics* **88**, 1356, doi:10.1063/1.373824 (2000).
82 Tajarobi, F., Larsson, A., Matic, H. & Abrahmsen-Alami, S. The influence of crystallization inhibition of HPMC and HPMCAS on model substance dissolution and release in swellable matrix tablets. *European journal of pharmaceutics and biopharmaceutics : official journal of Arbeitsgemeinschaft fur Pharmazeutische Verfahrenstechnik e.V* **78**, 125-133, doi:10.1016/j.ejpb.2010.11.020 (2011).